2008

Rheological studies on the flow behavior of two-phase solid-liquid materials

Gang Lu
Iowa State University

Rheological studies on the flow behavior of two-phase solid-liquid materials

by

Gang Lu

A dissertation submitted to the graduate faculty

in partial fulfillment of the requirements for the degree of

DOCTOR OF PHILOSOPHY

Major: Civil Engineering (Civil Engineering Materials)

Program of Study Committee:
Kejin Wang, Major Professor
Thomas J. Rudolphi
Halil Ceylan
Max Porter
Bruce R. Thompson

Iowa State University

Ames, Iowa

2008

TABLE OF CONTENTS

LIST OF FIGURES

CHAPTER 1.

CHAPTER 2.

CHAPTER 3.

CHAPTER 4.

CHAPTER 5.

CHAPTER 6.

LIST OF TABLES

CHAPTER 2.

CHAPTER 3.

CHAPTER 4.

CHAPTER 5.

ABSTRACT

Fresh concrete as well as mortar can be considered as a two-phase material with solid particles dispersing in non-Newtonian fluid. In this study, rheological models were developed to predict the flow behavior of cement-based two-phase materials. The models include four different aspects: aggregate particles direct shear stress, fresh cement paste yield stress, fresh mortar yield stress and shear stress.

Firstly, mathematical approach to model the direct shear of coarse granular material was performed in order to study the relationship between the bulk internal friction angle of granular materials and the friction coefficient of raw material of granular materials, the former can be measured directly by different methods, however, the later cannot. Three-dimension probabilistic and mechanical two-particle contact models were developed to calculate both the shear stress generated on shear plane when granular material is under direct shear and volume change due to shear. The models show that the friction angle of coarse granular materials is dependent on surface properties of granular material, and independent on the size of and size distribution of granular material. Direct shear tests on different type of particles were performed using standard direct shear box and a modified large size direct shear box. For different kind of granular materials, the peak friction angles showed good consistence with previous experimental results and proved that the present models are reasonable and experimentally correct.

Secondly, a yield stress model of cement paste was developed based on the DLVO theory. In this model, cement particles were considered as rigid spheres suspending in water. The interparticle cohesion force between two adjacent cement particles was assumed to be generated by the electrostatic and dispersion forces of the cement particles. The mean interparticle force of the cement paste system along the shear direction was determined based on a probability approach. The shear stress of the cement paste was then obtained by multiplying the mean interparticle force with the number of particles in a unit volume of the cement paste. To verify the validity of the newly developed model, two types of tests, direct shear and rheometer tests, were also performed for a group of cement pastes with different w/c. The results indicated that the yield stress of cement paste primarily depends on the w/c and properties of cement materials. The newly developed model can well predict the yield behavior of cement pastes made with different w/c. It can also describe the correlation among the shear stress test results obtained from different experimental methods using an experimental scaling parameter (D). The present experimental work indicated that the yield stress obtained from a direct shear test is close to the yield stress obtained from the up flow curve of the rheolometer test used. A normal stress has significant effect on yield stress of a cement paste, particularly on the pastes with low w/c ($\leq$0.4).

Then, a shear failure behavior of fresh mortars was investigated using a force balance approach from a microscale to macroscale level. In this approach, fresh mortar was considered as a two-phase material containing a matrix of cement paste and a group of rigid, spherical, non-cohesive aggregate particles. The shear force of a micro mortar unit,

consisting of two contacted aggregate particles surrounded by a layer of cement paste, was first assessed from all forces balanced on the micro slant surface of failure. The shear force was assumed resulting from the friction between these two contacted particles and the shear force carried by the cement paste of the micro unit. The shear force of a macro-unit volume of the mortar was then calculated based the number of the contacted aggregate particles in the mortar and the shear force carried by the rest of cement paste. The number of the contacted aggregate particles in the micro-unit volume of mortar was estimated based on the probability concept. In order to verify the validity of the newly developed model, 47 fresh mortar mixtures made with different water-to-cement ratios (w/c), sand-to-cement ratios (s/c), and different aggregate size and gradations were tested using a direct shear apparatus. The experimental results were compared with those obtained from the model. The study indicated that the newly developed shear failure stress model fits the data from the direct shear tests very well. Both the model and experimental results revealed that the shear failure behavior of mortar follows the Mohr-Coulomb equation. The internal friction angle (ϕ_M) and cohesion (C_M) obtained from the Mohr-Coulomb curves of mortar decrease with the interparticle distance (S), which is in turn associated with the aggregate size, gradation, voids, and volume fraction. The research results provide researchers and engineers an insight onto proportioning of workable mortar and concrete mixtures.

Finally, a particle-fluid model was developed for predicting the relationship between the shear stress and shear strain rate of highly flowable mortars. In this model, mortars was considered as a two-phase material, containing a fluid matrix (cement paste) and a group

of well-graded, non-cohesive, and rigid particles (fine aggregate) that were uniformly distributed in the matrix. The mortar shear stress was assumed to be the sum of the shear stresses resulting from the paste flow, the aggregate particle movement, and the interaction between the cement paste and aggregate. The shear stress resulting from the paste flow was assessed using constitutive equations. The shear stress resulting from the aggregate particle movement was evaluated based on the probability and mechanical concepts of aggregate particle collision. The shear stress resulting from the interaction between the paste and aggregate was considered as the normal stress that the moving aggregate particles apply onto the cement paste. The shear rate of the mortar was obtained from the rheological definition of viscosity. Using this model, the effects of mortar mixture properties (such as aggregate size, volume, gradation, and friction as well as paste viscosity and yield stress) on mortar rheology were studied.

CHAPTER 1. GENERAL INTRODUCTION

Background

Concrete has been the most versatile construction material. Since first appearance hundreds of years ago, many developments have been accomplished to improve its quality and reliability. Fresh concrete properties, principally workability, significantly affect transporting, placing, and compacting; therefore, these properties have significant effects on the quality and cost of concrete construction. They also potentially determine certain hardened concrete properties, such as strength and durability.

Based on the American Concrete Institute (ACI) [1], the workability is defined as "the property of freshly mixed concrete or mortar that determines the ease with which it can be mixed, placed, consolidated, and finished to a homogenous condition". In order to obtain desirable workability, concrete must have proper flowability, or rheology, which is a quantitative property that describes concrete deformation and flow. The importance of studying concrete rheological behavior has been known for many years, since the ease of flow and placement can significantly reduce costs and allow more flexibility in architectural and structural design. The experimental studies of the effects of mix components and proportions on concrete rheology have been widely conducted worldwide. However, the theoretical explanations for the rheological behavior of fresh concrete are still very limited.

Moreover, self-compacting concrete (SCC) has generated tremendous industrial interest since its initial introduction in Japan in 1990. The combination of high fluidity and segregation resistance makes it superior in construction due to reduced labor costs and improved quality control [2]. However, the development of SCC is still a trial-and-error process with little insight gained into the mechanisms that control the self-consolidating properties. The continued development of SCC also requires a fundamental understanding of the rheology of cement-based materials. As reported by Larrard and co-workers [3], the Herschel-Bulkley (HB) model is more suitable than the other rheology models for SCC. Following the model, $\tau = \tau_0' + a \cdot \dot{\gamma}^b$, where τ_0' is yield stress, $\dot{\gamma}$ is the shear strain rate, a and b are concrete parameters. This finding indicated that to obtain a new applicable rheology model for SCC with profound investigation of flow mechanism of SCC is necessary.

As been discussed, yield stress and shear stress are two basic physical properties in concrete rheology. The former one is the minimum shear stress that material is required to be applied to transfer from solid to flowing state. And later one is the shear stress that is needed to keep the material flow. Since concrete and mortar are composite materials with rigid aggregate and cement particles dispersing in water, their shear behaviors are similar. Thus, only mortar was modeled in this study.

The cohesion between cement particles, the friction between aggregate particles at both solid and flowing state of mortar, and the interparticle collisions during the flowing of materials are components of the shear stress of mortar. When studying the interparticle

collisions, the friction coefficient of the aggregate particles is required instead of the friction angle, which is handy and widely used in geotechnical engineering and material engineering. Meantime, the origin mechanism of the shear behavior of granular materials is still fully understood. Thus, at very beginning a theoretical study on the direct shear behavior of granular materials was developed.

Secondly, since the cement paste is the only cohesion matrix material in mortar/concrete, it controls the yield behavior of concrete/mortar. Further more, cement paste also contributes shear stress to mortar/concrete during flow since it is nun-Newtonian fluid with viscosity. Hence, the origin mechanisms of yield stress of cement paste and mortar were studied.

Finally, the shear stress required to maintain the flow was modeled by combing the shear stress generated from different phases in mortar (shear stress from cement paste, interaction between cement paste and aggregate particles, and interaction between particles due to collision).

Thus, the rheological modeling of mortar was finished with one model to explain the shear behavior of granular material, two models to predict the yield stresses of cement paste and mortar, respectively, and one model to predict the shear stress required to maintain the mortar flow, which is equal to the sum of the mortar yield stress and shear stress due to the flowing.

Objectives

The objectives of the present research are to:

1. To establish a theoretical formula to predict the internal friction angle of granular particles from the friction coefficient of material;
2. To quantitatively study material property effects on the internal friction angle of granular particles at static state;
3. To theoretically investigate the mechanism of the origin of the shear stress generated by fresh cement paste at static state;
4. To theoretically investigate the mechanism of the origin of the shear stress generated by fresh mortar at static state;
5. To quantitatively study material property effects on the origin of the shear stress generated by fresh mortar at static state;
6. To theoretically investigate the mechanism of the origin of the shear stress generated by fresh mortar at flowing state; and
7. To quantitatively study material property effects on the origin of the shear stress generated by fresh mortar at flowing state.

Research approach

In order to ensure successful models, the overall research strategy schematically outlined below in Figure 1 was used in present research.

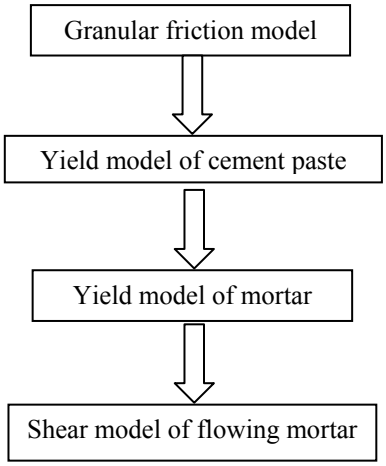

Figure 1. Flowchart of rheology model development

A mathematical model was first developed to predict the direct shear stress of granular particles in bulk condition. Results of this model were going to be used in modeling the yield stress and shear stress of solid and flowing mortar, respectively.

The DLVO theory was investigated to model the yield stress of cement paste, which is the non-Newtonian matrix fluid in mortar. After considering the friction of aggregate particles dispersing in cement paste, the yield stress of mortar was modeled.

Finally, in consideration of the aggregate particle collisions in flowing cement paste as well as the interaction between aggregate particles and cement paste, the total shear stress of a flowing mortar was calculated as the summary of the yield stress of cement paste, the interaction between aggregate particles and surrounding cement paste, and the shear stress from the aggregate particle collisions. The probability concept was employed to calculate the numbers of particle collisions occurring in the mortar.

Dissertation Organization

The dissertation contains seven chapters. The brief description of each chapter is presented in the following:

Chapter 1 is an introduction, which gives the background, objectives, and strategy of this study. The organization of this dissertation is also provided in this chapter.

Chapter 2 contains a literature review, which serves to provide the necessary background and terminology on concrete rheology. The utilization of two different equipments for cementitious material rheology is summarized. The factors that influence concrete rheology are reviewed. This section also provides a summary of current models to predict concrete rheology.

In Chapter 3, a theoretical model for prediction of the direct shear stress of a granular material (such as fine and coarse aggregate particles in concrete) is developed. Different granular materials, such as glass and steel ball, river sands, limestone and gravel particles, are also tested with a small and large dimension direct shear box.

In Chapter 4, the theoretical investigation of the origin of the yield stress of cement paste is investigated. The results of the cement paste rheology study, from both direct shear and rheometer tests, are presented as well as the previous results from rheometer tests by other researchers to verify the theoretical model for prediction of the yield stress of cement paste.

In Chapter 5, the theoretical investigation of the origin of the shear stress of mortar at static state is modeled. The results of the mortars shear stress from direct shear tests are also presented. The effects of the mortar material properties, such as aggregate property and cement paste property were studied. The newly developed model prediction of the shear stress of mortar is verified by these experimental results.

In Chapter 6, the theoretical investigation of the origin of the shear stress of mortar at flowing state is described. The predicted trends of material property effects on fresh mortar flow behavior are studied and compared with the published results on material effects on fresh mortar rheology.

Finally, Chapter 7 provides a summary of this research. It offers overall conclusions from this study and provides recommendations for future research.

References

[1] ACI Committee 116, (2000). "*Cement and concrete terminology*", ACI 116R-00, ACI Manual of Concrete Practice, Detroit, MI

[2] Okamura H, Ouchi M. Self-Compacting Concrete, Journal of Advanced Concrete Technology 2003; 1(1): 5-15

[3] Larrard D, Ferraris CF, Sedan T. Fresh concrete: A Herschel-Bulkley material. Material and Structures 1998; 31(211): 494-498

[4] Bird RB, Dai GC, Yarusso BJ. The rheology and flow of viscoplastic materials. Rev Chem Eng 1983; 1: 1-70

CHAPTER 2. LITERATURE REVIEW

In recent years, the research on fresh concrete rheology has been very active in the pursuit of highly reliable material. Many fruitful outcomes of such investigations are certainly useful in concrete industry as well as the mathematical modeling which will be presented in this desertion. Consequently the brief review of them would provide great value as references and the basic understanding. In this chapter, a through literature review on the rheology of cement-based materials, including cement paste, mortar, and concrete is included.

Introduction to Concrete Rheology

Rheology is the science of the deformation and flow of a matter, and the emphasis on flow means that it is concerned with the relationships between stress, strain, rate of strain, and time. Cementitous materials, such as cement paste, mortar and concrete, in their fresh state can be considered as a fluid, and therefore the basic principles of rheology can be applied to this material [1].

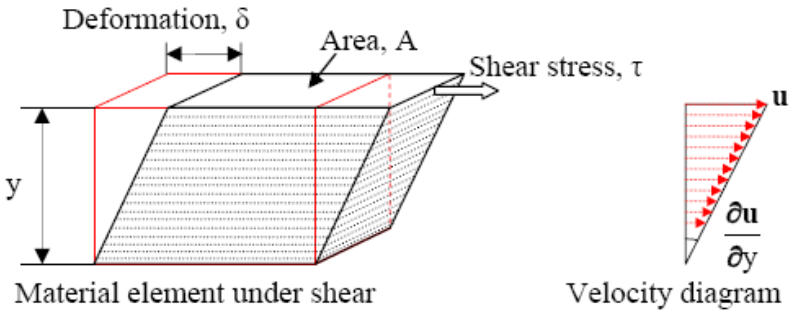

Figure 1. Material element under shear

As shown in Figure 1, flow is concerned with the relative movement of adjacent elements of liquid and in shear flows liquid elements flow over or past each other, while in extensional flows elements flow towards or away from each other. In a simple laminar flow, parallel layers of liquid move in response to a shear stress to produce a velocity gradient, $\frac{\partial u}{\partial y}$, which is referred to as the shear rate, equivalent to the rate of increase of shear strain. These gave the microscopic definition of the shear stress, as below:

$$\tau = \eta \cdot \dot{\gamma} \tag{1}$$

where τ is the shear stress, η is the microscopic viscosity and $\dot{\gamma}$ is the shear rate.

Equation 1 gives shear stress for both solid-like (elastic) and liquid-like (viscous) behavior for a particular material depending on the ratio between relaxation and experimental measurement time [1].

Clearly, cement-based materials are able to stand unsupported without flowing under their own gravity and during setting they develop strength and stiffness. Struble and de Larrard [2] found that concentrated suspensions such as concrete processes yield stress. Even the very high flowable concrete, such as self-compacting concrete, has some initial strength to resist flow. Tattersall and Banfill carried out systematic investigations in the rheology of concrete [3]. They found that there was a linear relationship between torque and the rotation speed of the viscometer after a certain torque had been exceeded. Thus, they stated that the simplest analysis involving concrete flow behavior, which was modified from Equation 1, is that of the Bingham model:

$$\tau = \tau_0 + \eta \cdot \dot{\gamma} \tag{2}$$

where the material is an elastic solid at shear stress $\tau < \tau_0$, which is the yield stress of material; but flows at higher stresses. The yield stress is a consequence of the interparticle forces, but these links are often broken irreversibly by shear and the measured shear stress is found to depend on time and previous shear history as well as on shear rate [1]. Figure 2 shows a typical curve for Bingham model.

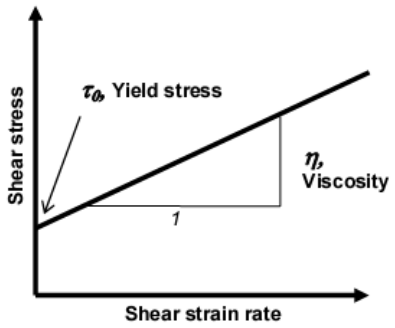

Figure 2. Bingham flow curve

Following Tattersall and Banfill's work, a great deal of research has been conducted to study the flow behavior of cement-based materials. Figure 3 shows the most commonly used types of curves that express the stress and shear rate relationship of cement-based materials.

As shown in this figure, a Bingham material needs to overcome the yield stress to initial flow, and its plastic viscosity is constant. In a shear thickening material, viscosity increases continuously with shear rate, while viscosity decreases continuously with shear rate. In the material having shear thinning with yield stress, viscosity decreases with shear rate once the yield stress has been exceeded.

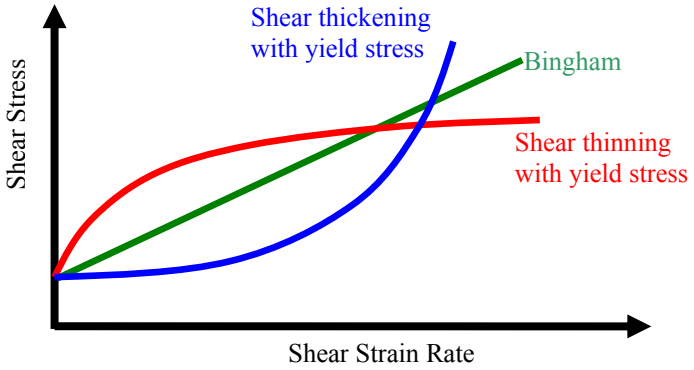

Figure 3. Common used flow curves [4]

These flow curves can be described with various relationships between shear stress and shear rate as summarized in Table 2-1. The Power equation can be used to describe shear thinning (n<1) or shear thickening (n>1) behavior. The Herschel-Bulkley equation can be used for the case of shear thinning or shear thickening with yield stress.

In all these equations, the yield stress and viscosity have a physical basis, while other terms such as "n", "K" have no exact physical meanings, which are always from the curve fittings as the constants for tested cement-based materials [6, 7, and 9].

Table 1. Equations relating shear stress and shear rate

Model	Equation	Reference
Bingham	$\tau = \tau_0 + \eta\dot{\gamma}$	[5] and [6]
Herschel-Bulkley	$\tau = \tau_0 + K\dot{\gamma}^n$	[5], [6], and [7]
Modified Bingham	$\tau = \tau_0 + \eta\dot{\gamma}^{n_1} + \eta\dot{\gamma}^{n_2}$ and $\tau = \tau_0 + \eta\dot{\gamma} + \eta\dot{\gamma}^2$	[5], and [6]
Papo-Piani	$\tau = \tau_0 + \eta_\infty\dot{\gamma} + K\dot{\gamma}^n$	[8]

Variable definitions:
τ=shear stress, $\dot{\gamma}$=shear rate, τ_0=yield stress, η=viscosity
n, n_1, n_2, and K=constants

Different models may only suitable for certain range of material or measurement. Some

researchers stated that the Herschel-Bulkley model is more suitable than the Bingham model for certain concretes like SCC [4]. Atzeni et al. compared the rheological properties of Portland cement pastes using different mathematical models; and he found that the best results were obtained with Herschel-Bulkley's equation [9]. However, fresh concrete, including cement paste and mortar, is most commonly described using the Bingham model because the flow of most concrete follows this equation fairly well and the two parameters in Bingham model; yield stress and viscosity, can be measured independently [3].

Various factors may affect the shape of the flow curve of cementitious materials, including testing equipment, testing time, experiment duration and procedure [10, 11, and 12]. The shear thickening phenomenon can also occur simultaneously with shear thinning [13]. When more networks in the material are destroyed, the shear resistance between the flow layers of the material is lower. Thus, the apparent viscosity decreases and shear thinning behavior is observed.

Factors Affecting Concrete Rheology

Concrete rheology is affected by all of the components of concrete and essentially every condition under which concrete is made and tested, including the material properties including the water amount, the cement properties and the amount, mineral and chemical admixture type and amount, and the degree of hydration, properties and proportion of fine and coarse aggregates, temperature, mixing time and method. Since fresh concrete is the dispersion of rigid solid particles in matrix fluid---cement paste, all

these issues can be logically divided into three categories, and they are:

1. Matrix material property --- cement paste properties

The matrix material in mortar and concrete is cement paste, which is the dispersion of cement particles in water. Thus, the water content and cement characteristics and content are two key issues in discussion of the matrix material properties.

Water content is the most important factor governing the rheology of concrete by changing the rheological properties of matrix fluid, cement paste. Increasing the water content while keeping the proportions of the other constituents constant will decrease yield stress and viscosity of the matrix material as well as the concrete. But sometimes increased yield stress and viscosity of cement paste may lead to segregation and to bleeding. Since the rheology of cement paste is an important indicateor of concrete rheology, and due to the equipment limitation, most research focuses on the effect of water content on rheology of cement, rather than concrete [14, 15]. Jones and Taylor showed an empirical equation that related the flow curves of a cement paste to its w/c [16]. Banfill summarized previous results and showed that the increase of water content would result in higher slump and less Vebe time [17].

The physical and chemical properties of cements are correlated to the rheological properties of cement pastes too. Vom Berg studied the influence of specific surface area (SSA) and concentration of solids on the flow behavior of cement pastes [13]. He found that the yield stress and plastic viscosity of cement paste increased as the cement

fineness or the solids concentration increased, which reflects the dominance of the water cement interface in this system. The fineness of cement particles controls the balance of attractive and repulsive force between cement particles, which has a profound impact on the flow of concrete. At a given water content, low cement content tends to produce harsh mixtures with poor workability, while high cement content produces better cohesiveness.

2. Properties of dispersing solid particles

The effect of various properties of aggregate will be described in this section into three main categories and they are aggregate volume fraction, particle size distribution and particle shape and surface texture.

- Aggregate volume fraction

The amount of aggregate and the relative proportions of fine and coarse aggregate are two factors that significantly affect the concrete rheology. The increase in the fine aggregate/coarse aggregate ratio generally increases the water content required for a given workability. For a given w/c, increasing the aggregate/cement ratio generally results in decrease of workability; furthermore, more cement is needed when finer aggregate grading is used. The greater portion of fine aggregate the particles and to fill the interstitial spaces between particles. An excess of fine aggregate will result in a somewhat more permeable and less economical concrete, and the potential of drying shrinkage of hardened concrete will also increase although the mix is more workable. Alternatively, an increase in the relative coarse aggregate proportion will initially lead to a more workable, stronger, and cheaper concrete. However, there is an optimum coarse

aggregate amount in considering workability. An excessively high amount of coarse aggregate results in a mix that is harsh, which means it is prone to segregation and difficult to finish. This will eventually lead to a weaker and less durable hardened concrete [18]. Small aggregate particles in concrete provide larger surface area and require a higher quantity of cement paste to coat all of aggregate particles.

Denis et al. studied the effect of coarse aggregate on the workability of sandcrete with two different mortar matrixes [19]. The results confirmed the significant effect of coarse aggregate concentration on workability. Results from Geiker et al. showed that the relative yield stress and relative viscosity, which were defined as the rheological parameters of concrete divided by the parameters of mortar, both significantly increased with the increase of coarse aggregate volume fraction, no matter what type of aggregate was used (Figure 4) [20].

- Particle size distribution

The particle size distribution, or gradation, of an aggregate is one of the most influential aggregate characteristics in determining how the concrete will perform as a pavement material. Gradation and the maximum size of aggregate in PCC affects the mix design as well as durability, porosity, workability, cement and water requirements, strength and shrinkage and durability of PCC. In order to obtain the proper workability of concrete, a certain amount of cement paste will be required to fill up the space between aggregate, hence the gradation and size of aggregate will significantly affect the workability of concrete. Very fine sand or very coarse aggregate cannot produce the most satisfactory

result. Aggregate that does not have a large deficiency or excess of any size and has a smooth grading curve is required to produce satisfactory and economical concrete [18].

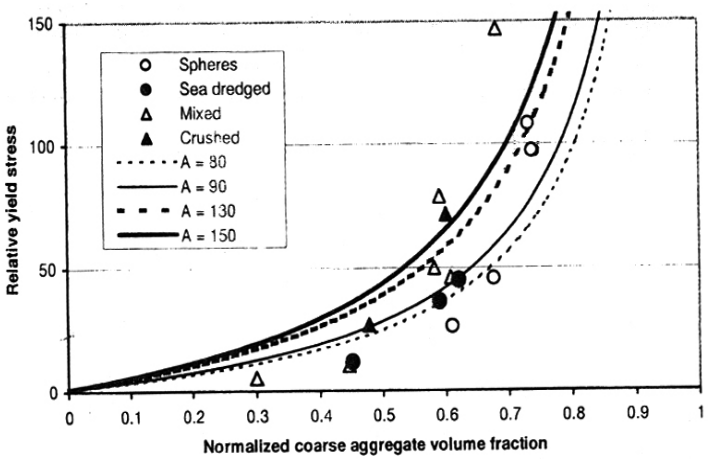

(a) Relative yield stress

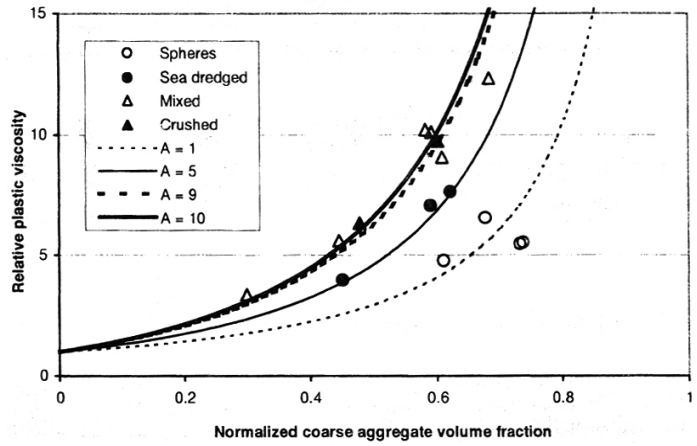

(b) Relative viscosity

Figure 4. Relative rheological parameters of concretes varying in amount and type of coarse aggregates [20]

Aggregates by themselves can display different levels of "compactability", depending on the grading and the method of compaction used. A term of "coarse aggregate factor" is used to describe the compaction degree of coarse aggregate gradation, which is defined as the ratio of the amount of coarse aggregate in a unit volume of concrete to the

amount of the same coarse aggregate compacted by the standard dry-rodding procedure into a mold of the same unit volume. This factor might be considered as the percent of maximum compacted density of the coarse aggregate in the concrete. Nichols found that the coarse aggregate factors are lower when the coarse aggregates size becomes smaller. As a result, decreasing maximum particle size normally requires an increase in the total fine aggregate content and a corresponding increase in water demand [21].

If a finer aggregate is substituted in a mixture, the water content typically must be increased to maintain the same workability because finer aggregate grading requires more cement to coat the particles. Mehta and Monteiro reported the approximate mixing water and air content requirements for different slumps and nominal maximum sizes of aggregates [22]. With the increase of aggregate size, the water demand for same slump decreases.

Graded aggregate offers a noticeable improvement in ability to fill the space between particles, so that an optimized aggregate blend results in a higher degree of packing and therefore requires lower amounts of paste. Research indicated that there is an optimum aggregate gradation that can produce the most effective w/c and highest strength. The optimum gradation should have the lowest possible surface area and void content per unit weight [23]. The grading of fine and coarse aggregate that is suitable for manufacture of ordinary concrete is specified by a national standard (ASTM C33). The purpose of setting up these limits on grading is to get close to the optimum grading for economical concrete mixes in general construction practice.

- Particle shape and surface texture

Aggregate composed of spherical shapes with smooth surface textures is generally considered to be good for the workability of concrete. Rounded particles create lower degrees of particle-to-particle interlock than angular particles and thus provide better workability. Particles with smoother surfaces have a lower surface-to-volume ratio than rough surfaced particles and thus may be easier to coat with binder. Particles with rougher surfaces provide more area to which the cement paste can bond, which requires more sand, cement and water to provide adequate workability. However, the requirement for workability does not match the requirement of concrete strength. Angular, irregular shapes with rough surface texture aggregate have greater surface area for bonding with cement paste and have better interlock between aggregate particles which creates stronger concrete.

Malhotra studied the correlation between the particle shape and surface texture of fine aggregates and their water requirement [24]. Research showed that crushed sands tend to have a higher water requirement than natural sands because of the higher angularity and differences in surface texture. Angular fine aggregate particles interlock and reduce the freedom of movement of particles in the fresh concrete. As a result, using angular fine aggregate (e.g., manufactured sand) increases the amount of fine aggregate that must be used for a given amount of coarse aggregate and generally requires that more water be added to achieve the workability obtained with rounded sand. Kosmatka et al. confirmed that the workability of fresh concrete and the bond between cement paste and a given aggregate is affected by particle shape and surface texture [25]. It was found that water

content must be increased to maintain workability if angular aggregate is substituted for rounded aggregate. Crushed aggregates having numerous flat or elongated particles will produce less workable concrete that requires higher mortar content and possibly higher paste content. Quiroga and Fowler systematically studied the effect of aggregates characteristics on the performance of PCC [26]. Their research confirmed that aggregates blended with well-shaped, rounded, and smooth particles require less paste for a given slump than those blended with flat, elongated, angular, and rough particles.

As shown previously in Figure 4, Geiker et al. used aggregates with different aspect ratios (*A*) to study the effect of fraction and shape of coarse aggregate on the rheology of concrete [20]. The investigation indicated that the aspect ratio, angularity, and surface texture of aggregates affect the viscosity and yield stress differently, round and smaller aggregates results in lower rheological parameters.

3. Other factors

The flowability of concrete can be significantly changed by using different kinds of aggregate [22]. The particle size of aggregate influences the water requirement for a given slump of concrete. Very fine sands will require more water for a given consistency; on the other hand, they will produce harsh and unworkable concrete compared to coarser sands at same water content. The shape and texture of aggregate particles can also affect the rheology. Generally, the more nearly spherical the particles, the more workable the resulting concrete will be. The gradation and fine-to-coarse aggregate ratio will also provide concrete with different rheology.

Besides all issues discussed previously, there are some other factors that can affect fresh concrete rheology, such as porosity of aggregates, impurities in aggregates, and density of aggregates. The porosity of aggregates and impurities can change the rheology properties of cement paste greatly. Absorption of mixing water causes a change of water content in cement paste, which increases the yield stress and viscosity. The amount of limestone dust or quarry dust in an aggregate was also found to have significant effects on concrete workability. Celik and Marar reported that the slump and air content of fresh concrete decreased as the percentage of dust content increased [27]. Ho et al. stated that mixes with quarry dust required a higher dosage of superplasticizer to achieve similar flow properties due to its shape and particle size distribution [28]. Research also indicated that finer and better graded limestone dust significantly increases the deformability of the paste [29].

Since the aggregate particles are dispersing in cement paste, the density of aggregate also affects the rheology properties of fresh concrete. Low density aggregate tends to float in the fresh mix and rise to the surface. As a result, high workability mixes with light weight aggregate will segregate more easily than normal mixes of the same workability. On the other hand, the use of high density aggregate also increases the potential of segregation.

Modeling of Concrete Rheology

Studies on the rheology of fresh concrete, especially from a materials science approach, have been conducted worldwide for a decade. Previously, it was considered adequate to

use an engineering approach for characterizing rheological properties, consisting of subjecting a concrete sample to a more-or-less controlled loading and deriving and index, such as slump, flow time, compacting factor, to classify the mixtures in terms of workability. This approach is limited as the classifications obtained by using different tests vary substantially [4].

Tattersall proposed using an instrumented mixer to obtain a more complete characterization of the flow characteristics of fresh concrete [30]. He proposed describing the behavior of fresh concrete using the Bingham model, see Equation 2. The last two quantities in Equation 2 (the Bingham parameters, τ_0 and μ) characterize the flow properties of the material. However, in Tattersall's apparatus, the velocity field is unknown and complex due to the lack of symmetry. Therefore, he limited himself to an empirical description of the material's behavior, by using the relationship between the torque and the rotation speed of the mixing blades.

Following Tattersall, different approaches have been conducted to relate Bingham parameters to concrete material properties. All these empirical and semi-empirical rheological models can be summarized as: 1) Empirical model [31]; 2) Volume friction model [32]; 3) Maximum packing density model [33]; 4) Two-phase theory [34, 35]; 5) Gap and aggregate spacing theory [19, 36]; and 6) Excess paste theory [37, 38, and 39]. As an efficient tool, finite element methods were adopted to simulate the deformation of fresh concrete [40].

Topcu and Kocataskin proposed a model to establish basic composition-property relations for fresh concrete, using the two-phase composite materials approach and the law of plastic viscosity [34]. Kurokawa and co-workers developed a model of concrete rheology based on the two-phase theory approach [35]. They stated that the yield stress of fresh concrete could be expressed by the sum of the yield values of matrix mortar and the contribution from the friction of coarse aggregate. The viscosity can be expressed by the sum of viscosities of the matrix mortar and that of the volume fraction and friction of coarse aggregate. Kennedy stated that the rheology of concrete depends on not only the rheology of cement paste, but also on the amount of excess paste to fill the voids between the aggregate [37]. Kennedy's theory indicated that in addition to the paste that fills up the space between aggregate, an excess paste will be required maintaining the flow. Su and his colleagues developed a design method for SCC according to this theory [39]. Oh and co-workers found that when the thickness of excess paste increased, both the yield stress and viscosity of concrete decreased [38]. Base on this phenomenon, an excess paste theory was developed by using model concrete with polymer as paste and artificial plastic beads as fine and coarse aggregate. The related excess paste thickness, which can be defined by the excess paste thickness divided by the average diameter of aggregate, was found to be directly related to the relative viscosity and yield stress of concrete, and the relationship was shown to be independent to the mix proportion of concrete. By trading fresh concrete as a multiphase material, Pimanmas and Ozawa developed a mathematical model to predict the flow of fresh concrete based on the energy conservation concept [41]. They studied the shear stress transfer mechanism of fresh concrete and concluded that the overall shear stress is the sum of the shear stress generated by different phases

and the interaction between them. From their works, a more systematic and comprehensive models were developed based on collision and flow mechanics. However, the consideration of gap and aggregate spacing, were missed in their approach as well as a reasonable probabilistic model to predict the number of collision of aggregate particles. According to the review from previous research, paste property, particle friction between aggregate, solid particle volume frictions, the inter-particle distance, are all important factors that should be considered in the concrete rheology model. A new microscopic approach will be developed in the present study, which will be based on the inter friction and collision of aggregate particles and interaction between aggregate particles and surrounding matrix material by considering concrete as two-phase of mortar and coarse aggregate.

Test Methods Related to Concrete Rheology

The choosing of suitable rheology measurement methods is important, because the success of a concrete rheology model in a large degree depends upon whether the test methods can completely and accurately reflect the rheology performance of concrete. A large number of workability tests have been proposed over the years since the early 20th century. Detailed information on the available 61 different test methods for measuring the concrete workability has been summarized and discussed thoroughly [42]. The complete comparison of concrete rheometers is also available from Ferraris and Brower's report [43]. Hence, only the rheology measurement methods directly related to this study will be discussed in this part. These methods include the vane shear rheometer test and direct shear box test.

1. Vane rheometer

Rotating vane rheometer is one of the most popular and important rheometer in concrete rheology due to the fully understood mechanism of the measurement of shear stress and viscosity and the relatively low cost.

Generally, the vane has 4 or 6 blades extending outward from the shaft at equal angles (Figure 5 shows a 4 blades vane). The vane is rotate at certain angular speed of less than 10 rpm and the torque acting on the vane is recorded [44, 45]. As the vane rotates, the torque increases until it reaches a maximum, corresponding to the yield point, then decays to steady state. The great advantage of the vane method is that slip is eliminated since shearing occurs completely within the material along the localized surface circumscribed by the vane [45]. Another advantage is that insertion of the vane results in much less disruption of the material in comparison to concentric cylinders. This is particularly advantageous due to the irreversible structural breakdown and thixotropy associated with shearing cement paste [3].

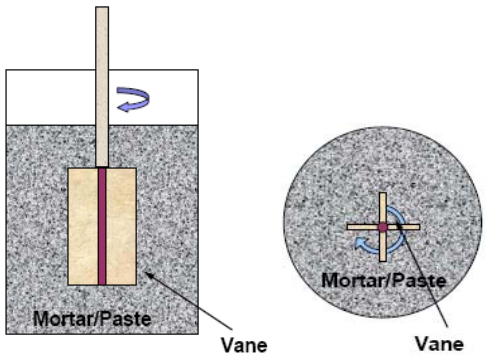

Figure 5. Schematic of vanes for vane rheometer

The torque on the vane surface is calculated by replacing the vane with a cylinder of equal dimensions (Figure 6). The shearing force is distributed uniformly over the entire cylindrical surface is assumed [45]. The torque is given by:

$$T = 2\pi r_v^2 H\tau_c + 4\pi\int_0^{r_v} \tau_r r^2 dr \tag{3}$$

where T is the torque, r_v is the radius of the vane, H is the height of the vane, τ_c is the shear stress at the radius of the vane, τ_e is the shear stress at the top and bottom surfaces of the vane, and r is the radial distance from the center of the vane. Assuming that the stress is uniformly distributed along the top and bottom surfaces and τ_e equals τ_c when r equals r_v, then Equation 3 reduces to:

$$T = 2\pi r_v^2 \tau_c \left(\frac{H}{r_v} + \frac{2}{3}\right) \tag{4}$$

Keentok et al. modeled the shearing surface around a vane in two dimensions using a finite element method [46]. The results from the model agreed with their experimental data, showing that shearing occurs along the cylinder circumscribed by the vane. The model also predicts stress concentrations at the blade tips. Christensen also confirmed that the yield surface existed along the circumference of the vane according to the finite element modeling [47]. However, the results suggest that the yielding zone is much smaller than Keentok's model predicts.

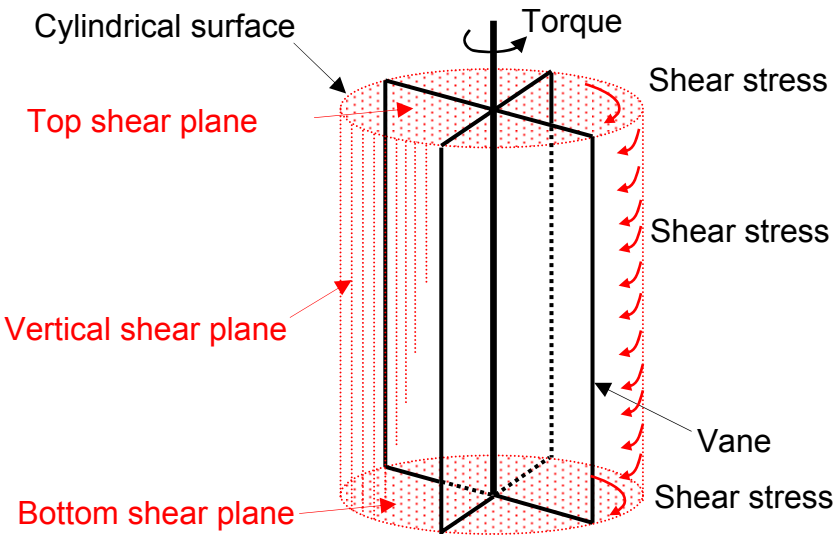

Figure 6. Shear surface of material in vane rheometer

The vane method has become a popular technique for evaluating the yield stress of suspensions, emulsions, and pastes [46, 48, and 49]. Hainoni and Hannant measured the yield stress of cement paste using a vane and found it to be greater than twice the value measured using smooth-walled concentric cylinders [50]. They also found the yield stress to be dependent on the rotational speed of the vane. Banfill and Kitching also reported a large difference in yield stress between vane and parallel plate measurements of cement paste, attributing the differences to slip [51].

Although the vane method has been widely used in testing the yield stress of cement paste, the shear rate is not calculable due to the unknown shearing pattern and the unknown thickness of the sheared layer. Barnes and Carnali suggested that the vane could be used in place of the inner concentric cylinder when measuring the viscosity of highly shear-thinning materials [52]. In this study, the authors used the shear rate values directly

output from the machine, which is obtained from multiplying the rotation speed of the vane with a calibrate constant.

2. Direct shear test

The direct shear test used for soil was suggested to be performed with fresh concrete to assess the cohesive strength of a concrete mixture. The results of the test are given in terms of soil mechanics parameters, not in terms of yield stress and plastic viscosity.

The device consists of a ring or square shapes container filled with compacted material sample. The lower half of the device is held in a fixed position while the upper half of the device is moved slowly, resulting in a maximum shear stress on the plane between the two halves of the container. A vertical load can be applied to the concrete during test. The test measures the displacement of the upper container and the corresponding load required to move the container (Figure 7).

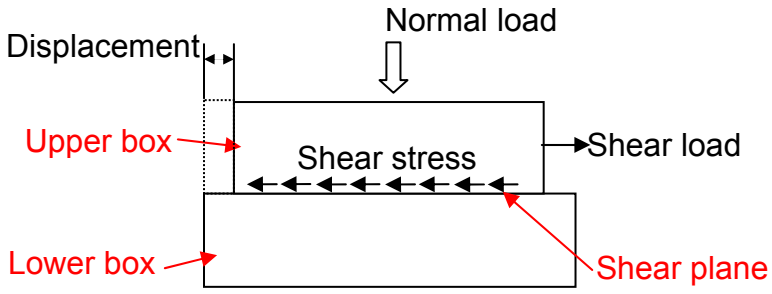

Figure 7. Schematic of direct shear test

A typical plot of load versus relative displacement shows an initial increase in load up to a maximum value and then a decline followed by a gradual leveling off of the curve. The maximum stress is considered the “static friction” and the stress after the plot has leveled

off is considered the “sliding friction”. The liner relationship between static friction and normal stress allows the calculation of the angle of internal friction. The test essentially determines the yield stress of the concrete.

From previous discussions on both vane rheometer and direct shear test, the basic measurements of the yield stress of concentrated material such as cement paste and mortar are theoretically similar. The only different is the number of shear plane. Furthermore, the vane rheometer is able to perform a wide range of loading rate from low to high, while the loading rate of the direct shear test is limited to very low to ensure the static state condition.

Summary

Concrete rheology is the science of deformation and flow of matter, and can be used as a tool to quantitatively study the workability of concrete. However, due to the complications of concrete composition and the limitation of measuring equipment, the study of concrete rheology is still very limit.

Yield stress and viscosity are normally used to describe concrete rheology. Currently, different rheology equations using these two rheological parameters are only determined from the rheology test of concrete mixtures. Obviously, the results are affected by almost all parameters, such as testing methods, environmental condition, and material properties. These rheological parameters of concrete are also decided by different factors, such as mixture components including water, cement, chemical and mineral admixtures, and the

mixing and environmental conditions. However, studying this factor is restricted by the measurement and characterization of aggregate. Even though the experimental studies have been widely performed, a theoretical study of the origin mechanism of the yield stress and viscosity is still missing. Thus, a theoretical study to model the concrete rheology is in need.

A variety of test methods can be used to study concrete rheology. With the progress of modern techniques, more equipment has been developed for measuring concrete workability. Rotational rheometer are found to be a promising tool to study concrete rheology, which can be used to learn both rheological parameters directly by analyzing the shear stress versus shear rate relation in concrete flow curve. The vane rheometer and direct shear tests give same yield stress of tested material. Thus, to compare the results from these two test methods is possible.

References

[1] Banfill, P. F. G., (2003). "The rheology of fresh cement and concrete – A review", *Proc 11th International Cement Chemistry Congress, May 2003, Durban*

[2] Struble, L. J.; Szecsy, R.; Lei, W.; and Sun, G., (1998). "Rheology of cement paste and concrete", *Cement, Concrete, and Aggregate,* Vol. 20, No. 2, pp. 269-277

[3] Tattersall, G. H.; and Banfill, P. F. G., (1983). "*The rheology of fresh concrete*", Pitman Publishing Inc.

[4] Ferraris, C. F.; and de Larrard, F., (1998). "*Testing and modeling of fresh concrete rheology*", NISTIR 6094

[5] Ferraris, C. F., (1999). "Measurement of the rheological properties of high performance concrete: State of the art report", *Journal of Research of the National Institute of Standards and Technology*, Vol. 104, No. 5, pp. 461-477

[6] Nehdi, M.; and Rahman, M. A., (2004). "Estimating rheological properties of cement pastes using various rheological models for different test geometry, gap and surface friction", *Cement and Concrete Research,* Vol. 34, No. 11, pp. 1993-2007

[7] Papo, A., (1988). "Rheological models for cement pastes", *Materials and Structures*, Vol. 21, No. 121, pp. 41-46

[8] Papo, A.; and Piani, L., (2004b). "Effect of various superplasticizers on the rheological properties of Portland cement pastes", *Cement and Concrete Research*, Vol. 34, No. 11, pp. 2097-2101

[9] Atzeni, C.; Massidda, L.; and Sanna, U., (1985). "Comparison between rheological models for Portland cement pastes", *Cement and Concrete Research*, Vol. 15, No. 3, pp. 511-599

[10] Shaughnessy, R. III; and Clark, P. E., (1988). "The rheological behavior of fresh cement pastes", *Cement and Concrete Research*, Vol. 18, No. 3, pp. 327-341

[11] Banfill, P. F. G.; and Saunders, D. C., (1981). "On the viscometric examination of cement pastes", *Cement and Concrete Research*, Vol. 11, No. 3, pp.363-370

[12] Roy, D. M.; and Asaga, K., (1979). "Rheological properties of cement mixes: III The effects of mixing procedures on viscometric properties of mixes containing superplasticizer", *Cement and Concrete Research*, Vol. 9, No. 6, pp. 731-739

[13] Vom Berg, W., (1979). "Influence of specific surface and concentration of solids upon the flow behavior of cement pastes", *Magazine of Concrete Research*, Vol. 31, No. 109, pp. 211-216

[14] Rosquoet, F; Alexis, A.; Kjelidj, A.; and Phelipot, A., (2003). "Experimental study of cement grout: Rheological behavior and sedimentation", C*ement and Concrete Research*, Vol. 33, No. 5, pp. 713-722

[15] Svermova, L.; Sonebi, M.; and Bartos, P. J. M., (2003). "Influence of mix proportions on rheology of cement grouts containing limestone powder", *Cement and Concrete Composites,* Vol. 25, No. 7, pp. 737-749

[16] Jones, T. E. R.; and Taylor, S., (1977). "Mathematical model relating the flow curve of a cement paste to its water/cement ratio", *Magazine of Concrete Research*, Vol. 29, No. 101, pp. 207-212

[17] Banfill, P. F. G. (1994). "Rheological methods for assessing the flow properties of mortar and related materials", *Construction and Building Materials*, Vol. 8, No. 1, pp. 43-50

[18] Mindess, S.; Young, J. F.; and Darwin, D., (2003). "*Concrete*", 2nd ed., Prentice Hall

[19] Denis, A.; Attar, A.; Breysse, D.; and Chauvin, J. J., (2002). "Effect of coarse aggregate on the workability of sandcrete", *Cement and Concrete Research,* Vol. 32, No. 5, pp. 701-706

[20] Geiker, M. R.; Brandl, M.; Thrane, L. N.; Bager, D. H.; and Wallevik, O., (2002a). "The effect of measuring procedure on the apparent rheological properties of self-compacting concrete", *Cement and Concrete Research*, Vol. 32, No. 11, pp. 1679-1850

[21] Nichols, F. P. Jr., (1982). "Manufactured sand and crushed stone in Portland cement concrete", *Concrete International: Design and Construction*, Vol. 4, No. 8, pp. 56-63

[22] Mehta, P. K.; and Monteiro, P. J. M., (1993). "*Concrete - structure, properties and materials*", 2nd ed., Prentice Hall

[23] Smith, M. R.; and Collis, L., (2001). "*Aggregates – sand, gravel and crushed rock aggregates for construction purposes"* 3rd ed., The Geological Society London

[24] Malhotra, V. M., (1964). "Correlation between particle shape and surface texture of fine aggregates and their water requirement", *Materials Research & Standard*, December, pp.656-658

[25] Kosmatka, S, H.; Kerkhoff, B.; and Panarese, W. C., (2002). "*Design and control of concrete mixture*", 14th ed., Portland Cement Association

[26] Quiroga, P. N.; and Fowler, D. W., (2004). "*The Effect of aggregates characteristics on the performance of Portland cement concrete*", ICAR Report 104-1F, International Center for Aggregates Research, The University of Texas at Austin

[27] Çelik, T.; and Marar, K., (1996). "Effects of crushed stone dust on some properties of concrete", *Cement and Concrete Research,* Vol. 26, No. 7, pp. 1121-1130

[28] Ho, D. W. S.; Sheinn, A. M. M.; Ng, C. C.; and Tam, C. T., (2002). "The use of quarry dust for SCC applications", *Cement and Concrete Research*, Vol. 32, No. 4, pp. 505-511

[29] Bosiljkov, V. B., (2003). "SCC mixes with poorly graded aggregate and high volume of limestone filler", *Cement and Concrete Research*, Vol. 33, No. 9, pp. 1279-1286

[30] Tattersall, G. H., (1991). "Workability and quality control of concrete", E & FN Spon

[31] Ouchi, M.; Edanarsu, Y.; Ozawa, K.; and Okamura, H., (1999). "Simple evaluation method for interaction between coarse aggregate and mortar's particles in self-compacting concrete", *Transactions of the Japan Concrete Institute*, Vol. 21, pp. 1-6

[32] Powers, T. C., (1968). "*The properties of fresh concrete*", John Wiley & Sons, Inc.

[33] De Larrard, F., (1999). "*Concrete mixture proportioning – A scientific approach*", E & FN Spon

[34] Topcu, I. B.; and Kocataskin, F., (1995). "A two-phase composite materials approach to the workability of concrete", *Cement and Concrete Composites*, Vol. 17, No. 4, pp. 319-325

[35] Kurokawa, Y.; Tanigawa, Y.; Mori, H.; and Nishinosono, K., (1996). "Analytical study on effect of volume fraction of coarse aggregate on Bingham's constants of fresh concrete", *Transactions of the Japan Concrete Institute*, Vol. 18, pp. 37-44

[36] Bui, V. K.; Akkaya, Y.; and Shah, S. P., (2002b). "Rheological model for self-consolidating concrete", *ACI Materials Journal*, Vol. 99, No. 6, pp. 549-559

[37] Kennedy, C.T., (1940). "The design of concrete mixes", *Proceedings of the American Concrete Institute*, Vol. 36, pp. 373-400

[38] Oh, S. G.; Noguchi, T.; and Tomosawa, F., (1999). "Toward mix design for rheology of self-compacting concrete", *RILEM International Symposium on Self-Compacting Concrete, 1999, University of Tokyo*

[39] Su, N.; Hsu, K.; and Chai, H., (2001). "A simple mix design method for self-compacting concrete", *Cement and Concrete Research*, Vol. 31, No. 12, pp. 1799-1807

[40] Mori, H.; and Tanigawa, Y., (1992). "Simulation methods for fluidity of fresh concrete", *Memoirs of the School of Engineering, Nagoya University,* Vol. 44, No. 1, pp. 71-134

[41] Pimanmas, A.; and Ozawa, K., (1996). "Mathematical modeling of shear constitutive relationship for flowing fresh concrete". In: Proceedings of ICUEACC, Bangkok, Thailand. p. D.128-D.133

[42] Koehler, E. P.; and Fowler, D. W., (2003). "*Summary of concrete workability test methods*", ICAR Report 105-1, International Center for Aggregates Research, The University of Texas at Austin

[43] Ferraris, C. F.; and Brower, L. E., (2001). "*Comparison of concrete rheometers: International tests at LCPC (Nantes, France) in October, 2000*", US Department of Commerce and National Institute of Standards and Technology

[44] Nguyen, Q. D.; and Boger, D. V., (1985). "Direct yield stress measurement with the vane method", *Journal of Rheology*, Vol. 29, No.3, pp.335-347

[45] Nguyen, Q. D.; and Boger, D. V., (1983). "Yield stress measurement for concentrated suspensions", *Journal of Rheology*, Vol. 27, No.4, pp.321-349

[46] Keentok, M.; Milthorpe, J. F.; and O'Donovan, E., (1985). "On the shearing zone around rotating vanes in plastic liquids: theory and experiment", *Journal of Non-Newtonian Fluid Mechanics*, Vol. 17, pp. 23-35

[47] Christensen, G., "*Modeling the flow of fresh concrete*," Ph.D. dissertation, Princeton University, 1991

[48] Yoshimura, A. S.; and Prud'Homme, R. K., (1987). "A comparison of techniques for measuring yield stresses", *Journal of Rheology*, Vol. 31, No.8, pp.699-710

[49] Alderman, N. J.; Meeten, G. H.; and Sherwood, J. D., (1991). "Vane rheometry of bentonite gels", *Journal of Non-Newtonian Fluid Mechanics*, Vol. 39, pp.291-310

[50] Haimoni, A.; and Hannant, D. J., (1998). "Developments in the shear vane test to measure the gel strength of oilwell cement slurry", *Advanced Cement Research*, Vol. 1, No. 4, pp.221-229

[51] Banfill, P. F. G.; Kitching, D. R., (1991). Use of a controlled stress rheometer to study the yield value of oilwell cement slurries, The rheology of fresh cement and concrete, Spon, pp.125−136

[52] Barnes, H. A.; and Carnali, J. O., (1990). "The vane-in-cup as a novel rheometer geometry for shear thinning and thixotropic materials", *Journal of Rheology*, Vol. 34, No.6, pp.841-866

CHAPTER 3. PREDICTING FRICTION OF GRANULAR MATERIALS USING 3-D PROBABILISTIC AND TWO-PARTICLE MODEL APPROACH

A paper submitted to ASCE International Journal in Civil Engineering Material

Gang Lu and Kejin Wang

Abstract

A 3-D probabilistic and two-particle contact model is developed for predicting the shear stress and volume change of a granular material under a direct shear. Lu added: The inter-friction force and volume change during particles shear were calculated based on the force balance and relative movement between two contact particles. The models show that the friction angle of coarse granular materials is dependent on surface properties of granular material, and independent on the size of and size distribution of granular material. Direct shear tests are conducted for various types of granular materials using a standard direct shear box and a modified (large-sized) direct shear box. The test results indicate that the peak friction angles are consistent with previously published experimental results, and they prove that the present models are rational and reliable.

Keywords: *Granular material; Friction angle; Angle of repose; Shear stress; Friction.*

Introduction

Granular materials are widely used in construction, mining, and agriculture. Friction of the granular materials, such as aggregates in concrete and subbases of an infrastructure, is an important property that controls the material strength and stability, or flowability.

Over 200 years ago, Coulomb (1773) described the yielding of granular materials as a frictional process, which follows the Mohr-Coulomb failure criterion [1]. Today, this failure criterion is still used in civil engineering foundation design. A great amount of experimental measurements have been conducted measuring friction of granular materials used for soil foundations and subbased. The experiments have revealed that the angle of the repose of the materials depends strongly on the shape and surface roughness of the grains or particles [2, 3, 4, and 5].

The granular materials are also used in concrete as aggregate. Research has demonstrated that aggregate shape and surface roughness strongly influence concrete workability and rheology [6, 7, 8, and 9]. However, there are no specific description and practical measurements for the overall shape and surface roughness of concrete aggregate. Thus, effects of these aggregate properties on concrete behavior become ambiguous. Very recently, the authors of this paper developed a microscopic model for rheology of fresh mortar and illustrated that the friction of aggregate has significant effect on fresh mortar rheology [10]. Evidently, using friction coefficient as a parameter to describe aggregate shape and surface roughness is of great significance in concrete research.

Although extensively studied, the flow behavior of granular materials observed from soil, foundation, and subbase, can not be directly applied to the study of aggregate in fresh mortar and concrete. This is because the behavior of granular materials depends not only on the properties of the individual particles but also on the properties of the bulk material: the boundary condition, arrangement of particles, particle size, etc. In a fresh mortar or

concrete, aggregate particles are not arrayed in the same way as those in soil, foundation and subbase. Even though the friction angle is directly correlated to its primary physical material friction, to use the bulk material friction angle measured for soil foundations to study fresh mortar and concrete flow behavior is not appropriate.

In the present study, a mathematic model is established for the behavior of granular materials under shear. This model includes two different approaches: 1) the force balance approach and 2) the deformation approach. Since the direct shear test of granular material is theoretically based on the force balance at static state, it should be considered as the first order consideration. Additionally, the shearing of granular materials is a kinetic process. During the shear of granular material, the relative displacement between particles will dissipate energy, and this is the second order consideration. This model is an attempt for an efficient and simple theoretical explanation on why the shear behavior of granular materials is independent on the particle size, size distribution, and only dependent on the material properties such as raw material, surface texture, and this is still not fully understood. Further more, the theoretical relationship between the individual material friction coefficient and global friction angle of the granular is studied. With these relationships, one may predict the friction coefficient of a granular material, which is very difficult to be accurately measured, from the friction angle, which can be easily measured.

Background

Friction of material

Friction is a force that acts on two surfaces in contact in the direction against a relative motion of an object. The friction force is classically known as Coulomb friction and expressed as:

$$f = \mu \cdot n \tag{1}$$

where μ is the coefficient of friction which is a dimensionless value and depending on the surface condition, n is the force normal to the contact surface and pressing the surface together, and f is the force exerted by friction, in the direction opposite the motion.

The coefficient of friction is generally measured experimentally. Rougher surfaces tend to have higher values. Most dry materials in combination give friction coefficient values from 0.3 to 0.6. To maintain values outside this range is difficult.

Friction angle of granular material

Figure 1 shows a typical experimental device for direct shear test. It consists of two open boxes with individual compartments shaped like a comb. The two boxes are filled with a granular medium and placed upside down on top of each other. A lateral shearing force F is applied to the upper box, which is also subjected to a vertical load N.

The shearing force required to set the upper half in lateral motion is strictly proportional to the load N and is independent of the surface area under shear.

$$F = N \cdot \tan\theta \tag{2}$$

where θ is defined as the friction angle of granular material in bulk state. It is correlated to the coefficient of friction of material of granular particles. Generally, the friction angle of bulk granular material and friction coefficient of material of particles cannot be

obtained at once. Previous experimental results indicate the bulk granular material friction angle is only dependent on the material properties of particles, such as mineral content, surface texture, and so on. The internal correlation between material coefficient of friction and bulk granular material friction angle is still not theoretically known. Thus, the correlation between friction angle and friction coefficient will be studied in this paper.

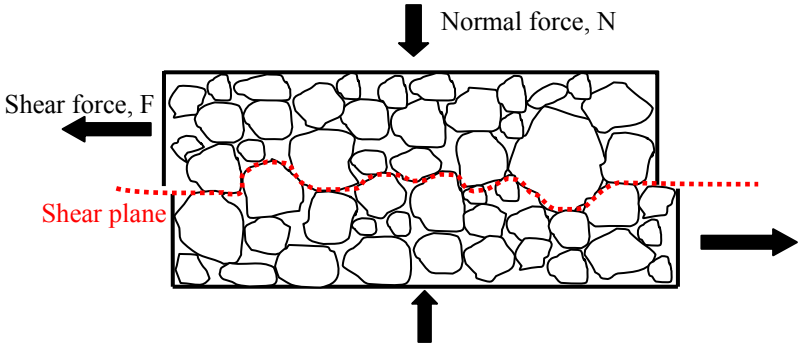

Figure 1 Direct shear of granular material

Internal force transmission in a granular material

Recently, Camphell presented a critical overview of the field of granular flow and discussed the basic internal force transmission and contact mechanics in a granular flow [11]. As he pointed out that the unique feature of a granular material result from the manner in which internal forces are transmitted. Mehrabadi and co-workers first proposed that the internal force of a dense granular material were transmitted by the contacting particles at a microscale, and they derived the relationship between the friction angle and strain increment ratio [12]. Although prominent, the work is more complicated rather than simple and effective.

Currently, the behavior of granular frictional materials, such as sand, is frequently modeled with the Finite Element Method (FEM), where the material is considered as a continuum. With such a model discontinuities between separate particles cannot be described. The Distinct Element Method (DEM) is therefore used as an alternative method, where individual material elements, each assumed as a rigid solid, are separate and (possibly) connected only along their boundaries by appropriate interaction laws based on the principles of physics. Although available computer program makes the modeling much easier, the interface between the granular particles is not appropriately described and the difficulties in development of a 3-D model are still important concerns [13].

In the present study, a dense granular material is considered by calculating the interparticle friction force and relative movement of two contact particles.

Analytical Investigation

Assumption and simplification

The following assumptions were made to simplify a unit volume of mortar to be studied:

1. All aggregate particles can be simplified as rigid, spherical, dry, and non-cohesive particles with gradation diameters corresponding to the opening of the sieve which the aggregate retaining on;
2. The initial compact condition of aggregate particles is dense. Every particle has contact points with others;

3. The shear force results from only the friction between the moving particles at contact points.

Two particle interaction

Based on the above assumptions, a macro-unit volume of an actual aggregate particle assembly, composed of well-graded, irregular-shaped aggregate particles, can be simplified as an "idea" aggregate particle assembly, consisting of rigid, spherical particles with different sizes in dense condition. Thus, the shear force applied on these particles can be calculated as the sum of the shear forces generated by two adjacent particles in contact on the shear plane. The core issue is to calculate the mean shear force and normal force generated by the contact particles. Figure 2 (a) shows two contacting real aggregate particles that are under a normal stress (σ) and moving in a contrary direction. At the contact point, the normal force (n) generates a friction force (f), which is perpendicular to the normal force ($f = \mu \cdot n$) according to Equation 1. The shear resistance generated by this two contact particles results from both normal stress (n) and friction force (f). In order to simplify calculation, two spheres with different diameters were considered as shown in Figure 2 (b). The gravity force is neglected in present study since it is relatively small when compared to external normal force.

Figure 2 (b) shows two spherical particles (i and j) in contact under a normal stress (N). The two particles are moving in an opposite direction. In this case, the shear resistance is generated by the interaction between these two particles. The unit vector **n** in Figure 2(b) along the line linking the centers of these spherical particles (i and j) is determined by

angles α and β. The unit vector **t**, which is on the same plane as vector **n** and shear direction ($\mathbf{x_i}$) and perpendicular to vector **n**, gives the direction of friction force generated by normal force along collision direction (**n**). Thus, the directions of **n** and **t** are determined by:

$$\mathbf{n} = (\sin\alpha \cdot \cos\beta \cdot \mathbf{i} + \cos\alpha \cdot \mathbf{j} + \sin\alpha \cdot \sin\beta \cdot \mathbf{k}) \tag{3}$$

$$\mathbf{t} = \frac{\cos\alpha}{\sqrt{\cos^2\alpha + \sin^2\alpha \cdot \cos^2\beta}} \cdot \mathbf{i} - \frac{\sin\alpha \cdot \cos\beta}{\sqrt{\cos^2\alpha + \sin^2\alpha \cdot \cos^2\beta}} \cdot \mathbf{j} + 0 \cdot \mathbf{k} \tag{4}$$

where $\alpha \in \left[0,\ \frac{\pi}{2}\right]$ and $\beta \in \left[-\frac{\pi}{2},\ \frac{\pi}{2}\right]$.

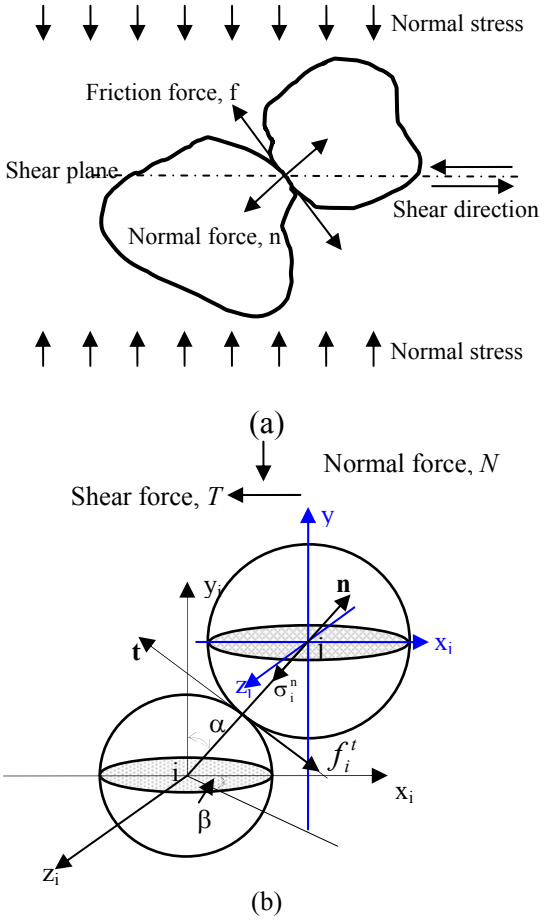

Figure 2 Two-particle shear model

Force equilibrium approach

In the following section, the correlation between the mean shear and normal force of two contact particles are obtained from the force equilibrium equations. Thus, the correlation between the friction angle of the granular particles and friction coefficient of the material is established.

Figure 2(b) illustrates two granular particles sliding against each other on a potential sliding plane. Each particle is applied normal force, which is along the direction of vector that connects the centers of gravity of these two particles. In Figure 2(b), σ_i^n is the normal force applied on particle i; and f_i^t is the friction force generated on the contact surface of particle j by the normal force σ_i^n, and $f_i^t = \mu \cdot \sigma_i^n$, where μ is the friction coefficient of the material. According to the equilibrium of the inter-particle forces on the contact plane of these two particles, the components of the normal force (σ_i^n) and friction force (f_i^t) acted on these two contacting particles along global normal direction (y_i in Figure 3(b)) can be given below,

$$\sigma_n^y = \sigma_i^n \cdot \cos\alpha \tag{5}$$

$$f_t^y = \mu \cdot \sigma_i^n \cdot \frac{\sin\alpha \cdot \cos\beta}{\sqrt{\cos^2\alpha + \sin^2\alpha \cdot \cos^2\beta}} \tag{6}$$

Thus, the overall normal force (N_i) generated from one contact point can be expressed by:

$$N_i = \sigma_i^n \cdot \cos\alpha + \mu \cdot \sigma_i^n \cdot \frac{\sin\alpha \cdot \cos\beta}{\sqrt{\cos^2\alpha + \sin^2\alpha \cdot \cos^2\beta}} \tag{7}$$

Similaly, the overall shear force (F_i) generated from one contact point is given by:

$$F_i = \sigma_i^n \cdot \sin\alpha \cdot \cos\beta - \mu \cdot \sigma_i^n \cdot \frac{\cos\alpha}{\sqrt{\cos^2\alpha + \sin^2\alpha \cdot \cos^2\beta}} \tag{8}$$

And, the normal and shear force generated by all contacting particles on the shear plane in a bulk granular material can be given by:

$$N = \sum_{i=1}^{m} N_i = m \cdot \overline{N} \tag{9}$$

$$F = \sum_{i=1}^{m} F_i = m \cdot \overline{F} \tag{10}$$

where m is the number of contact of particles; $\overline{N}$ and $\overline{F}$ are the mean normal and shear force generated by two particles in a bulk granular material studied.

From the probability point of view, the contact can happen at any point of the top right quarter part of particle i, or the bottom left quarter part of particle j ($\alpha \in \left[0,\ \frac{\pi}{2}\right]$ and $\beta \in \left[-\frac{\pi}{2},\ \frac{\pi}{2}\right]$). The probability that contact happens at a certain location is the ratio of the small area of contact point, and the whole quarter surface area of the particle (P), and it can be expressed as:

$$P = \frac{\sin\alpha \cdot d\alpha \cdot d\beta}{\pi} \tag{11}$$

where $\alpha \in \left[0,\ \frac{\pi}{2}\right]$ and $\beta \in \left[-\frac{\pi}{2},\ \frac{\pi}{2}\right]$.

Thus, the mean normal and shear force ($\overline{N}$, $\overline{F}$) given by Equation (7) and (8) are

$$\overline{N} = \iint_{\alpha,\beta} N_i \cdot P \text{ and } \overline{F} = \iint_{\alpha,\beta} F_i \cdot P \tag{12}$$

and these yield

$$\overline{N} = 0.5 \cdot \sigma_i^n \text{ and } \overline{F} = 0.637 \cdot \mu \cdot \sigma_i^n \tag{13}$$

The friction angle of a granular material can be obtained as:

$$\tan(\phi) = \frac{F}{N} = 1.274 \cdot \mu \tag{14}$$

Microscopic deformation approach

Instead of force equilibrium during the direct shear of granular material, volume change of a bulk granular material is another concern. The important role of volume change of a bulk granular material during shear was firstly recognized by Taylor [14]. He found that the energy dissipated by the friction is equal to the sum of the work done by shearing and that needed to increase the volume. Based on Taylor, the following equation was established:

$$\frac{\tau_{peak}}{\sigma_n} = \mu + \frac{\Delta y}{\Delta x} \tag{15}$$

where τ_{peak} is the maximum value of the applied shear stress, σ_n is the confining normal stress on the shear plane, Δx is the incremental horizontal displacement at peak stress, Δy is the incremental vertical displacement at peak stress, and μ is the friction coefficient of material.

As shown in Figure 3 (a), the particle assembly is imagined to comprise a cube with sides of unit dimension on the mobilized shear plane (MS plane). A shear stress τ is applied on the unit cube. This imaginary cube is composed of many particle layers that are perpendicular or parallel to the MS plane, as shown in Figure 3 (a).

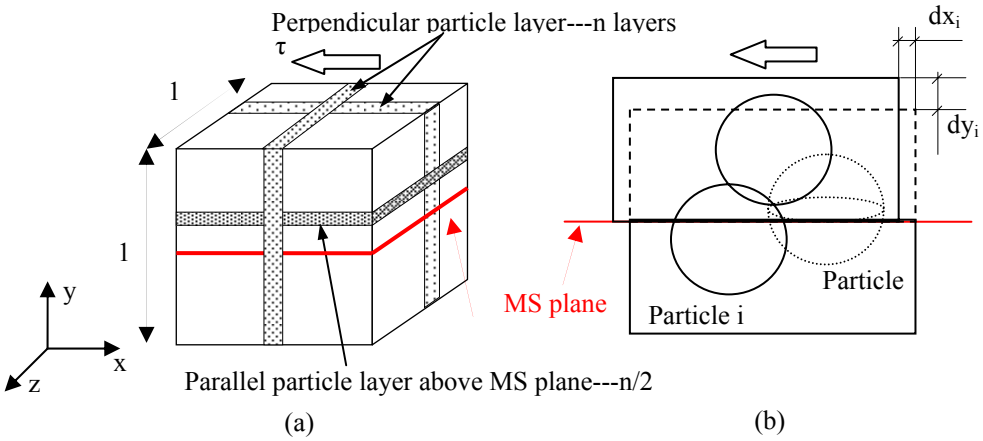

Figure 3 Microscopic view of granular material under shear

Assume that the mechanical behaviors of the particles in any perpendicular particle layer (see Figure 3(a)) are the same, and the shear deformation of any vertical particle layer is equal to that of this cube. Thus, this vertical unit particle layer can be further divided into smaller basic cube on the shear plane, which only includes two contacting granular particles, as shown in Figure 3 (b). Under a shear stress, the movement of any one particle i or j will result in the horizontal, dx and vertical displacements, dy (Figure 3 (b)).

The overall horizontal displacements of buck material along MS plane (x and z direction in Figure 3) are equal to the global the horizontal displacements of the imaginary unit cube, as:

$$\Delta x = dx_i \tag{16}$$

and

$$\Delta z = dz_i \tag{17}$$

Figure 4 illustrates how the individual particles may move in a bulk material under a shear force. It is assumed that there exist m particle layers in the vertical direction relative to the shear plane, and the incremental length Δy due to the shear in the vertical direction of a unit cube can be expressed as shown below, if the particles are rigid.

$$\Delta y = \sum_{i=1}^{n} dy_i \tag{18}$$

In Equations 16-18, dx_i dy_i and dz_i denote the change of relative position of two contacting particles under shear along shear direction, normal direction, and direction perpendicular to the shear-normal plane, respectively. The n in Equation 22 denotes the number of particle layers above and parallel to the MS plane in a unit cube.

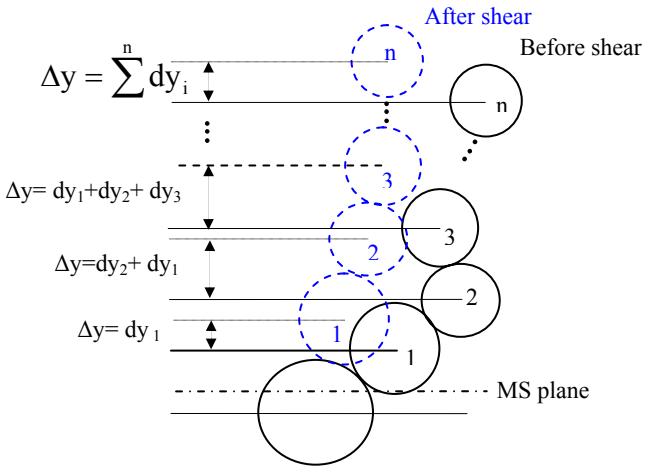

Figure 4 Microscopic mechanism of dilatancy

The displacements generated by two contacting particles can be obtained based on the 3-D model shown in Figure 2 (b). The initial relative position of two particles is determined by two angles, α and β. At the peak shear stress, the particle above the shear plane moves angles $\Delta\alpha$ and $\Delta\beta$ to reach the final position $\alpha+\Delta\alpha$ and $\beta+\Delta\beta$. Thus, the relative displacement between particles i and j can be calculated as:

$$dx_i = (r_i + r_j)\cdot[\sin(\alpha+\Delta\alpha)\cdot\cos(\beta+\Delta\beta) - \sin\alpha\cdot\cos\beta] \tag{19}$$

$$dy_i = (r_i + r_j)\cdot[\cos(\alpha+\Delta\alpha) - \cos\alpha] \tag{20}$$

and

$$dz_i = (r_i + r_j)\cdot[\sin(\alpha+\Delta\alpha)\cdot\sin(\beta+\Delta\beta) - \sin\alpha\cdot\sin\beta] \tag{21}$$

As mentioned before, $\alpha \in \left[0,\ \frac{\pi}{2}\right]$ and $\beta \in \left[-\frac{\pi}{2},\ \frac{\pi}{2}\right]$, and the probability that contact happens on a given location can be determined by Equation 11. Thus, the mean value of the relative displacements along shear direction can be calculated as:

$$d\bar{x} = \iint_{\alpha,\beta} (r_i + r_j)\cdot[\sin(\alpha+\Delta\alpha)\cdot\cos(\beta+\Delta\beta) - \sin\alpha\cdot\cos\beta]d\alpha d\beta \tag{22}$$

or,

$$d\bar{x} = \frac{(r_i + r_j)}{2\pi}\cdot[\pi\cos\Delta\alpha\cdot\cos\Delta\beta + 2\cos\Delta\beta\sin\Delta\alpha - \pi] \tag{23}$$

Similarly,

$$d\bar{y} = \frac{(r_i + r_j)}{2}\cdot\left[\cos\Delta\alpha - \frac{1}{2}\sin\Delta\alpha\cdot\pi - 1\right] \tag{24}$$

and

$$d\bar{z} = \frac{(r_i + r_j)}{2\pi} \cdot \sin\Delta\beta \cdot [\pi\cos\Delta\alpha + 2\sin\Delta\alpha] \tag{25}$$

One important control condition of direct shear is that the movement of material along the direction perpendicular to the shear direction is constrained (Δz=0 in Figure 3(b) and 4). The displacement only happens along the other two directions, parallel and vertical to shear direction (x_i and y_i in Figure 3(b) and 4). Thus, from Equation 25, the average values of $\Delta\alpha$ and $\Delta\beta$ can be calculated as:

$$\Delta\alpha = -1.004 \text{ and } \Delta\beta \in \left[-\frac{\pi}{2}, \frac{\pi}{2}\right] \tag{26}$$

Apply Equation 26 into Equation 24 and 25 $d\bar{x}$ and $d\bar{y}$ can be simplified as:

$$d\bar{x} = 1.5710 \cdot (r_i + r_j) \tag{27}$$

and

$$d\bar{y} = 0.4310 \cdot (r_i + r_j) \tag{28}$$

Furthermore, Equations (16) and (18) can be simplified as:

$$\Delta x = n \cdot 1.5710 \cdot (r_i + r_j) \tag{29}$$

and

$$\Delta y = n \cdot 0.2155 \cdot (r_i + r_j) \tag{30}$$

Thus, Equation 15 can be rewrite as:

$$\frac{\tau_{peak}}{\sigma_n} = \mu + 0.137 \tag{31}$$

Discussions

On the assumptions that the particles are spherical, and the granular media is densely compacted, Equations 14 and 31 give the relationships between the surface friction coefficients of a granular material which is generally difficult to measure and its internal friction angle, which is commonly measured from a direct shear test. Equation 14 indicates that under the fully compacted condition, the internal friction angle of a granular material is dependent on the particle surface roughness as represented by factor μ, and independent of the particle size and its distribution. As the particle surface roughness increasing, internal friction angle of granular material increases. These findings are in consistence with the previous test results [15]. Equation 32 also gives a linear correlation between friction coefficient of material and the internal friction angle. Again, the internal friction angle of granular material is independent of the particle size and its distribution. These two models also indicate that for different granular materials with same raw material and surface condition, the internal friction angle should be same. Previous experimental studies also found that the friction angle of granular materials at same state is independent of their size and only determined by material itself [15].

The predictions of the relationship between the friction coefficient and internal friction angles of a granular material according to Equation 14 and 31 are shown in figure 5. These two equations give similar predicting curves of internal friction angle based on the values of friction coefficient.

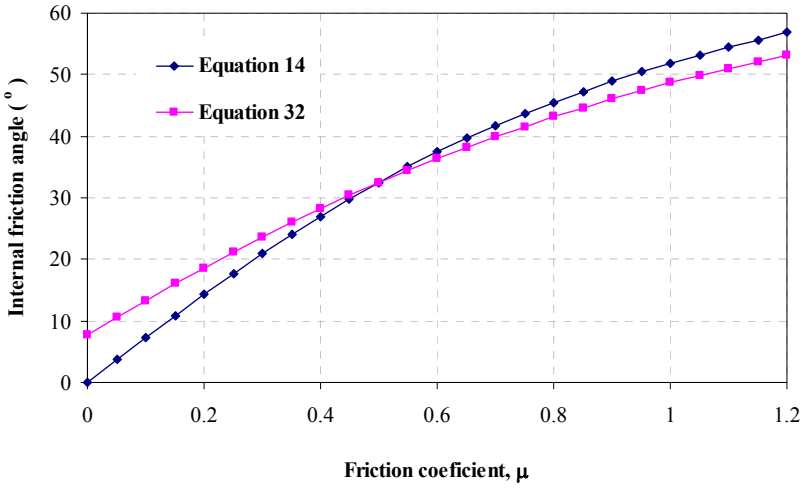

Figure 5 Friction coefficient effect on peak mobilized friction angle

The typical range of dry friction coefficient of normally used materials is from 0.3 to 0.75 [16], the friction angles calculated according to these two values are 21° and 44° for ideally maximum compacted particle materials by using Equation 14, and 24° and 42° by using Equation 31. The correlation between the internal friction angles predicted by Equations 14 and 31 in this range is 0.9999.

Experimental Investigation

In order to verify validity of the newly developed model different kinds of granular material were tested by using direct shear test equipment.

The tested materials include single-sized and graded river sand, gravel, limestone, glass and steel beads. The river sand (RS) had four different single sizes (1.770, 0.890, 0.450, and 0.225mm) and three different gradations (G1, G2, and G3, see Figure 8). Similarly,

the gravel (GR) and limestone (L) had four different single sizes (3.555, 7.125, 11.000, and 15.750mm) and three different gradations (GA, GB, and GC, see Figure 8), respectively. In order to evaluate the reliability of the modified large size direct shear box, 7 different river sand listed in Table 1 were tested with both direct shear boxes presented previously. For each sample, 6 repeated tests were performed. For rest of materials listed in Table 1, trials were performed only with modified large size direct shear box.

Steel and glass balls with two different single-sizes (5.000, and 10.000mm for steel balls; and 2.000 and 10.000mm for glass balls) were tested with the modified large size direct shear box.

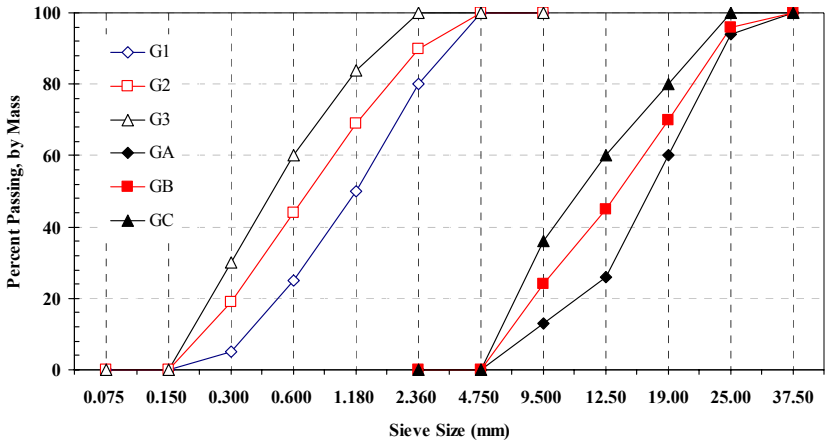

Figure 6 Particle gradations

The small size aggregate particles (Figure 6) were tested with a small shear box according to ASTM D 3080 [17]. And the materials with large aggregate particles were tested with a modified large dimension direct shear box. The modified direct shear box

consists of a container for being filled with granular material. The lower half of the device is fixed on the bottom plate while the upper half is movable. The movement of the upper half, which has the maximum capacity as 25.4 mm, results in a maximum shear stress on the gap plane between the top and bottom, which is 254 mm x 254 mm. During testing, a bulk granular material was pulled into the shear boxes and rodded into as compacted condition as possible. Different normal loads were then applied on the specimen, and shear stresses were measured. The results are plotted as the relationship between the shear stress and normal stress, from which the angle of internal friction was calculated.

Figure 7 ASTM standard direct shear box for small dimensional granular material

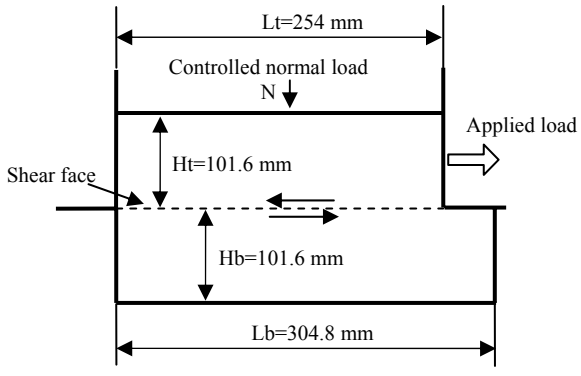

Figure 8 Modified direct shear box for large dimensional granular material

Table 1 Granular materials used in direct shear box tests

Number	Material	Grain shape	Average diameter (mm)	Direct shear tests	
				Small box	Large box
RS#16	River sand	Well Rounded	1.770	√	√
RS#30	River sand	Well Rounded	0.890	√	√
RS#50	River sand	Well Rounded	0.450	√	√
RS#100	River sand	Well Rounded	0.225	√	√
RS-G1	River sand	Well Rounded	Gradation 1(G1)	√	√
RS-G2	River sand	Well Rounded	Gradation 2(G2)	√	√
RS-G3	River sand	Well Rounded	Gradation 3(G3)	√	√
GR1	Gravel	Rounded	3.555	√	√
GR2	Gravel	Rounded	7.125	√	√
GR3	Gravel	Rounded	11.000	√	√
GR4	Gravel	Rounded	15.750	√	√
G-GA	Gravel	Rounded	Gradation A(GA)	√	√
G-GB	Gravel	Rounded	Gradation B(GB)	√	√
G-GC	Gravel	Rounded	Gradation C(GC)	√	√
L1	Limestone	Angular	3.555	-	√
L2	Limestone	Angular	7.125	-	√
L3	Limestone	Angular	11.000	-	√
L4	Limestone	Angular	15.750	-	√
L-GA	Limestone	Angular	Gradation A(GA)	-	√
L-GB	Limestone	Angular	Gradation B(GB)	-	√
L-GC	Limestone	Angular	Gradation C(GC)	-	√
SB1	Steel ball	Spherical	5.000	-	√
SB2	Steel ball	Spherical	10.000	-	√
GB1	Glass ball	Spherical	2.000	-	√
GB2	Glass ball	Spherical	10.000	-	√

Experimental Results and Discussions

Typical results of the direct shear test from the RS#30 sample are shown in Figure 9(a). It is observed that the force required shearing the river sand sample increased with the normal load. Figure 9b gives the relationships between the maximum shear forces obtained from the curves in Figure 9(a) and their corresponding normal forces. These relationships follow the format of Mohr-Coulomb equation, and therefore they are also called Mohr-Coulomb failure curves of the granular materials. The angle between the linear line and the normal load axis signifies the peak friction angle, which indicates the effect of normal stress on shear stress.

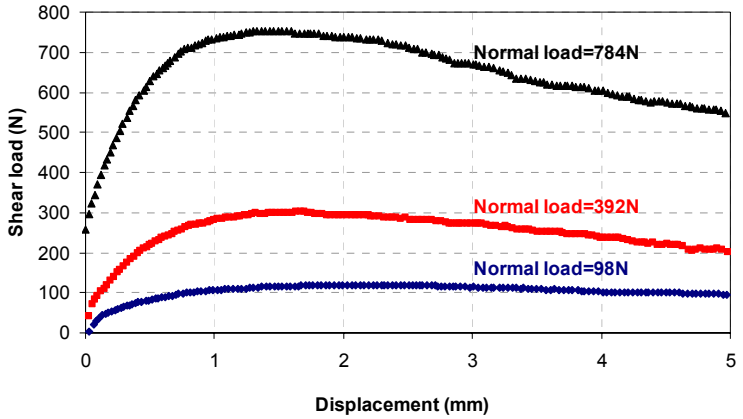

(a) shear load (N) vs. displacement (mm)

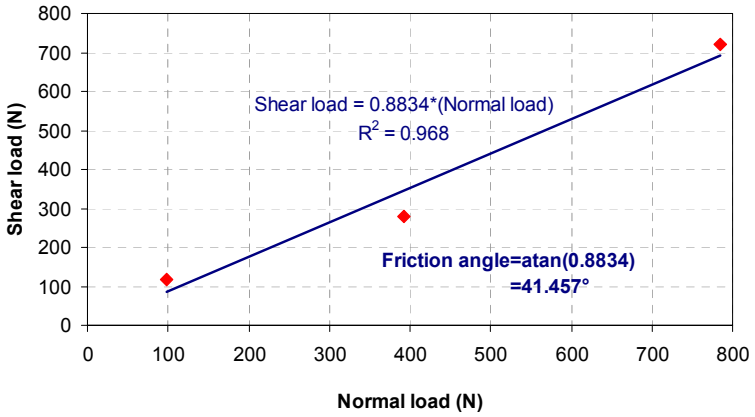

(b) Mohr-Coulomb failure curve of river sand sample (RS#30)

Figure 9 Typical results from direct shear test (RS#30)

The results of direct shear tests for river sand are summarized in Table 2. For each test equipment, the peak friction angles for single size and graded rivers and are similar, the standard deviation is small. The average value of ratios between peak friction angles obtained from same sand samples and different test equipments is equal to 1.00, and the standard deviation is 0.01, which means the two peak friction angles obtained from ASTM standard method and modified large direct shear box are statistically similar. This modified large direct shear box is reliable in testing direct shear resistance of large size granular material, such as gravel and limestone.

Tables 3 to 5 list all direct shear test results on coarse particles of limestone, gravel, steel and glass balls. The tables demonstrate that the peak friction angle of a given granular material is almost a constant, regardless to the particle size and gradation. This is consistent with the previous findings [15]. This also testifies one finding from the modeling that the friction angle is independent of the size and size distribution of granular material.

Since the glass and steel particles are perfect spheres with perfect surface, and the present models are based on the assumption that the shape of particles is perfect sphere, they are ideal samples to verify the present models. The peak friction angles of steel and glass particles are obtained from direct shear test as 40.9° (steel) and 50.9° (glass). By using Equation 14 and 32, the material friction coefficients of steel and glass can be calculated. Table 6 shows the values of material friction coefficient from presented models and references. The present models give a reasonable prediction.

The limestone particles used in experimental studies are angular. A higher value of peak friction angle is expected compared to the rounded particles. The peak friction angle is 55.8°, and this gives a value of friction coefficient of 1.15 (Equation 14) and 1.30 (Equation 32). Similarly, the friction coefficient of gravel can be calculated as 0.97 (Equation 14) and 0.87 (Equation 32).

Summary and Conclusions

The present models are the relatively simple model compared to the FEM or DEM, which are popularly used nowadays to simulate the granular material flow, and they are still capable to describe the 3D behavior of granular flow with direct shear. Overall shear resistance of granular materials is described as a function of friction coefficient of granular materials, which is one of the most important properties of material. Based on current considerations, the shear resistance of granular materials is directly correlated to inter-particle friction, or friction coefficient of granular materials, and it is independent of the size and size distribution of granular materials. These findings explained the observation that same granular materials with different size and size distributions have nearly constant friction angles.

Table 2 River sand direct shear box test results

Number	Large direct shear box results			Small direct shear box results			Ave φ_l/φ_s
	Peak friction angle φ_l (°)	Ave. φ_l	Std. Φ_l	Peak friction angle φ_s (°)	Ave. φ_s	Std. φ_s	
RS#16	41.480	41.38	0.14	41.361	41.03	0.19	1.01
	41.461			41.023			
	41.228			40.817			
	41.192			41.082			
	41.364			40.876			
	41.538			40.994			
RS#30	41.457	41.45	0.40	41.672	41.31	0.23	1.00
	40.768			41.345			
	41.419			41.383			
	41.984			40.974			
	41.425			41.260			
	41.666			41.218			
RS#50	41.043	40.92	0.52	41.956	41.31	0.50	0.99
	41.049			40.919			
	40.643			40.945			
	41.066			41.905			
	41.627			41.280			
	40.071			40.873			
RS#100	40.074	40.88	0.62	40.600	41.24	0.55	0.99
	41.170			41.927			
	41.483			41.283			
	41.312			41.409			
	41.092			40.580			
	40.121			41.627			
RS-G1	41.425	41.09	0.23	41.586	41.17	0.37	1.00
	41.036			40.774			
	40.814			41.105			
	41.196			40.692			
	40.843			41.470			
	41.196			41.367			
RS-G2	40.778	40.54	0.31	41.682	40.99	0.39	0.99
	40.097			41.017			
	40.368			40.603			
	40.659			40.728			
	40.381			40.791			
	40.955			41.131			

Table 2 River sand direct shear box test results (con.)

Number	Large direct shear box results			Small direct shear box results			Ave φ_l/φ_s
	Peak friction angle φ_l (°)	Ave. φ_l	Std. Φ_l	Peak friction angle φ_l (°)	Ave. φ_l	Std. φ_s	
RS-G3	40.672	41.16	0.48	41.486	41.24	0.39	1.00
	41.244			40.689			
	40.577			40.840			
	41.499			41.560			
	41.131			41.599			
	41.829			41.277			
Ave.	-	41.06	-	-	41.18	-	1.00

Table 3 Limestone direct shear box test results

Number	Friction angle φ	Friction angle φ	
		Ave	Std
L1-1	55.599	55.702	1.658
L1-2	54.097		
L1-3	57.409		
L2-1	53.589	54.424	1.178
L2-2	55.772		
L2-3	53.913		
L3-1	55.389	53.744	1.434
L3-2	53.086		
L3-3	52.757		
L4-1	56.338	53.986	2.038
L4-2	52.885		
L4-3	52.736		
L-GA-1	57.406	55.412	2.249
L-GA-2	52.974		
L-GA-3	55.855		
L-GB-1	57.369	56.359	0.961
L-GB-2	56.253		
L-GB-3	55.456		
L-GC-1	57.254	55.924	1.160
L-GC-2	55.404		
L-GC-3	55.116		
Ave	-	55.08	1.02

Table 4 Gravel direct shear box test results

Number	Friction angle φ (°)	Friction angle φ (°)	
		Ave	Std
G1-1	49.366	49.861	0.511
G1-2	49.832		
G1-3	50.386		
G2-1	45.883	46.753	0.929
G2-2	47.731		
G2-3	46.644		
G3-1	50.079	50.040	0.583
G3-2	50.602		
G3-3	49.438		
G4-1	47.526	46.842	0.725
G4-2	46.082		
G4-3	46.918		
G-GA-1	46.990	47.355	0.341
G-GA-2	47.408		
G-GA-3	47.667		
G-GB-1	48.460	47.757	0.663
G-GB-2	47.142		
G-GB-3	47.669		
G-GC-1	46.865	46.498	0.486
G-GC-2	46.682		
G-GC-3	45.947		
Ave	-	47.87	0.65

Table 5 Steel and glass particles direct shear box test results

Number	Friction angle φ(°)	Friction angle φ(°)		Friction angle φ(°)	
		Ave	Std	Ave.	Std.
SB1-1	41.079	41.313	0.581	40.91	0.09
SB1-2	41.975				
SB1-3	40.886				
SB2-1	40.974	40.506	0.453		
SB2-2	40.474				
SB2-3	40.071				
GB1-1	51.041	51.226	0.341	50.89	0.18
GB1-2	51.620				
GB1-3	51.018				
GB2-1	50.512	50.562	0.087		
GB2-2	50.662				
GB2-3	50.512				

Table 6 Summary of direct shear results on different materials

material	peak friction angle (°)	calculated friction coefficient		friction coefficient from literatures
		Eq.14	Eq.31	
steel	40.90	0.68	0.73	0.7-0.78 [18, 19, 20, 21]
glass	50.89	0.97	1.09	0.9-1.0 [20, 21]
rive sand	41.06	0.68	0.73	N/A
limestone	55.08	1.15	1.30	N/A
gravel	47.87	0.97	0.87	N/A

References:

1. Coulomb, CA. Sur une application des regles de Maximis et Minimis a quelques problemes de statique relatifs a l'Architecture, Acad. Roy. des Sciences Memoires de math, et de physique par divers savans, 1773; 7: 343-382.
2. Jaeger HM, Liu CH, Nagel SR. Relaxation at the Angle of Repose. Physical Review Letters 1989; 62(1): 40-43.
3. Jaeger HM, Nagel SR. Physics of the Granular State. Science 1992; 255: 1523-1531.
4. Evesque P, Fargeix D, Habib P, Luong MP, and Porion P. Pile density is a control parameter of sand avalanches. Physical Review E 1991; 47(4): 2326–2332.
5. Brown RL, Richards JC. Principles of Powder Mechanics. Oxford: Pergamon Press, 1970.
6. Barnes, HA, Hutton, J.F., and Walters, K. *An Introduction to Rheology*, New York: Elsevier, 1989.
7. Erdoðan, ST. Determination of Aggregate Shape Properties Using X-ray Tomographic Methods and the Effect of Shape on Concrete Rheology, 2005, PhD Dissertation, The University of Texas at Austin.
8. Tattersall, GH. “Workability and Quality Control of Concrete,” London: E&FN Spon, 1991.

9. Quiroga, PN. The Effect of Aggregate Characteristics on the Performance of Portland Cement Concrete, PhD Dissertation, The University of Texas at Austin. Austin, TX. 2003.

10. Lu G, Wang KJ, and Rudophi TJ. Modeling rheological behavior of highly flowable mortar using concepts of particle and fluid mechanics. Cement, Concrete Composite, accepted June 1, 2006.

11. Charles S. Campbell, Granular Material Flows – An overview Powder Technology, 2006, 162(3): 208-229

12. Mehrabadi MM, Nemat-Nasser S, and Oda M. On statistical description of stress and fabric in granular materials. International Journal for Numerical and Analytical Methods in Geomechanics, 1982, 6(1):95-108

13. Oda M, Nemat-Nasser S, and Mehrabadi MM. A statistical study of fabric in a random assembly of spherical granules. International Journal for Numerical and Analytical Methods in Geomechanics, 1982, 6(1):77-94

14. Taylor DW. Fundarnentals of soi1 mechanics, New York: JWS Inc. 1948

15. Holtz RD, Kovacs WD. An introduction to geotechnical engineering. Prentice hall, 1981.

16. Bowden FP, Tabor D. Friction and Lubrication of Solids. Oxford: Clarendon Press, 1950.

17. ASTM D3080. Standard Test Method for Direct Shear Test of Soils Under Consolidated Drained Conditions.

18. Sullivan JF. Technical Physics. New York: Wiley, 1988

19. Grigoriev IS, Meilikhov EZ, Radzig AA. Handbook of Physical Quantities. Boca Raton, FL: CRC Press, 1997: 145-156

20. Friction Center Coefficient Database. http://frictioncenter.siu.edu/databaseSearch.html

21. Friction Coefficients. http://www.physlink.com/Reference/FrictionCoefficients.cfm

CHAPTER 4. A DLVO MODEL FOR YIELD BEHAVIOR OF FRESH CEMENT PASTE

A paper submitted to ACI Material Journal

Gang Lu and Kejin Wang

Abstract

In the present study, a yield stress model of cement paste is developed based on the DLVO theory. In this model, cement particles are considered as rigid spheres suspended in water. The interparticle force between two adjacent cement particles is assumed to be generated by the electrostatic and dispersion forces of the cement particles. The mean interparticle force of the cement paste system along the shear direction is determined based on a probability approach. The shear stress of the cement paste is then obtained by multiplying the mean interparticle force with the number of particles in a unit volume of the cement paste. To verify the validity of the newly developed model, two types of tests, direct shear and rheometer tests, are also performed on a group of cement pastes made with different water-to-cement ratios (w/c). The results indicate that the yield stress of cement paste primarily depends on the w/c and properties of cement materials. The newly developed model can not only predict well the yield behavior of cement pastes but also describe the correlations among the yield stresses obtained from different experimental methods. The present experimental results illustrate that the rheological yield stress obtained from the direct shear test is close to the "true" yield stress obtained from the up flow curve of the rheometer test used. A normal stress has significant effect on yield stress of the cement paste with a low w/c ($\leq$0.4).

Keywords: *Rheology, cement paste, double-layer, yield stress, suspension*

INTRODUCTION

The rheological behavior of a cementitious system, or a freshly made paste, is greatly related to the hydration process of its cementitious materials. The hydration process depends not only upon the material characteristics (such as particle distribution, chemical composition, water-to-cementitious material ratio, and admixtures) but also upon the hydration time, construction process (such as mixing and placement procedures), and environmental conditions (such as temperature and relative humidity) [1]. The complexity of the hydration process made study of the rheology behavior of a fresh cementitious material very challenging. Currently, most studies on cement and concrete rheology are experimentally dependant. The experimental results vary largely because of different materials investigated, equipments used, and test methods applied. Little work has been done studying cement paste rheological behavior based on a theoretical approach.

In the science of rheology, two important parameters are often used to describe rheological behavior of a material: yield stress and viscosity. Yield stress is the shear stress required by a viscoelastic material for initiating a plastic deformation. It is the maximum shear stress under which the material is in a solid state. Yield stress is strongly influenced by the magnitude of the interparticle forces and spatial particle distribution of the material studied. A material must overcome the yield stress to transform from solid to liquid behavior[2]. Differently, viscosity is the resistance of a material to flow, and it

describes the material behavior in a dynamic state. The present study is to investigate the yield behavior of a cement paste that is in a solid state.

A great deal of study has been conducted to measure yield stress of fresh cementitious materials, most of which measure Bingham yield stress rather than the "true" yield stress[3-6]. According to the science of rheology, the "true" yield stress is defined as the maximum shear stress at the strain rate of zero. However, in many commonly used test methods, the reliable "true" yield stress of a fresh cementitious material is hard to obtain. Therefore, the yield stress is often determined by the intercept of the linear portion of a flow curve, or the shear stress-strain rate curve, of the tested material on the shear stress axis (or at zero shear rate). This yield stress is commonly referred as "apparent" yield stress. For a cement-based material, shear stress generally increases non-linearly with increased shear rate because of the particle agglomeration in an insufficiently mixed testing sample, which also makes the determination of "apparent" yield stress of the material difficult. Hence, the down load portion (or down curve) of a rheological hysteresis curve, which describes how the shear stress of a material decreases with reduced strain rate, is often used. The yield stress determined from the linear portion of the down curve is called Bingham yield stress [7]. Bingham yield stresses of various fresh cementitious materials have been reported by many researchers in the absences of their "true" yield stresses[4, 6]. Researchers have found that a normal stress, often resulting from a material self-weight and an external load, has significant influence on shear stress of the material[8]. However, in most rheological studies, the effect of normal stress on the shear stress of a cementitious material is often neglected[9-11].

Qualitative and quantitative disagreements among the rheological parameters of cementitious materials measured from different experiments have been reported by many researchers[12]. According to Banfill, these disagreements cannot be wholly explained by the variations in the materials used, and they must be associated with the experimental technique and apparatus used[12]. The differences in shear history of a test, undetected plug flow, and slippage of the tested material at the surfaces of the device (viscometer) can all contribute to the large variations of the experimental results. Since results obtained from each individual test device and method do describe rheological behavior of the tested materials, some relationships may exist among the results from the commonly used test devices and methods. A theoretical approach to the material rheological behavior may be able to explain the variations and to express the relationships among these test results.

In 1940s, Derjaguin, Landau, Verwey and Overbeek developed a theory, called DLVO theory, and described the force between charged surfaces interacting through a liquid medium[13, 14]. In this theory, the combined effect of van der Waals attraction and the electrostatic repulsion is considered by using the double layer of counter-ions. Many researchers have used this theory in the study of a cement paste[15]. Based on the DLVO theory, Flatt developed a model for the interaction between two adjacent cement particles with consideration of the interparticle potential and sedimentation behavior of a cement suspension in a polymer[2]. Although his model showed consistent results with those from experiment, the model was not suitable for studying the effects of cement paste material properties, such as water-to-cement ratio (w/c). Li et al. studied concrete rheological behavior based on the interparticle action generated by the friction and linking force

resulting from the surface tension and suction of pore water[16]. Although the model qualitatively explained the yield behavior of a cementitious material, the researchers did not consider the cohesion between the cement particles in their theoretical approach.

The objective of the present study is to develop an improved model for predicting rheological behavior of cementitious materials. This study contains two parts: (1) theoretical model development and (2) experimental verification of the validity of the new model. In the model development, cement particles are simplified as rigid spheres with the same (average) diameter. The shear force between two adjacent cement particles is then assessed based on the interparticle potential through modification of the work done by Flatt[2]. The DLVO theory is employed to determine the interaction, the attractive and repulsive forces, between two cement particles. The average shear force of all cement particles in a unit volume of a cementitious material is then determined based on the concept of probability. In the verification of the validity of the newly developed model, a group of cement pastes made with different w/c are tested using a direct shear box and a Brookfield rheometer. The yield stresses calculated from the present model are compared with those measured from the direct shear and rheometer tests.

RESEARCH SIGNIFICANCE

Most existing studies on cement and concrete rheology are dependent on the experimental protocol. Qualitative and quantitative disagreements among the rheological parameters measured from different experiments have been reported. However, limited work has been done studying the rheological behavior of cement-based materials based

on a theoretical approach. In the present study, a yield stress model of cement paste is developed based on the DLVO theory. This newly developed model can well predict the yield behavior of cement pastes, explain important factors that affect paste yield behavior, and describe the correlations among the yield stresses obtained from different experimental methods. These research results fill the above-mentioned gap in cement rheology study.

THEORETICAL APPROACH

Assumptions for modeling

To assist in modeling, a cement paste system is simplified, and the following assumptions are made:

(1) The cement paste studied is freshly made and the cement hydration has little effect on the paste rheological behavior at this stage; also, measurements are done at very early age, before initial set.

(2) There is no entrapped or entrained air void in the cement paste;

(3) All cement particles are rigid spheres and have the same diameter;

(4) The distance between any two cement particles is always larger than zero; and

(5) Attraction and repelling forces exist between cement particles in the paste.

A fresh cement paste can be considered as a suspension system with cement particles suspended in water[2, 16]. The cement particles can be simplified as equal-sized rigid spheres with the average diameter of the cement particles. For a given specific gravity of cement (S_c) and $\frac{w}{c}$, the volume of mixing water ($V_{mixing\ water}$), volume of cement (V_{cement}),

number of cement particles, and total surface area in a unit volume of paste ($A_{all\ particles}$) can be calculated as below:

$$V_{mixing\ water} = \frac{1}{1 + \frac{1}{S_c \cdot \frac{w}{c}}} \tag{1}$$

$$V_{cement} = \frac{1}{1 + S_c \cdot \frac{w}{c}} \tag{2}$$

$$N = \frac{V_{cement}}{\frac{4}{3} \cdot \pi \cdot \bar{r}^3} = \frac{3}{4 \cdot \pi \cdot \bar{r}^3} \frac{1}{1 + S_c \cdot \frac{w}{c}} \tag{3}$$

$$A_{all\ particles} = N \cdot A_{single\ \ particles} = \frac{3}{\bar{r}} \cdot \frac{1}{1 + S_c \cdot \frac{w}{c}} \tag{4}$$

Where, $\bar{r}$ is the average radius of cement particles, N is the number of cement particles in a unit volume of cement paste, and $A_{single\ particles}$ is the surface area of an individual cement particle. (In the present study, the cement density (S_c) of 3.15 and the average cement particle diameter ($2\bar{r}$) of 15 micrometer are used[17].)

In order to keep a cement paste in a suspension state, the distance between two adjacent cement particles in the paste is assumed larger than zero, and the spaces among the cement particles is filled with water. At the compacted state, the cement particles are all in contact with no separation. The water that fills the spaces between compacted cement particles is defined as “water between particles”. The volume of the water between particles ($V_{water\ between\ particles}$) in a unit volume of a paste is mainly depending upon the

particle packing of the cement. The rest of the mixing water ($V_{mixing\ water}$) that separates the cement particles is defined as excess water. In the present study, cement particles are assumed to be non-deformable, spherical, with a single average size, and well dispersed in water. Thus, the volume of the excess water ($V_{excess\ water}$) and the average interparticle distance (h) in a unit volume of a paste can be expressed as follows:

$$V_{excess\ water} = V_{mixing\ water} - V_{water\ between\ particles} = (1 - \frac{p}{1-p} \cdot \frac{1}{S_c \cdot \frac{w}{c}}) \cdot \frac{1}{1 + \frac{1}{S_c \cdot \frac{w}{c}}} \quad (5)$$

$$h = 2 \times \frac{V_{excess\ water}}{A_{all\ particles}} = \frac{2}{3} \cdot \bar{r} \cdot \left[S_c \cdot \frac{w}{c} - \frac{p}{1-p} \right] \quad (6)$$

where, p is the void ratio of the paste ($p=1-V_{cement}$)

The DLVO theory

As mentioned previously, in the DLVO theory, the combined effect of van der Waals attraction and the electrostatic repulsion is considered by using the double-layer of counter-ions. Many researchers have used the DLVO theory to study fresh cement pastes since cement particles have electron charged surfaces in a water suspension[2, 15]. Due to the net charge on the surface of a particle, a compact layer of oppositely charged ions is attracted to the interface[18, 19]. This compact thin layer is called the inner layer or Stern layer. Outside the Stern layer, there is a region called the diffuse layer. The diffuse layer carries a significant charge due to high concentrations of ions repelled from the inner layer. These repelled ions have the same sign charge as the surface of the particle, producing an electrical potential (ψ) that begins at the shear plane and decays with

distance. As a result, the diffuse layer is often described by two parameters: the electrical potential (ψ) and the thickness (l/κ, where κ is the Debye-Huckel parameter). The boundary between the Stern and diffuse layers (referred as double layer) is known as the shear plane. Approximately at 3/k from the surface of the diffuse layer, positive and negative ions become to balance, the electrical potential disappears, and ions start to move freely. This double-layer theory is often used to determine the interaction between two charged particles.

Shear force between two cement particles

In a bulk suspension solution, a repulsive potential, U_R, which arises from the electrostatic force between two particles with the same electron charges, can be given as:[15]

$$U_R = 2\pi\varepsilon_0\varepsilon_r\bar{r}\psi^2 \ln\{1 + \exp[-\kappa h]\} \quad (7)$$

where $\bar{r}$ is the mean particles radius; h is the distance of between particle surfaces; Ψ is the zeta potential, which can be determined experimentally; κ is given by $\kappa = e\sqrt{\frac{I_C N_A}{\varepsilon_0\varepsilon_r kT}}$; e is the charge of an electron; N_A is Avogadro's number; ε_r is the relative dielectric constant of the liquid medium; ε_0 is the dielectric permittivity of free space; and k is Boltzmann's constant. A value of k=1.7 can be taken in calculation of cement suspension[15]. T is the environmental temperature. The ionic strength of the bulk solution, I_C, is defined as $I_C = \frac{1}{2}\sum C_i z_i^2$, where C_i is the ionic concentration of ion i in moles per liter, z_i is the valency of ion i, and the summation is over all ion species.

In the same solution, an attractive potential, U_A, arising from the London-van der Waals force, can be expressed as[15, 20]:

$$U_A = -\frac{A_H}{12}\left[\frac{4\bar{r}^2}{h^2+4\bar{r}h}+\frac{4\bar{r}^2}{h^2+4\bar{r}h+4\bar{r}^2}+2\ln\left(1-\frac{4\bar{r}^2}{h^2+4\bar{r}h+4\bar{r}^2}\right)\right] \quad (8)$$

where A_H is the Hamaker constant, which is determined by properties of the suspending material and the suspension liquid medium.

Reliable values of Hamaker constants (A_H) for cementitious materials are not available although different values have been proposed. Sakai and Daimon suggested the value of Hamaker constant for tricalcium silicate as 4.55×10^{-6} J/mol[19]. Flatt used the Hamaker constant of 4.2×10^{-6} J/mol of magnesium oxide for cement suspensions[2]. Yang et al. proposed the value of 2.23×10^{-20} J of calcite for cement suspensions[15]. As discussed later, the value of Hamaker constant can also be found out from a curve fitting of experimental data.

Based on Equations 7 and 8, the interparticle electrostatic (F_E) and dispersion forces (F_U) of a buck suspension solution can be derived as[2]:

$$F_E = -2\pi\varepsilon_0\varepsilon_r\bar{r}\psi^2\frac{\kappa e^{-\kappa h}}{1+e^{-\kappa h}} \quad (9)$$

$$F_U = \frac{A_H\bar{r}}{12h^2} \quad (10)$$

Thus, the total interparticle attractive force (F_t) between adjacent two cement particles is

$$F_i = F_E + F_U = \frac{A_H\bar{r}}{12h^2} - 2\pi\varepsilon_0\varepsilon_r\bar{r}\psi^2\frac{\kappa e^{-\kappa h}}{1+e^{-\kappa h}} \quad (11)$$

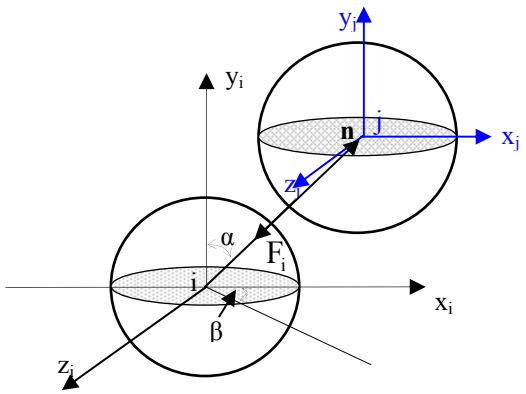

Fig. 1—Cement particles interaction model.

Assuming that cement particles are equal-sized rigid spheres, the interparticle attraction force of any two adjacent cement particles can be calculated according to the 3-D model as shown in Figure 1. In this figure, the vector **n** connects the centers of two particles, and it is determined by angles α and β as described below:

$$\mathbf{n} = (\sin\alpha \cdot \cos\beta \cdot \mathbf{i} + \cos\alpha \cdot \mathbf{j} + \sin\alpha \cdot \sin\beta \cdot \mathbf{k}) \tag{12}$$

The interparticle force F_i, determined by Equation 11, is on the vector **n**. The probability that the interparticle force generates in a given direction (P(α,β)) can be expressed by[21]:

$$P(\alpha,\beta) = \frac{\sin\alpha \cdot d\beta \cdot d\alpha}{\pi} \tag{13}$$

Where, the range of α and β are $\alpha \in \left[0,\ \frac{\pi}{2}\right]$ and $\beta \in \left[-\frac{\pi}{2},\ \frac{\pi}{2}\right]$, respectively.

Hence, the average value of interparticle force along x_i direction is given as:

$$\bar{F}_x = \iint F_i \cdot \mathbf{n}_x \cdot P(\alpha,\beta) = \iint \left(\frac{A_H \bar{r}}{12h^2} - 2\pi\varepsilon_0\varepsilon_r \bar{r}\psi^2 \frac{\kappa e^{-\kappa h}}{1+e^{-\kappa h}}\right) \sin\alpha \cdot \cos\beta \cdot \frac{\sin\alpha}{\pi} d\alpha d\beta \tag{14}$$

where $\alpha \in \left[0,\ \frac{\pi}{2}\right]$ and $\beta \in \left[-\frac{\pi}{2},\ \frac{\pi}{2}\right]$. Equation 14 above can be simplified as:

$$\bar{F}_x = 0.5 \cdot \left(\frac{A_H \bar{r}}{12h^2} - 2\pi\varepsilon_0\varepsilon_r \bar{r}\psi^2 \frac{\kappa e^{-\kappa h}}{1+e^{-\kappa h}} \right) \tag{15}$$

Shear stress of a cement paste

Equation 15 gives the shear force generated by two adjacent cement particles dispersed in water. Considering a horizontal plane of a unit volume of a cement paste cube, one can assume that there are N cement particles having the average diameter of $2\bar{r}$. Thus, the overall shear force applied on this plane due to all interparticle action is $N \cdot \bar{F}_x$, where N is the number of particles in a unit shear plane (Equation 3).

Combining Equations 3, 6, and 15, the shear stress of cement paste (τ_p) can be obtained as:

$$\tau_p = \frac{3}{8\pi\bar{r}^3} \cdot \frac{1}{S_c \cdot \frac{w}{c} + 1} \cdot \left\{ \frac{A_H \bar{r}}{12\left(\frac{2}{3} \cdot \bar{r} \cdot \left[S_c \cdot \frac{w}{c} - \frac{p}{1-p} \right] \right)^2} - 2\pi\varepsilon_0\varepsilon_r \bar{r}\psi^2 \frac{\kappa e^{-\kappa\left\{ \frac{2}{3} \cdot \bar{r} \cdot \left[S_c \cdot \frac{w}{c} - \frac{p}{1-p} \right] \right\}}}{1+e^{-\kappa\left\{ \frac{2}{3} \cdot \bar{r} \cdot \left[S_c \cdot \frac{w}{c} - \frac{p}{1-p} \right] \right\}}} \right\} \tag{16}$$

Equation 16 gives the theoretical calculation of the overall shear stress of a freshly-made cement paste. Due to the presence of excess water in the cement paste which separates cement particles, it can be assumed that the friction force between the cement particles is zero and the shear stress of the cement paste results only from the cohesion force between

the cement particles, and. This cohesion force is correlated to the specify gravity (S_c) of cement particles; w/c; and mean cement particle radius ($\bar{r}$).

Simplification of the shear stress model

For a practical application, Equation 16 can be simplified by replacing some parameters with typical values. Table 1 lists the selected parameters and values used in the present study (assuming water temperature of the cement paste is 25ºC). Using the values of the parameters selected in Table 1, Equation 16 is further simplified as Equation 17:

$$\tau_p = 2.8294\times10^{14}\cdot\frac{1}{3.15\cdot\frac{w}{c}+1}\cdot\left\{\frac{2.5\times10^{4}\cdot A_H}{\left[3.15\cdot\frac{w}{c}-0.9417\right]^2}-2.6707\times10^{-19}\frac{e^{-2.6776\times10^{-5}\cdot\frac{w}{c}+4.0022\times10^{-6}}}{1+e^{-2.6776\times10^{-5}\cdot\frac{w}{c}+4.0022\times10^{-6}}}\right\} \quad (17)$$

Table 1—Selected parameters and their values used in the model simplification

Parameter	ε_0	ε_r (C^2/Nm^2)	ψ	S_c	p	$\bar{r}$ (μm)	κ
Typical Value	80	8.8542×10^{-12}	2.17	3.15	48.5%	15	1.7
Source/Reference	[20]	[20]	[13]	[15]	[15]	[15]	[2]

As shown in Equation 17, the shear stress of a cement paste is now varying only with w/c since Hamaker constant A_H is a constant, not a variable. A_H is related to the cement

material characteristics, and its value varies from 4.2×10^{-6} to 2.23×10^{-20} J based on the published research[2, 15].

There are significant differences between the actual and typical values for Equation 17 (see Table 1). To consider these differences, the authors of this paper introduce an experimental scaling parameter (D) into the new shear stress model. When D is multiplied with w/c of a cement paste, it will only increase or decrease w/c but not change the form of Equation 17. When different test methods are selected for a cement rheology study, different D values can be used in Equation 17, and thus the effects of the test methods on the rheological test results may be described. Using the experimental scaling parameter (D), Equation 17 becomes:

$$\tau_p = 2.8294\times10^{14}\cdot\frac{1}{3.15\cdot D\cdot\frac{w}{c}+1}\cdot\left\{\frac{2.5\times10^{4}\cdot A_H}{\left[3.15\cdot D\cdot\frac{w}{c}-0.9417\right]^2}-2.6707\times10^{-19}\,\frac{e^{-2.6776\times10^{-5}\cdot D\cdot\frac{w}{c}+4.0022\times10^{-6}}}{1+e^{-2.6776\times10^{-5}\cdot D\cdot\frac{w}{c}+4.0022\times10^{-6}}}\right\} \tag{18}$$

As described below, proper values of the modification factor D and A_H can be determined by the curve fitting of actual experimental data.

EXPERIMENTAL WORK

In order to verify validity of the newly developed model and investigate the relationship between "true" yield stress and Bingham yield stress, experimental work is conducted for

cement pastes with different w/c. The yield stresses of these pastes are measured using a direct shear apparatus and a Brookfield rheometer. The test results are then compared with those obtained from the newly developed shear stress model.

Materials, proportions, and mixing procedures

Type I Portland cement was used in the experiments and its chemical and physical properties are shown in Table 2. Cement pastes were made with different w/c and without any supplementary cementitious materials (SCMs) and chemical admixtures. The pastes with w/c of 0.30, 0.35, 0.40, 0.42, 0.45, and 0.48 were used for the direct shear tests, and the pastes with w/c of 0.30, 0.35, 0.40, 0.45, 0.50, 0.55, and 0.60 were used for the Brookfield rheometer tests. All cement paste samples were mixed according to ASTM C305: Standard Practice for Mechanical Mixing of Hydraulic Cement Pastes and Mortars of Plastic Consistency [23]. The temperatures of mixing water and cement were all controlled at 25°C. The environmental temperature and relative humidity during the paste mixing and testing were 25 ±1.5 °C and 36±3 %, respectively.

Table 2—Chemical and physical properties of cement

Major Oxide Composition (%)	CaO	SiO_2	Al_2O_3	Fe_2O_3	MgO	SO_3
	64.20	20.80	5.55	2.25	1.91	2.96
Chemical Composition (%)	C_3S	C_2S	C_3A	C_4AF	Gypsum	
	53.71	19.58	6.14	10.59	0.78	
Physical Properties	Specific gravity			Fineness		
	3.15			$373 m^2/kg$		

Test methods

1. **Direct shear test**

ELE Direct/Residual Shear Apparatus for geotechnical material was used for dry cement paste mixes. The apparatus had a round shear area of 3167 mm^2 (4.9089 in^2). The shear rate of all cement paste samples was controlled as 1 mm/min. The total shear deformation was 5 mm (0.1969in). In order to prevent leakage of cement paste from the shear box, the gaps between upper and lower shear boxes and the gaps between the loading plate and the vertical surface of upper shear box were sealed with the mineral grease. Three different normal loads (0, 1 and 2 kg (0, 2.2046 and 4.4092 lb)) were applied to obtain the different shear stresses in the tested cement pastes. The entire shear test process (from the contact of the cement with water to the end of the test) took about 15 minutes.

2. **Brookfield rheometer test**

A Brookfield R/S SST200 rheometer was used to measure the rheology parameters of the cement pastes. The vane of the rheometer has 4 blades, 7.5 mm (0.2953 in) in width and 30 mm (1.1811 in) in height, extending outward from the shaft at 90º angles. The capacity of the torque of the rheometer ranges from 1.5 to 50 mNm (522.6 to 17420 in.lb.in).

In the present study, after placing the paste into the rheometer, the specimens were pre-sheared at a low rotation speed of 130rpm for 60 seconds. Then, the vane was stopped for 60 seconds, within which time the mixing vane was lifted and the sample was gently stirred to mitigate the formation of preferential shear planes due to particle orientation. The sample was then subjected to a controlled rate hysteresis loop where the rotation

speed was increased from 0 to 218 rpm over a 60 seconds period and then immediately decelerated back to 0 rpm.

Although the vane rheometer has been widely used in testing cement-based materials, the shear rate applied to the tested material is not calculable due to the unknown shearing pattern and the unknown thickness of the sheared layer. Some researchers have suggested using a calibration factor to convert the vane rotation speed and torque to shear rate and shear stress; however, the reference material for the calibration often has different behavior from cement-based materials[25]. Therefore, in this study, the torque (mNm) and vane rotation speed (rpm), instead of the shear stress and shear rate, are used in discussion of the test results.

RESULTS AND DISCUSSIONS

Direct shear test results

Due to the difficulties in mixing and testing a very dry or very wet paste, only the pastes with w/c ranging from 0.30 to 0.48 were performed for the direct shear test. Typical results of the direct shear tests from two sets of cement paste samples (w/c =0.30 and 0.40) are shown in Figure 2. It is observed that at the low w/c (0.3), the shear stresses of cement paste samples clearly increased with the normal stress applied. However, at the high w/c (0.4), the shear stresses of the corresponding cement paste samples was much lower and did not change very much with increased normal stress.

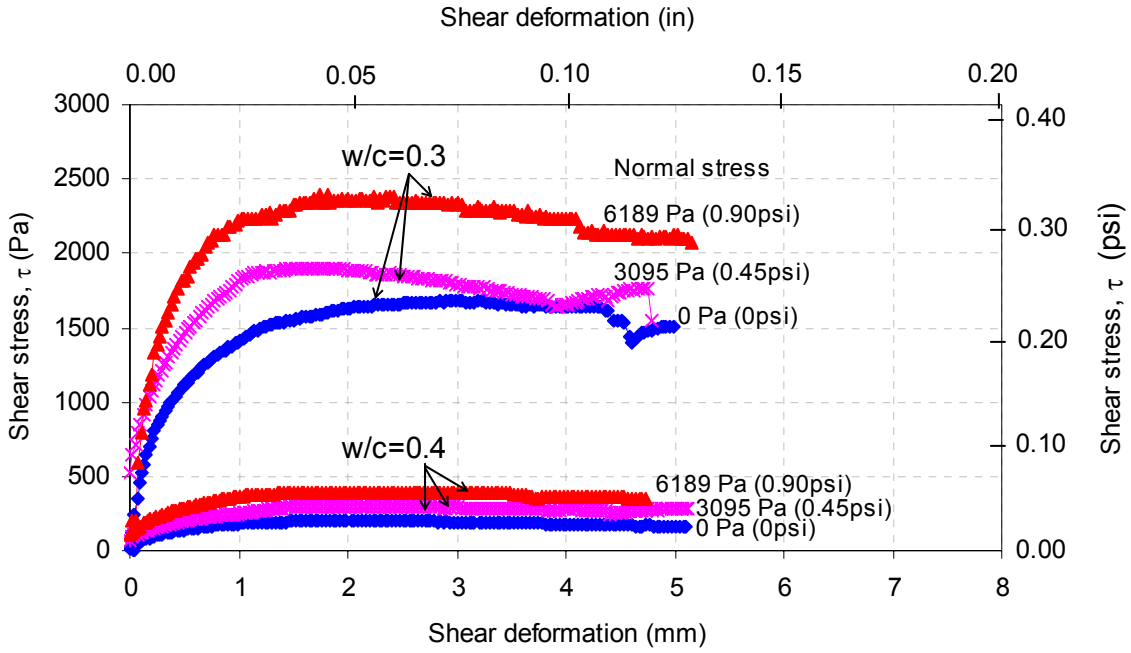

Fig. 2—Typical direct shear test results.

Figure 3 gives the relationship between the maximum shear stresses obtained from the curves in Figure 2 and their corresponding normal stresses. The relationship follows the format of Mohr-Coulomb equation, and therefore also called Mohr-Coulomb failure curves. The intercept of the linear line on the shear stress axis indicates the cohesion of the cement paste. The shear stress of the cement paste under zero normal stress in Figure 3 represents the rheological "true" yield stress, under which the cement paste material is in a static state. The angle between the linear line and the shear stress axis signifies the friction angle, which indicates the effect of normal stress on shear stress. It is noted that the friction angle is about 6.0^{o} for cement paste with w/c=0.3, and it decreases with increased w/c (1.8^{o} for w/c=0.4).

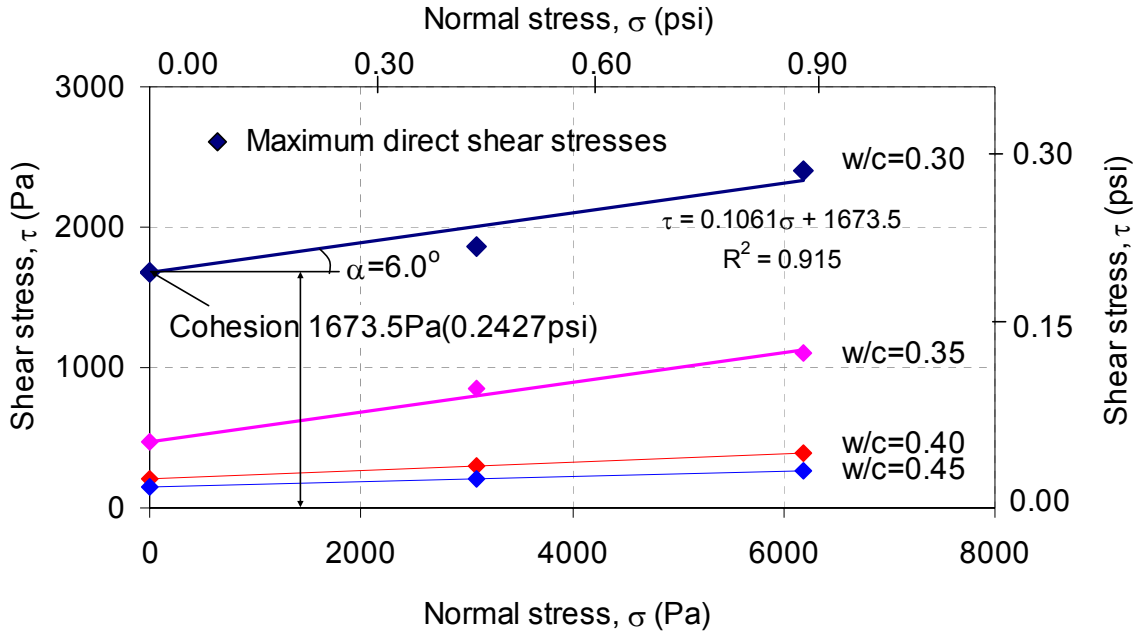

Fig. 3—Mohr-Coulomb failure curves of cement pastes.

Figure 3 depicts that the Mohr-Coulomb failure curves of cement pastes decrease with increased w/c. The "true" yield stresses from direct shear test, the shear stresses under zero normal stress in Figure 3, of the cement pastes also decrease with increased w/c. (They are 1673.5, 473.6, 202.1, and 148.4 Pa (0.2427, 0.0687, 0.0293, and 0.0215 psi) for pastes with w/c of 0.30, 0.35, 0.40, and 0.45, respectively.) This trend is consistent with the result from general rheological study of cement paste since increased w/c improves flow ability of a cement paste[4]. Figure 3 also illustrates that the friction angle of a cement paste decrease as its w/c increases. A significant change in shear stress is observed when w/c increases from 0.3 to 0.40.

As illustrated in Figure 3, for a cement paste with a low w/c (<0.4), shear stress increases significantly with its normal stress; while for a cement paste with a higher w/c, because

of higher flow ability and less particle assembly, the shear stress of the paste does not change very much with its normal stress, and the friction angle of the paste is small. This is very important information for studying the rheological behavior of cement paste with a low w/c (<0.4). It implies that conducting a rheometer test for a cement paste with w/c lower than 0.4 without considering the effect of normal stress is not appropriate. Such a normal stress may result from the self weight of the cement paste located above the shear zone or a confining stress from the boundary of the rheometer device.

Rheometer test results

Figure 4 shows the flow curves of cement pastes with different w/c from rheometer tests. Consistent with that observed from direct shear tests, significant change in the shapes of the flow curves occurs when w/c decreases from 0.4 to 0.3. As seen in Figure 4, the rheometer test generally produces a hysteresis loop, which contains two parts: the up and down curves. The area enclosed by the up and down curves reflects the thixotrophical behavior of a paste. Figure 4 demonstrates that the thixotrophical behavior of the paste with a low w/c is more significant than that of paste with a high w/c. This indicates that higher energy is required for the low w/c paste to make the shear deformation happen.

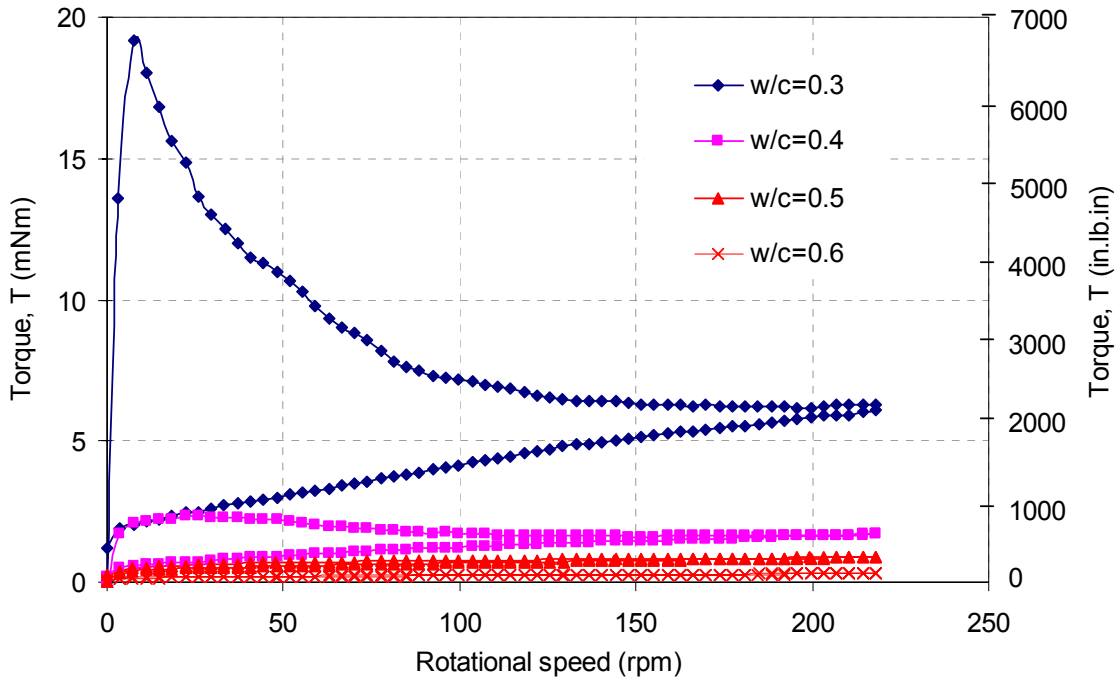

Fig. 4—Effect of w/c on paste rheological behavior.

In order to identify experimental scaling parameter (D) in the newly developed yield stress model and to compare the results from direct shear tests with those from the Brookfield rheometer tests, the shear stresses of the materials tested with the Brookfield rheometer are calculated from the torque measured by the rheometer using Equation 20: [24]

$$T = 2\pi r_v^2 \tau_c \left(\frac{H}{r_v} + \frac{2}{3} \right) \tag{20}$$

where T is the torque, r_v is the radius of the vane, H is the height of the vane, τ_c is the shear stress at the radius of the vane. As discussed below, when a particular torque is applied into Equation 20, the shear stress τ_c calculated from Equation 20 may become a

"yield stress". This yield stress can be compared with the yield stress measured from the direct shear test.

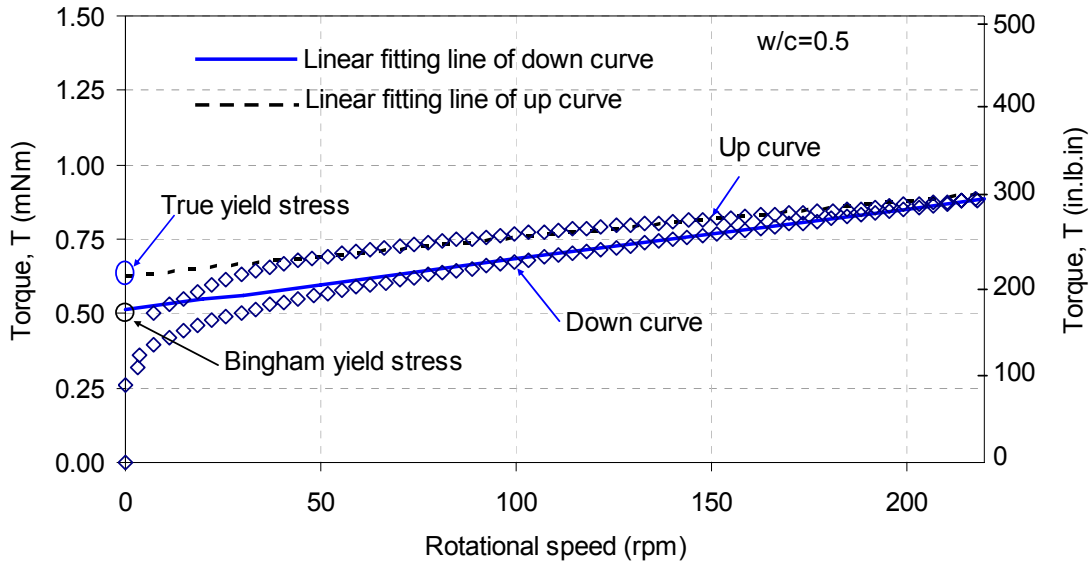

(a) Up curve without a peak value

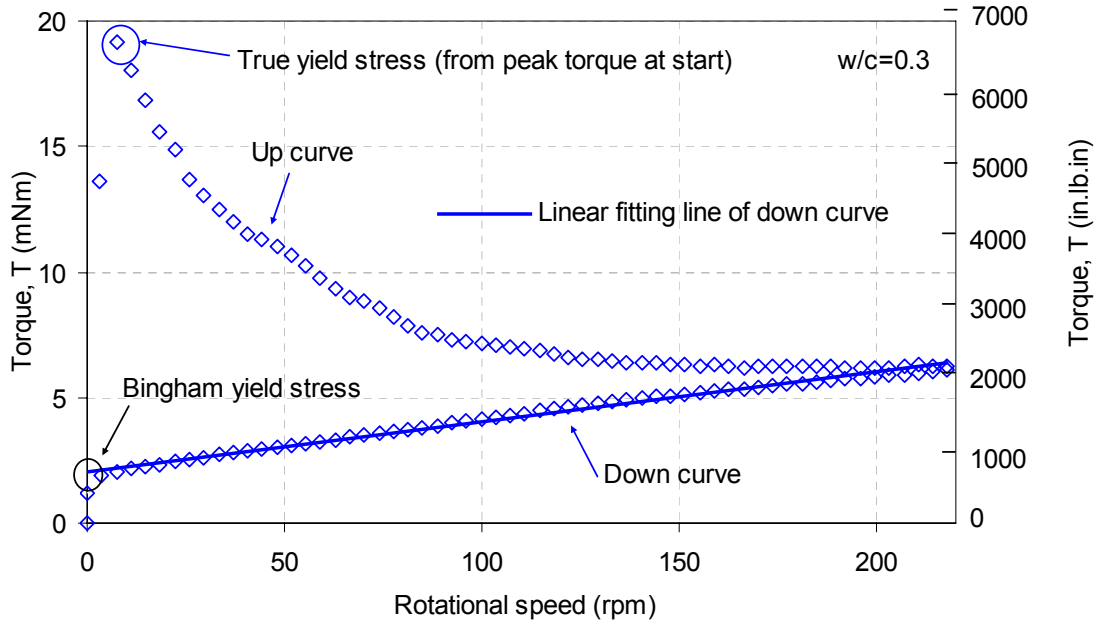

(b) Up curve with a peak value

Fig. 5— "True" and Bingham yield stress defined from typical flow curves.

In the present paste rheometer tests, the up curve of a hysteresis loop reflects the behavior change of the original cement paste (without de-agglomeration) from a solid state to a flow state. Thus, the yield stress calculated from the torque of this up curve corresponding to the vane rotation speed or the paste deformation of zero, is most likely the "true" yield stress. On the other hand, the down curve of a rheometer test reflects the behavior of the tested paste under a shear after its particle agglomerations are broken down. During this testing period, the cement paste possesses Bingham behavior. Thus the Bingham yield stress can be calculated from the torque of the down curve corresponding to the vane rotation speed of zero.

Figure 5 illustrates that the up curves have two different types of shapes: one with a clear peak torque (for the pastes with w/c =0.3 and 0.4) and one without a visible peak torque (for the pastes with w/c =0.5 and 0.6). For the up curve without a clear peak, as shown in Figure 5a, since there is no distinguished maximum torque before the paste flows and the minimum stress value is zero, a linear curve fitting of the up-curve appears the best way to obtain the yield stress of the up curve. In the present study, a linear curve fitting of the up flow curve is performed for the up curve without a clear peak value, and the shear stress calculated from the torque corresponding to the interception of the linear curve with the torque axis is defined as the "true" yield stress. For the up curve with a clear peak, as shown in (Figure 5b), the "true" stress of a cement paste is calculated according to Equation 20 from the peak value of the torque of the up curve since the peak generally occurs at a very small rotation speed. Bingham yield stress is determined from the torque corresponding to the interception of the linear portion of the down curve with the torque

axis [7]. The "true" and Bingham yield stresses from both rheometer and direct shear tests for all samples are listed in Table 3, and the discussions of these test results are given in the following section.

Table 3—Rheological yield stress of cement pastes

w/c	0.30	0.35	0.40	0.45	0.48	0.50	0.55	0.60
Bingham yield stress from rheology test, Pa(psi)	153.5 (0.0223)	51.3 (0.0074)	38.8 (0.0056)	30.5 (0.0044)	n/a*	25.5 (0.0037)	10.8 (0.0016)	10.0 (0.0015)
"True" yield stress from rheology test, Pa (psi)	1547.2 (0.2244)	395.7 (0.0574)	189.2 (0.0274)	53.3 (0.0077)	n/a*	53.2 (0.0076)	16.5 (0.0024)	15.7 (0.0023)
"True" yield stress from direct shear test at 0 normal stress, Pa (psi)	1673.5 (0.2427)	473.6 (0.0687)	202.1 (0.0293)	148.4 (0.0215)	142.1 (0.0200)	n/a*	n/a*	n/a*

* The test is not performed and the result is not available.

Comparison of test results

Table 3 illustrates that the "true" yield stresses measured from the direct shear tests and rheometer tests are very close, both of which are much higher than the Bingham yield stresses obtained from the rheometer tests. All yield stresses in Table 3 decreases with increased w/c regardless the testing and measuring methods. Such a similar trend provided by the different tests implies that there may be a correlation between the yield stress measurements from different test methods.

The small differences between the "true" yield stresses obtained from the direct shear and rheometer tests may result from the effect of thixotrophical behavior of the cement pastes. As displayed in Figure 4 and 5, at the very beginning of a rheometer test (or the

beginning part of the up flow curve), the vane of the rheometer needs much higher torque to conquer the yield stress of the tested cement paste so as to initiate a significant flow. This is due to the cement particle agglomeration, which is also the reason that cement paste has a yield stress and occurs more severely in the pastes with a low w/c even though a pre-shear procedure is applied in the rheometer test. In the direct shear test, no pre-shear procedure is applied. The shear rate is relative small when compared with that used in the rheometer test. As a result, the small difference in "true" yield stresses from the two test methods is anticipated.

Bingham yield stress is obtained from the down flow curve, where all cement particle agglomerations have been broken down. Thus, less stress is required for the cement paste to flow. Consequently, Bingham yield stress is lower than the "true" measured from the up flow curve.

Comparison of model and test results

The previous discussions on Table 3 have proven that even though the values of the yield stress obtained from different tests are different, the trends related to w/c influences the yield stress of cement pastes are similar. Because of this, an experimental scaling parameter (D) can be introduced in Equation 18. Using different D values, as described below, the relationships between the results from different rheological tests can be established.

First, Equation 18 is used to fits the "true" yield stress obtained from the direct shear tests (Figure 6). This good curve fitting results in a R^2 value of 0.9988. From the curve fitting, factors A_H and D are obtained as 2.80×10^{-17} and 1.25, respectively. (The A_H value of 2.8×10^{-17} falls in the range of $4.2x10^{-6}$~$2.3x10^{-20}$ as suggested by previous researchers.[2,13]) Since A_H is related to only the properties of the tested material, it should not change for the same material tested with different methods.

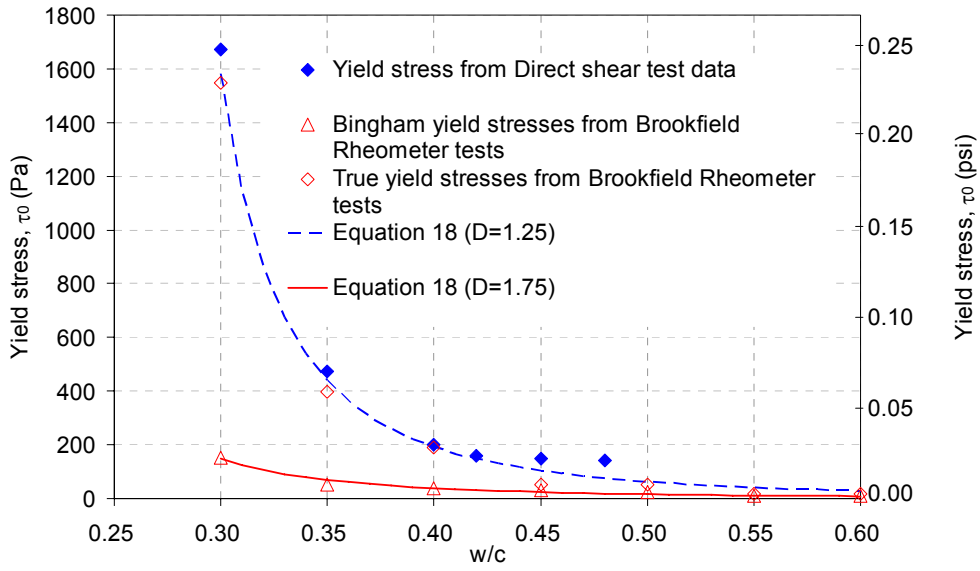

Fig. 6—Fitting of test data using Equation 18.

Given $A_H = 2.80\times10^{-17}$, Equation 18 is then applied to fit the "true" yield stress data obtained from the rheometer tests. This curve fitting results in a R^2 value of 0.9990 and an unchanged D value of 1.25. The same D value obtained from the curve fittings of the "true" yield stresses from the direct shear and rheometer tests indicates that these two test methods are directly correlated.

Using $A_H = 2.80 \times 10^{-17}$, Equation 18 is once again used to fit the Bingham yield stress data obtained from the rheometer tests (Figure 6). Consequently, the curve fitting results in a R^2 value of 0.9669 and a different D value of 1.75. This suggests that there is a difference but also a correlation between the yield stress from the direct shear and the Bingham yield stress from the rheometer tests.

Application of the present model to the published rheometer test results

In order to verify the validity of the newly developed model, Equation 18 is also employed to fit some published experimental data. Figure 7 shows the yield stress data collected from selected literatures, which cover different types of rheometer used and different ranges of w/c in pastes, as well as the results of the Equation 18 curve fitting on these data. Here, the Hamaker constant (A_H) of 2.80×10^{-17} is used again.

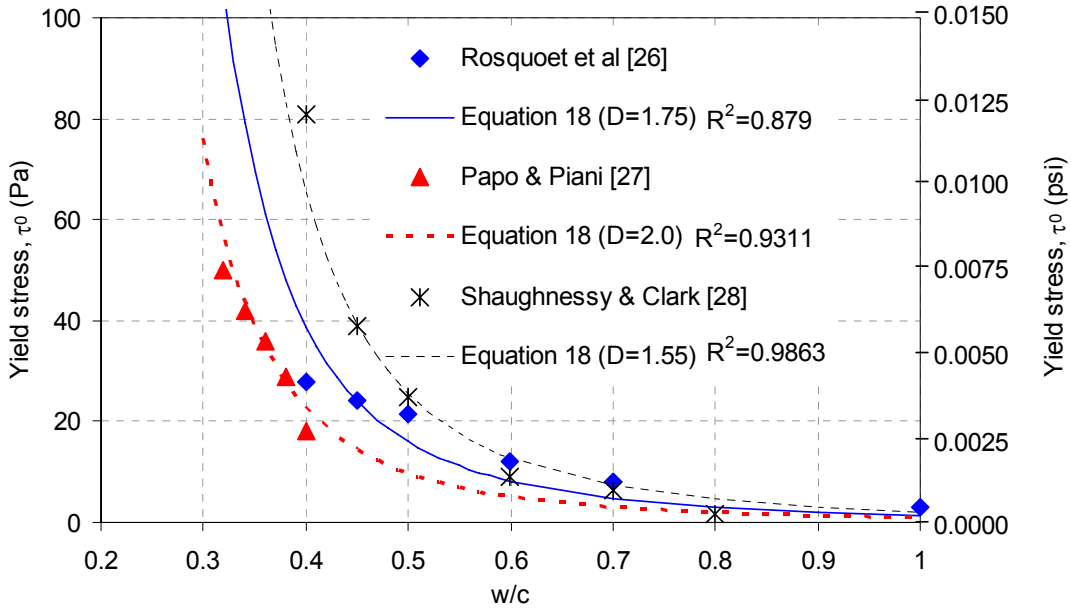

Fig. 7—Curve fitting of published data using Equation 18

Figure 7 indicates that the newly developed yield stress model fits all selected, published experimental data very well (R^2=0.8794-0.9863). The experimental scaling parameter (D) is 1.75 for the test data provided by Rosquoet et. al., who tested the yield stresses of cement pastes with a large variation of w/c (from 0.35 to 1.00) using a type Rhéomat 115 rheometer with a MS 145 type coaxial cylinder spindle[26]. The experimental scaling parameter (D) is 2.0 for the test data provided by Papo and Piani, who studied the cement pastes with w/c of 0.35~0.40 by using a rate-controlled coaxial cylinder viscometer Rotovisko-Haake[27]. The experimental scaling parameter (D) is 1.55 for the test data provided by Shaughnessy and Clark who studied the rheological properties of cement pastes with w/c of 0.4~0.8 using both concentric cylinder rotary viscometer and cone and plate viscometer[28].

The information presented in Figure 7 confirms that it is feasible not only to predict the yield stress of a cement paste but also to correlate the yield stresses from different experimental methods using an experimental scaling parameter (D=1.25~2.00). The newly developed yield stress model, based on the DLVO theory, well describes the basic physical principle that all cement pastes follow under shear stress.

CONCLUSIONS

In the present study, a yield stress model of cement paste is developed based on the DLVO theory. In this model, cement paste is considered as a suspension system and cement particles are rigid spheres in the suspension system. The shear stress of cement paste is determined by the interparticle electrostatic and dispersion forces alone with

probabilistic approach. To verify the validity of the newly developed model, two types of tests (direct shear and rheometer tests) are performed for a group of cement pastes with different w/c, and the model has been applied to three sets of published experimental data. The results indicate that:

1. The newly developed model can not only predict the yield stress of a cement paste but also correlate the yield stresses from different experimental methods using an experimental scaling parameter (D);
2. A normal stress has significant effect on yield stress of a cement paste with a low w/c (≤0.4). Therefore, the normal stress, possibly resulting from the material self weight and external loads, should be considered in paste rheology tests.
3. The "true" yield stresses measured from the direct shear test and rheometer tests are very close, especially at a low w/c (≤0.4), both of which are much higher than the Bingham yield stress measured from the rheometer test.

REFERENCES

1 Aïtcin, P. C.; Jolicoeur, C.; and MacGregor, J. G., "Superplasticizers: how they work and why they occasionally don't," *Concrete International*, V.16, No.5, 1994, pp. 45-52.

2 Flatt, R. J., Interparticle forces and superplasticizers in cement suspensions. Ph.D desertation,1999.

3 Kurokawa, Y.; Tanigawa, Y.; Mori, H.; and Komura, R., "Study on Slump Test and Slump-Flow Test of Fresh Concrete," *Transactions of the Japan Concrete Institute*, V. 16, 1994, pp. 25-32.

4 Tattersall, G. H., and Banfill, P. F. G., The rheology of fresh concrete, Pitman Publishing Inc., 1983.

5 Wallevik, O. H., and Gjorv, O. E., "Modification of the two-point workability apparatus," *Magazine of Concrete Research*. V. 42, No.152, 1990, pp. 135-142.

6 Hu, C., and de Larrard, F., "The rheology of fresh high performance concrete," *Cement and Concrete Research*, V.26, No.2, 1996, pp. 283-294.

7 Nehdi, M., and Mindess, S., "Applicability and significance of rheometric tests for rheology of fluid and self-leveling high-strength concrete," *Transportation Research Record*, V.1574, 1996, pp. 41-48.

8 Mori, H., and Tanigawa, Y., "Simulation methods for fluidity of fresh concrete," Memoirs of the School of Engineering, Nagoya University, V.44, No.1, 1992, pp. 71-134.

9 Collyer, A. A., and Clegg, D. W., Rheological Measurement. London and New York: Elsevier Applied Science, 1990.

10 Dzuy, N. Q., and Boger, D. V., "Direct yield stress measurement with the vane method," *Journal of Rheology*. V.29, No.3, 1985, pp. 335-347.

11 Dzuy, N. Q., and Boger, D. V., "Yield stress measurement for concentrated suspensions," *Journal of Rheology*, V.27, No.4, 1983, pp. 321–349.

12 Banfill, P. F. G., "The rheology of fresh cement and concrete - a review," Proceedings of the 11th International Congress on the Chemistry of Cement, Durban, South Africa, (Grieve, G., Owens, G., editors). V.1, 2003, pp. 50-62.

13 Derjaguin, B. V., and Landau, L., Acta Physicochim. *URSS,* V. 14, 1941, pp. 633–662.

14 Verwey, E. J. W., and Overbeek, J. Th. G., *Theory of Stability of Lyophobic Colloids*, Elsevier, Amsterdam, 1948.

15 Yang, M.; Neubauer, C. M; and Jennings, H. M., "Interparticle potential and sedimentation behavior of cement suepensions," *Advanced cement based material*, V.5, No.1, 1997, pp.1-7.

16 Li, Z.; Ohkubo, T.; and Tanigawa, Y., "Yield Model of High Fluidity Concrete in Fresh State," *Journal of Material in Civil Engineering*, V.16, No.3, 2004, pp. 195-201.

17 Kosmatka, S. H.; Kerkhoff, B.; and Panarese, W. C., Design and control of concrete mixture, 14th edition, Portland Cement Association, 2002.

18 Russell, W. B.; Saville, D. A.; and Schowalter, W. R., Colloidal Dispersions, Cambridge University Press: Cambridge, UK,1989.

19 Hunter, R. J., Foundations of Colloid Science, V. I; Oxford University Press: New York, 1987.

20 Sakai, E., and Daimon, M., "Dispersion mechanisms of alite stabilized by superplasticizers containing polyethylene oxide graft chains," American Concrete Institute, SP-173: 1997, pp. 187-201.

21 Mehrabadi, M. M.; Nemat-Nasser, S.; and Oda, M., "On statistical description of stress and fabric in granular Mechanics," *International Journal for Numerical and Analytical Methods in Geomechanics*, V.6, No.1, 1982, pp. 95-108.

22 CRC Handbook of chemistry and physics, R.C. Weast, Chemical Rubber Company: Cleveland, Ohio, 1970

23 ASTM C305-99, "Standard practice for mechanical mixing of hydraulic cement pastes and mortars of plastic consistency," ASTM International, West Conshohocken, Pa, 2003.

24 Nguyen, Q. D.; and Boger, D. V., (). "Yield stress measurement for concentrated suspensions", *Journal of Rheology*, V. 27, No.4, 1983, pp.321-349.

25 Barnes, H. A., and Carnali, J. O., "The vane-in-cup as a novel rheometer geometry for shear thinning and thixotropic materials," Journal of rheology, V. 34, No. 6, 1990, pp. 841-866

26 Rosquoet, F.; Alexis, A.; Khelidj, A.; and Phelipot, A., "Experimental study of cement grout - Rheological behavior and sedimentation," *Cement and Concrete Research*, V.33**,** No.5, 2003, pp. 713-722.

27 Papo, A., and Piani, L., "Flow behavior of fresh Portland cement pastes," *Particular Science and Technology*, V.22, No.5, 2004, pp. 201-212.

28 Shaughnessy, R., and Clark, P. E., "The rheological behavior of fresh cement pastes," *Cement and Concrete Research*, V.18, No.3, 1988, pp. 327-341.

LIST OF SYMBOLS

A_H	the Hamaker constant
$A_{all\ particles}$	total surface area of all cement particles in a unit volume of cement paste
$A_{single\ particle}$	surface area of single cement particle in a unit volume of cement paste
F_E	the interparticle electrostatic force
F_U	the interparticle dispersion force
$\overline{F}_x$	average value of interparticle force along x direction
h	interparticle distance
I_C	the ionic strength of the bulk solution defined as $I_C = \frac{1}{2}\sum C_i z_i^2$, where C_i is the ionic concentration of ion i in moles per liter, z_i is the valency of ion i
k	the Boltzmann's constant
N	number of cement particles in a unit volume of cement paste
N_A	the Avogadro's number
$P(\alpha,\beta)$	probability of a collision occurring at certain location
p	void content of cement particles
$\bar{r}$	mean radius of cement paste
S_C	specific gravity of cement
T	temperature

U_A the attractive potential

U_R the repulsive potential

V_{cement} volume of cement particles in a unit volume of cement paste

$V_{excess\ water}$ volume of excess water in a unit volume of cement paste

$V_{voids\ among\ cement}$ volume of voids in cement particles

V_{water} volume of water in a unit volume of cement paste

$\frac{w}{c}$ water to cement ratio

α angle of direction, see Figure 1

β angle of direction, see Figure 1

ε_0 the dielectric permittivity of free space

ε_r the relative dielectric constant of the liquid medium

ψ the zeta potential

κ the thickness of the electrical double layer defined by $\kappa = e\sqrt{\frac{I_C N}{\varepsilon_0 \varepsilon_r kT}}$

τ_P the shear stress of cement paste

CHAPTER 5. THEORETICAL AND EXPERIMENTAL INVESTIGATION INTO SHEAR FAILURE BEHAVIOR OF FRESH MORTAR

A paper submitted to ACI Material Journal

Gang Lu and Kejin Wang

Abstract

The shear failure behavior of fresh mortars was investigated using a force balance approach. In this approach, fresh mortar was considered as a two-phase material containing a matrix of cement paste and a group of rigid, spherical, non-cohensive aggregate particles. The shear force of a micro unit mortar, which consists of two contacted aggregate particles surrounded by a layer of cement paste, was first assessed based on the friction between these two contacted particles and the shear force carried by the cement paste of the micro unit. The shear force of a macro unit mortar was then calculated based the number of the contacted aggregate particles in the mortar and the shear force carried by the rest of cement paste. Forty-seven fresh mortar mixtures made with aggregate and paste having different characteristics and different mix proportions were tested using a direct shear apparatus. The experimental results were compared with those obtained from the model. The study indicated that the model and experimental results correlated well. The shear failure behavior of mortar follows the Mohr-Coulomb equation. The internal friction angle (ϕ_M) and cohesion (C_M) obtained from the Mohr-Coulomb curves of mortar decrease with the interparticle distance (S), which is in turn associated with the aggregate size, gradation, voids, and volume fraction. These research

results can provide researchers and engineers an insight onto proportioning of workable mortar and concrete mixtures.

Key words: mortar, shear failure, yield stress, friction, rheology

INTRODUCTION

Mortar occupies over 50% of concrete volume and has significant influence on concrete properties. In the development of a concrete mix proportion, the mortar phase is often designed and evaluated first so as to select appropriate combinations of water, powder, and admixtures and to take forward to concrete trial mixtures[1]. To ensure a workable concrete mixture, a layer of mortar with a sufficient thickness is required to coat the coarse aggregate particles for the mixture to have an adequate flow. In self-consolidating concrete (SCC), mortar has to have proper deformability for the concrete mixture to achieve self-consolidation and adequate yield stress to prevent segregation of coarse aggregate[2, 3]. Understanding the shear failure behavior of mortar is essential for designing a workable concrete mixture[4].

Concrete mixtures flow when subjected to a certain shear force. Two important rheological parameters are often used to describe the flow behavior of concrete materials: yield stress and viscosity. A “true” yield stress is the shear stress required by an elastic-visco material for initiating a plastic deformation. It is the maximum shear stress under which the material keeps in a static state[5]. A material must overcome the yield stress to transform from solid to liquid behavior. The present study is to investigate the yield behavior of a mortar and deals with the mortar material under a static state. Differently,

viscosity is the resistance of a material to flow, and it describes the material behavior in a dynamic state, which is not studied in the present paper.

Presently, yield stress of a concrete material is often determined by some workability tests [5, 6, 7]. The yield stresses measured from these tests are actually called Bingham yield stress, rather than the "true" yield stress. Due to the variations in the test equipment and procedures, the Bingham yield stresses obtained from different experiments often vary largely[5]. Some research has been conducted studying the relationship between the "true" and Bingham yield stresses[5, 7]. However, most of these studies are still based on experimental approaches. Recently, the authors of the paper investigated the yield behavior of cement pastes based on a theoretical approach and revealed the relationship between the "true" and Bingham yield stresses and the relationship between the yield stresses obtained from different experiments[8]. Nevertheless, the study on the "true" yield stress of mortar is still limited.

Li et. al. attempted to model the "true" yield stress of high flow ability fresh concrete[9]. They considered concrete as a particle assembly and assumed that the interparticle force was generated by the friction between the particles and the link resulting from the surface tension and suction of pore water. Although their model qualitatively described yield behavior of some cementitious materials, they neglected the factor that the cement particles are cohesive and aggregate particles are non-cohesive.

The objective of the present study is to investigate the shear failure behavior and "true" yield stresses of fresh mortars. In this study, the shear failure model is developed using a force balance approach from a microscale to macroscale level. Forty-seven (47) fresh mortar mixtures made with different water-to-cement ratios (w/c), sand-to-cement ratios (s/c), and different aggregate size and gradations were tested using a direct shear apparatus. The model was finalized by adopted the present experimental results.

RESEARCH SIGNIFICANCE

Limited work has been done studying the shear failure behavior of fresh mortar mixtures. Existing studies on the rheological yield stress of mortar materials are often experimental dependent. The results from the experimental tests vary largely depending upon the test equipment and methods, and they often provide researchers and engineers with only Bingham yield stress rather than "true" yield stress. In the present study, the shear failure behavior and "true" yield stresses of fresh mortars are investigated using a theoretical model as well as a direct shear test method. This new model, developed from the force balances of a mortar at both microscale and macroscale levels, can not only well predict the shear failure behavior of mortar materials but also explain the direct shear test results. The research provides a better understanding of the effects of the material properties and microstructure on the failure behavior of a fresh mortar. It offers an insight onto proportioning of workable mortar or concrete mixtures.

MODEL DEVELOPMENT

In the present model development, fresh mortar was considered as a two-phase material containing a matrix of cement paste and a group of rigid, spherical, non-cohensive aggregate particles. The shear force of a micro-scale mortar unit, also called a micro unit, which consists of two contacted aggregate particles surrounded by a layer of cement paste, was first assessed from all forces balanced on the micro slant surface of failure. The shear force was assumed resulting from the friction between these two contacted particles and the shear force carried by the cement paste of the micro unit. The shear force of a conventional unit volume of the mortar (such as a cubic centimeter or cubic meter of mortar), also called a macro-unit mortar, was then calculated based the number of the contacted aggregate particles in the macro unit and the shear force carried by the rest of cement paste. The number of the contacted aggregate particles in the macro-unit mortar was estimated based on the probability concept. The details in the shear stress model development are presented in the following sections.

Assumption and simplification

The following assumptions were made to simplify the mortar to be studied:

1. The cement paste of the mortar is an ideal elastic-viscous material with known rheological properties;
2. All aggregate particles in the mortar can be simplified as rigid, spherical, dry, and non-cohesive particles.

3. The different sizes of the aggregate particles can be represented by the single-sized spheres having a mean diameter (D_0) calculated based on the actual aggregate gradation;
4. The mortar is freshly mixed. Cement paste properties are constant. There is no bond between the cement paste and aggregate particles;
5. No static aggregate segregation occurs in the mortar mixture; and
6. No entrained or entrapped air voids are in the mortar.

Based on the above assumptions, a macro-unit volume of an actual mortar, composed of well-graded, irregular-shaped aggregate particles in a cement paste (Figure 1a), can be simplified as an "idea" mortar that consists of single-sized, rigid, spherical particles in a elastic-viscous paste (Figure 1c via Figure 1b).

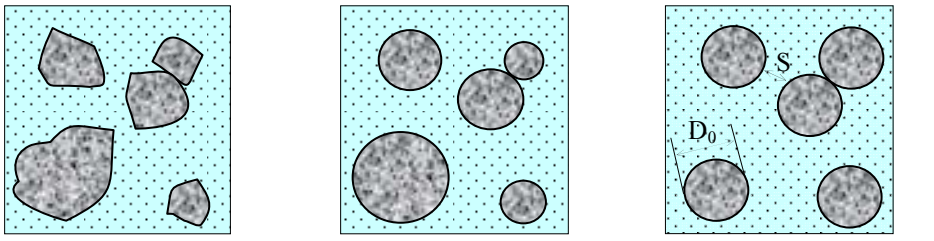

(a) a "real" mortar
(b) a simplified mortar (aggregate particles are rigid spheres)
(c) a further simplified mortar (aggregate particles are equal-sized rigid spheres)

Fig. 1—Simplification of fresh mortar system

Volumetric calculations

The mean diameter (D_0) of the single-sized spherical aggregate particles in Figure 1c can be determined by Equation 1, according to the actual aggregate gradation[10]:

$$D_0 = \left[\frac{1}{\sum p_i D_i^{-3}} \right]^{1/3} \quad (1)$$

where

D_0 the average diameter of the aggregate particles retained on a given sieve, i;

p_i volume fraction of the aggregate particles on the given sieve;

D_i the average diameter of the i-th group, $D_i = \frac{(D_i)_{max} + (D_i)_{min}}{2}$, where $(D_i)_{max}$ is the maximum diameter of i-th group and $(D_i)_{min}$ is the minimum diameter of i-th group; and

i the order of the sieves used.

The number of aggregate particles (N_{agg}) in a macro-unit volume of mortar having the aggregate volume fraction of V_{agg} is given by:

$$N_{agg} = \frac{V_{agg}}{\frac{4}{3} \cdot \pi \cdot \left(\frac{D_0}{2} \right)^3} = \frac{6V_{agg}}{\pi D_0^3} \quad (2)$$

The volume of void among the un-compacted aggregate particles ($V_{uncompacted\ agg\ voids}$) in the macro-unit volume of the mortar can be obtained from the un-compacted void ratio of aggregate particles ($n_{uncompacted\ agg}$) measured according to ASTM C1252:

$$V_{\text{uncompacted agg voids}} = \frac{n_{\text{uncompacted agg}}}{1 - n_{\text{uncompacted agg}}} \cdot V_{\text{agg}} \tag{3}$$

The volume of cement paste (V_{paste}) in the macro-unit volume of the mortar is:

$$V_{\text{paste}} = 1 - V_{\text{agg}} \tag{4}$$

The cement paste in a mortar that separates the aggregate particles and ensures the mortar to have a proper flow is called excess cement paste. The volume of the excess cement paste ($V_{\text{excess paste}}$) is defined as the total volume of the cement paste (V_{paste}) subtracts the volume of cement paste that fills the voids among the aggregate ($V_{\text{paste in voids}}$), which is equal to the volume of void among the un-compacted aggregate particles ($V_{\text{uncompacted agg voids}}$). The volume of the excess cement paste ($V_{\text{excess paste}}$) can be expressed as below[11]:

$$V_{\text{excess paste}} = V_{\text{paste}} - V_{\text{paste in voids}} = 1 - \frac{1}{1 - n_{\text{uncompacted agg}}} \cdot V_{\text{agg}} \tag{5}$$

The mean interparticle distance ($\overline{S}$) can be calculated from the volume of the excess cement paste in a macro-unit volume of mortar ($V_{\text{excess paste}}$), the number of aggregate particles in the mortar (N_{agg}), and the surface area of a single aggregate particle ($A_{\text{particle}} = \pi D_0^2$), as given below:

$$\overline{S} = \frac{2V_{\text{excess paste}}}{N_{\text{agg}} \cdot A_{\text{particle}}} = \frac{D_0}{3V_{\text{agg}}} \cdot \left(1 - \frac{V_{\text{agg}}}{1 - n_{\text{uncompacted agg}}} \right) \tag{6}$$

Stress Analyses

Figure 2 illustrates the mechanism by which the shear force (τ) in a macro-unit volume of a freshly mixed mortar subjected to a normal force (σ) generates in a given shear plane. (Note that these forces are equal to the corresponding stresses since a unit volume of mortar is considered in the model.) Based on the force balance concept, the external shear force (τ) generated by the applied normal force (σ) should be balanced by the internal shear force of the mortar material. Two sources of the shear forces are considered in the present model: (1) the friction between contacted aggregate particles and (2) the shear force carried by the cement paste (τ_p).

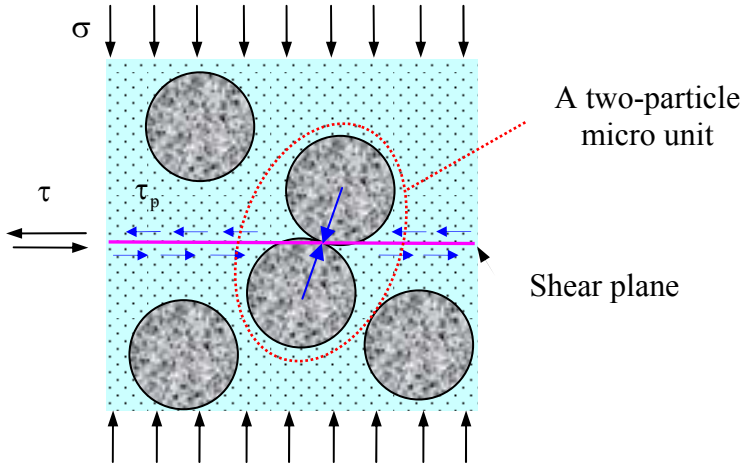

Fig. 2—Force acted on a macro unit of mortar

In order to obtain the overall stress of the mortar, the interaction of two particles is studied first. Figure 3a show a two-particle micro unit (i) out of a macro-unit of mortar (Figure 2). The two particles are coated with a uniform layer of cement paste except for the touching point C. The normal force applied on the micro-unit system (σ_i) and the shear force generated by these two contacted particles (τ_i) can be calculated as[13]:

$$\tau_i = f_i^x = f_i \cdot \sin\alpha \cos\beta ; \quad \text{and} \tag{7}$$

$$\sigma_i = f_i^y = f_i \cdot \cos\alpha \tag{8}$$

Where, f_i is the total force resulting from the two particle interaction (see Figure 3a, where it is assumed that particle j acts on particle i); f_i^x and f_i^y are shear and normal components of force f_i, respectively (see Figure 3a and 3c); α and β are position angles of force f_i in x-y-z coordinate (see Figure 3b).

The mean values of shear and normal stresses of a typical micro unit ($\bar{\tau}_i$ and $\bar{\sigma}_i$) are the product of the values provided by Equations 7 and 8 and the value of probability (P_i) that the force (f_i) falls in the range of a half sphere, as determined by the position angles α and β in Figure 3b, respectively. This probability value (P_i) can be expressed as Equation 9[12].

$$P_i(\alpha,\beta) = \frac{\sin\alpha \cdot d\beta \cdot d\alpha}{\pi} \tag{9}$$

Where, $\alpha \in \left[0 \ , \ \frac{\pi}{2}\right]$ and $\beta \in \left[-\frac{\pi}{2} \ , \ \frac{\pi}{2}\right]$.

Thus, the average shear and normal force of a typical micro unit can be obtained as:

$$\bar{\tau}_i = \int P_i(\alpha,\beta) \cdot \tau_i = 0.637 \cdot f_i \tag{10}$$

$$\bar{\sigma}_i = \int P_i(\alpha,\beta) \cdot \sigma_i = 0.5 \cdot f_i \tag{11}$$

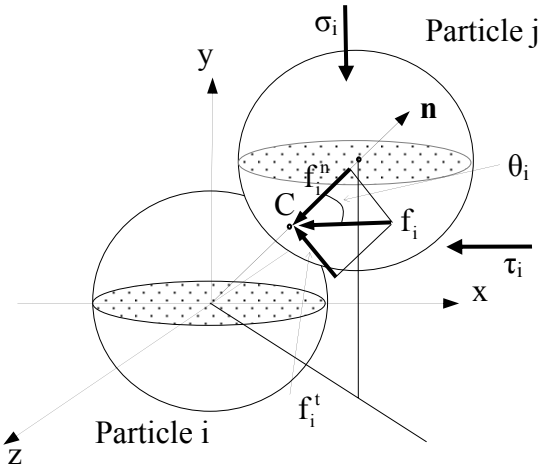

(a) Forces acted on a micro unit of morta

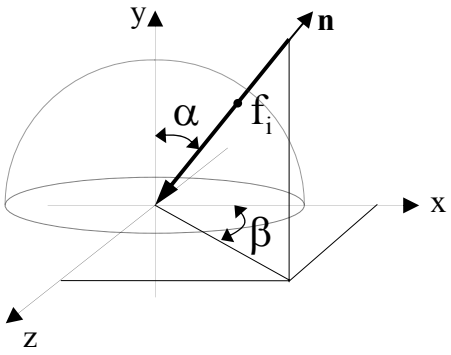

(b) Position of force f_i

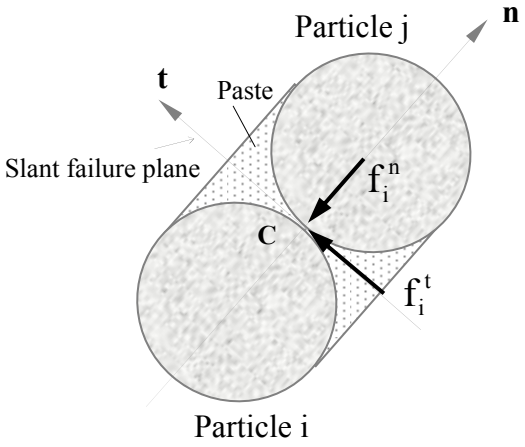

(c) Slant failure plan of the micro unit

Fig. 3─Stresses development in a micro unit of mortar

The forces balance on the slant failure plane of the micro unit (f_i^t, see Figures 3 a and c), is assumed resulting from the friction between the two contacted particles and the shear force carried by the cement paste of the micro unit, and it can be expressed as:

$$f_i^t = f_c + f_i^n \cdot \mu \tag{12}$$

where $f_i^t = f_i \cdot \sin\theta$, $f_i^n = f_i \cdot \cos\theta$, θ is the local concentrated angle of two contact aggregate particles, which will be discussed in detail later; μ is the friction coefficient of the aggregate particles; and f_c is the shear force generated by cement paste on the slant plane. f_c is determined by:

$$f_c = \tau_P \cdot A_{\text{paste of a micro unit}} \tag{13}$$

where, $A_{\text{paste of a micro unit}}$ is the area of the cement paste enclosed by the two aggregate particles of a micro unit and projected on the slant failure plane, or $A_{\text{paste of a micro unit}} = \pi D_0^{\,2}/4$.

Combining Equations 10 to 13, the following equation can be obtained:

$$\frac{\bar{\tau}_i}{0.637} \cdot \sin\theta = \frac{\bar{\sigma}_i}{0.5} \cdot \cos\theta \cdot \mu + \tau_p \cdot A_{\text{paste of a micro unit}} \tag{14}$$

Through a different study, the authors have found the correlation between aggregate particles friction angle (ϕ_{agg}) and their friction coefficient (μ) as $\tan(\phi_{agg}) = 1.274 \cdot \mu$ [13]. Thus, Equation 14 can be rewritten as:

$$\bar{\tau}_i = \frac{\tan\phi_{agg}}{\tan\theta} \cdot \bar{\sigma}_i + \frac{0.637\tau_p \cdot A_{\text{paste of a micro unit}}}{\sin\theta} \tag{15}$$

Equation 15 gives the mean value of the shear force generated by a micro unit containing two contacted aggregate particles.

It is assumed that in a macro-unit shear plane, there are N_{agg} aggregate particles (see Equation 2), and the probability that these aggregate particles getting in touch is known as P. (The calculation of P value will be discussed later.) Thus, the subtotal shear stress resulting from the friction of the contacted aggregate particles in the shear plane (τ_{agg}) can be expressed as:

$$\tau_{agg} = P \cdot N_{agg} \cdot \tau_i = P \cdot N_{agg} \cdot A_{\text{paste of a micro unit}} \left(\frac{\tan \phi_{agg}}{\tan \theta} \cdot \sigma + \frac{0.637}{\sin \theta} \cdot \tau_p \right) \quad (16)$$

The shear force resulting from the net cement paste (τ_{NP}), not including the paste enclosed by the touched aggregate particles, in the macro-unit shear plane of mortar is:

$$\tau_{NP} = \tau_P \cdot A_P = \left(1 - P \cdot N_{agg} \cdot A_{\text{paste of a micro unit}} \cdot \cos\alpha\right) \cdot \tau_P \quad (17)$$

where, A_p is the net area of cement paste in a macro-unit volume of mortar. It is the area of the macro-unit shear plane subtracting the area of the paste enclosed in all micro units of contacted aggregate particles. A_p can be calculated as:

$$A_P = 1 - P \cdot N_{agg} \cdot A_{\text{paste of a micro unit}} \cdot \cos\alpha \quad (18)$$

Combining Equation 16, 17, and 18, the total shear force generated in the macro-unit mortar shear plane (τ_M) becomes:

$$\tau_M = \tau_{NP} + \tau_{agg} = \left(1 - 0.5 \cdot P \cdot N_{agg} \cdot A_{\text{paste of a micro unit}}\right) \cdot \tau_P + P \cdot N_{agg} \cdot A_{\text{paste of a micro unit}} \left(\frac{\tan \phi_A}{\tan \theta} \cdot \sigma + \frac{0.637}{\sin \theta} \cdot \tau_p \right) \quad (19)$$

Equation 19 can be simplified as:

$$\tau_M = \frac{3 \cdot P \cdot V_{agg}}{2 \cdot D_0 \cdot \tan \theta} \cdot \tan \phi_{agg} \cdot \sigma + \left[1 + \left(\frac{0.9555}{\sin \theta} - 0.75 \right) \cdot \frac{P \cdot V_{agg}}{D_0} \right] \cdot \tau_P \quad (20)$$

$$\text{Given} \quad \tan \phi_M = \frac{3 \cdot P \cdot V_{agg}}{2 \cdot D_0 \cdot \tan \theta} \cdot \tan \phi_{agg} = P_1 \cdot \tan \phi_{agg} \quad (21)$$

$$\text{and } C_M = \left[1 + \left(\frac{0.9555}{\sin \theta} - 0.75 \right) \cdot \frac{P \cdot V_{agg}}{D_0} \right] \cdot \tau_P = [1 + P_2] \cdot \tau_P, \quad (22)$$

Equation 20 can be rewritten as:

$$\tau_M = \tan \phi_M \cdot \sigma + C_M \quad (23)$$

$$\text{or } \tau_M = P_1 \cdot \tan \phi_{agg} \cdot \sigma + (1 + P_2) \cdot \tau_P \quad (24)$$

$$\text{Where, } P_1 = \frac{3 \cdot P \cdot V_{agg}}{2 \cdot D_0 \cdot \tan \theta} = \frac{\tan \phi_M}{\tan \phi_{agg}}; \text{ and } P_2 = \left(\frac{0.9555}{\sin \theta} - 0.75 \right) \cdot \frac{P \cdot V_{agg}}{D_0} = \frac{C_M}{\tau_P} - 1.$$

Since P_1 and P_2 containing the probability term (P), they are called probability parameters. τ_p is the yield stress of cement paste, which can be obtained from either rheology test or modeling[8].

It is noted that the form of Equation 23 is the same as that of the Mohr-Coulomb equation, which is commonly used to express the shear failure condition of rock or soil. Correspondingly, ϕ_M can be defined as the friction angle and C_M can be defined as the

cohesion of mortar. C_M is also the yield stress under zero normal stress, or the rheological "true" yield stress of the mortar.

Based on Equations 23 and 24, the value of $\tan\phi_M$ is dependant upon the aggregate characteristics (ϕ_{agg} and D_0) and volume fraction (V_{agg}), the probability with which the aggregate particles in a mortar under a shear force may get in touch (P), and the local force concentrate angle (θ). As explained in the following, both θ and P depend upon the mean interparticle distance (S), which also relies on aggregate characteristics and volume fraction.

The angle θ randomly varies in the range of (0 º, 90 º]. When θ=90 º, a layer of excess cement paste exists between aggregate particles of the mortar (or S>0), and there is no touch between the aggregate particles ($\tan\phi_M = 0$). Thus, the yield condition of fresh mortar (Equation 23) becomes $\tau_M = C_M$. When θ=0 º, all forces applied onto two adjacent aggregate particles are coaxial with the axis connecting the gravity centers of the two particles, which is an extreme interlock situation. In this case, the mortar is not a particle assembly but a piece of solid. As a result, θ of a mortar should be larger than zero.

As discussed later, the probability parameters P_1 and P_2 can be obtained from their relationship with S through the curve fitting of test data. Like parameters V_{agg}, D_0, and S, P_1 and P_2 are also material-related parameters and depending on the mortar mix proportion. Therefore, the quantitative predictions for the friction angle (ϕ_M) and

cohesion (C_M) of mortar can still be achieved from Equations 23 and 24 with no need of any experimental results.

Note that Equation 24 is a different format of Equation 23. As discussed later, using Equation 24, the parameters (ϕ_M and C_M) of Equation 23 can be studied more easily.

EXPERIMENTAL WORK

In order to verify validity of the newly developed model and find out the effects of mortar material properties on yield stress, a group of mortar mixtures made with different w/c, s/c, and sand gradations were tested by using a direct shear test.

Materials

Type I portland cement was used in mortar, and its chemical and physical properties are shown in Table 1. No chemical admixture was employed. River sand was used as fine aggregate, and its specific gravity was 2.63 under the saturated surface dried (SSD) condition and 2.59 under the oven dried (OD) condition. Four single-sized aggregates (#16, #30, #50 and #100) and three graded aggregates (G1, G2, and G3, with fineness modulus (F.M.) of 3.40, 2.81 and 2.25 respectively) were used. G1 and G3 are the high and low limits of ASTM C33, Standard Specification for Concrete Aggregates, and G2 is in the middle of G1 and G3. The other properties of the aggregate are presented in Table 2. The uncompacted void content of the aggregates were measured according to ASTM C1252, the Standard Test Method for Uncompacted Void Content of Fine Aggregate. The

average diameter of the aggregates (D_0) was calculated from Equation 1. The friction angles of the aggregates (ϕ_{agg}) were obtained from a direct shear test[13].

Table 1 – Chemical and physical properties of cement

Oxide Composition (%)	CaO	SiO_2	Al_2O_3	Fe_2O_3	MgO	SO_3
	62.96	20.96	4.54	3.48	2.91	2.77
Chemical Composition (%)	C_3S	C_2S	C_3A	C_4AF	Gypsum	
	53.71	19.58	6.14	10.59	0.78	
Physical Properties	Specific gravity			Fineness		
	3.15			$373 m^2/kg$		

Table 2 – Aggregates and properties

ID	Uncompacted void content	Average diameter, D_0 (mm)	Friction angle*, ϕ_{agg} (º)
RS#16	0.420	1.770	41.03
RS#30	0.445	0.890	41.31
RS#50	0.450	0.450	41.31
RS#100	0.458	0.225	41.24
RS-G1	0.358	0.523	41.17
RS-G2	0.372	0.364	40.99
RS-G3	0.395	0.222	41.24

Mix Proportions

Three cement pastes made with different w/c were used in mortar. Table 3 gives the yield stresses of the pastes, measured by a BROOKFIELD rheometer[8]. Table 4 shows the

mortar mix proportions with different w/c, s/c, aggregate size and gradations. A total of 47 mortar mixtures were studied.

Table 3 – Cement pastes and properties

Paste #	P1	P2	P3
w/c	0.35	0.40	0.45
Yield stress, τ_p (Pa)	473.6	205.2	148.4

Table 4 – Mortar mix proportions

Aggregate	Paste	s/c
#16	P1, P2, P3	1
#30	P1, P2, P3	1
#50	P1, P2, P3	1
#100	P3	1
G1	P1, P2, P3	1
G2	P1, P2, P3	1
G3	P1, P2, P3	1
#16	P1, P2, P3	2
#30	P2, P3	2
#50	P2, P3	2
#100	P3	2
G1	P1, P2, P3	2
G2	P1, P2, P3	2
G3	P1, P2, P3	2
#16	P3	3
#30	P3	3
G1	P1, P2, P3	3
G2	P1, P2, P3	3
G3	P1, P2, P3	3

Mixing Procedure

All cement and mortar samples were mixed according to ASTM C305 “Standard Practice for Mechanical Mixing of Hydraulic Cement Pastes and Mortars of Plastic

Consistency"[14]. The temperature of mixing water was controlled at 25°C (77°F). The environmental temperature and relative humidity were 25±1.5°C (77±2.7°F) and 36±3%, respectively, during the sample mixing and the Rheometer and direct shear tests.

Direct Shear Test

ELE Direct/Residual Shear Apparatus for geotechnical material was used in present study. The apparatus have a round shear area, which is 3167 mm^2 (4.9089in^2). The shear rate was controlled as 1 mm/min. The total shear deformation is 5 mm (0.1969in). In order to prevent the leaking of cement paste in the shear box, the gapes between upper and lower shear boxes and the gapes between the loading plate and the vertical surface of upper shear box were sealed with the mineral grace. Three different normal stresses (0; 30,945; and 61,890 Pa (0; 4.4883; and 8.9765 psi)) were applied to the mortar samples. The whole shear test process (from the contact of the cement with water to the end of the test) is about 15 minutes.

RESULTS AND DISCUSSIONS

Typical direct shear test results

Figure 4a shows the typical direct shear test results of a mortar sample (w/c=0.35; s/c=1, RS#30) under three different levels of normal stresses (0; 30,945; and 61,890 Pa (0; 4.4883; and 8.9765 psi)). It is observed in the figure that shear stress of the mortar increases with normal stress. The peak shear stress of each curve can be considered as the failure shear stress of the mortar under the given normal stress. As a result, the relationship between the failure shear stress and its normal stress of the mortar samples

presented in Figure 4a can be plotted as Figure 4b. This relationship, approximately linear, is similar to that described by the Mohr-Coulomb equation that is commonly used to express the shear failure condition of rock and soil. Comparably, the internal friction angle (ϕ_M) of the mortar can be determined from the slope of the failure shear stress-normal stress curve, and the cohesion (C_M) can be determined from the intercept of the linear fitting line on shear stress axis. Based on the rheological definition, the rheological yield stress of the tested mortar is the failure shear stress at zero normal stress, under which the fresh mortar will not have shear deformation. This rheological yield stress from the direct shear test can be considered as the "true" yield stress of mortar.

Since both Equation 23 and the failure shear stresses measured by the direct shear tests of a mortar under different normal stresses follow the format of the Mohr-Coulomb equation, the validity of Equation 23 is primarily proven. Thus, the prediction of Equation 23 can be compared with the experimental results obtained from the direct shear tests, and the parameters in Equation 23 can also be obtained from the fitting of the test data. The features of the Mohr-Coulomb failure curves of the designed mortars are further discussed in the rest parts of the paper.

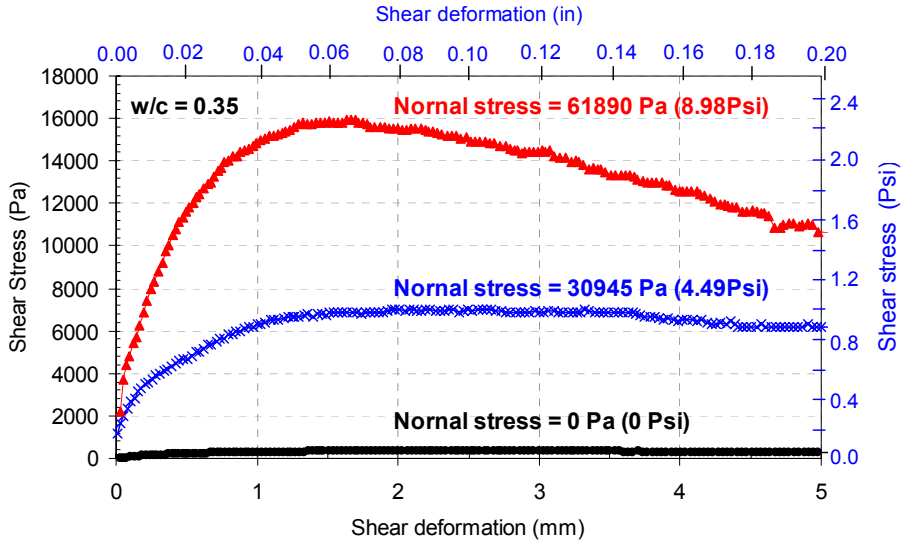

(a) Effect of normal stress on the direct shear test results

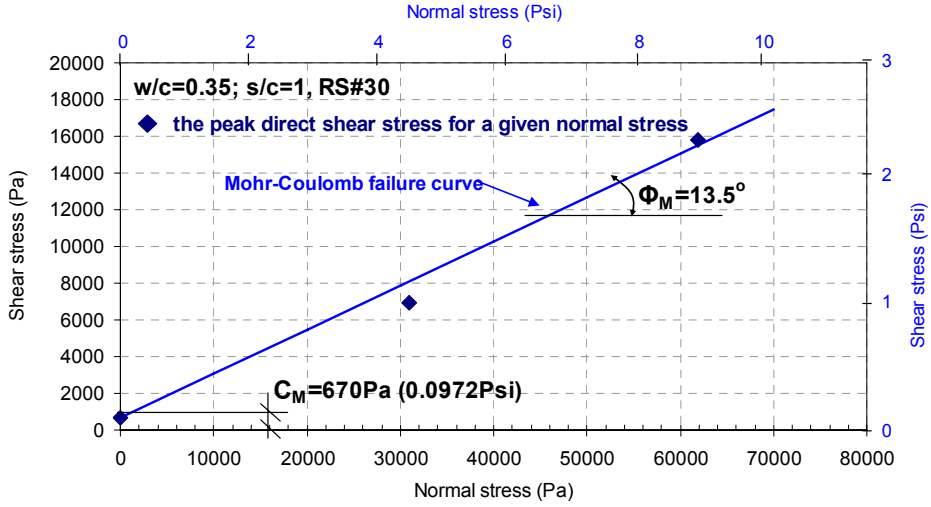

(b) Mohr-Coulomb failure curve of a mortar

Fig. 4—Typical direct shear results of a mortar sample (w/c=0.35; s/c=1, RS#30)

Effect of cement paste

Figure 5 shows the Mohr-Coulomb failure curves of the mortar samples made with the same aggregate volume fraction (s/c=1) and average particle size (#30) but different cement paste yield stress (τ_p): 473.6, 205.2, and 148.4Pa (0.069, 0.030, and 0.022 psi) (w/c: 0.35, 0.40, and 0.45, correspondingly). As observed in the figure, the cohesion of a mortar (C_M) increases as the yield stress of a cement paste (τ_p) increases or the w/c of the cement paste decreases. This indicates that a larger force is required to initiate a flow for a cement paste with a higher yield stress or lower w/c, which is consistent with the widely accepted knowledge[15]. However, the friction angle (ϕ_M) of the mortar has no significant change with the cement pastes. This is also consistent with the Equation 17b, which indicate that the yield stress of a cement paste (τ_p) influences only the cohesion of a mortar.

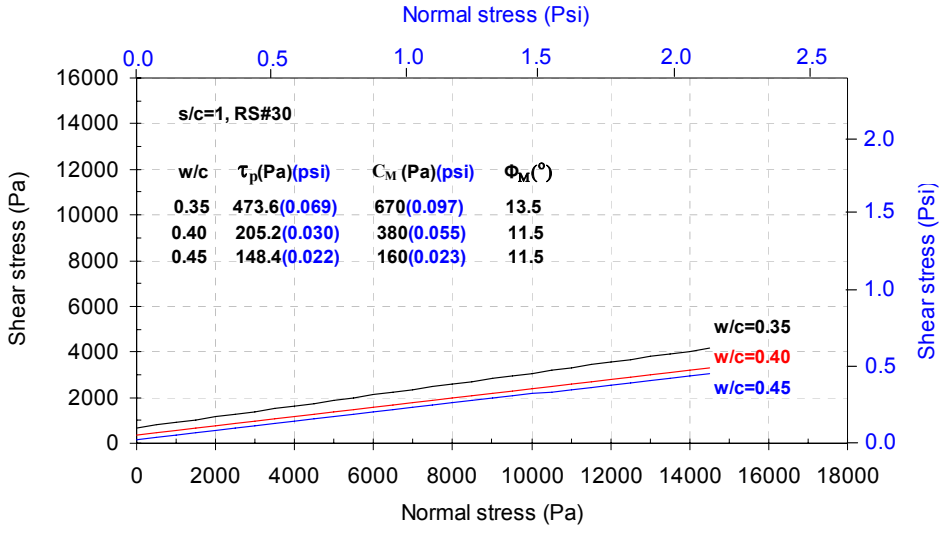

Fig. 5—Effect of cement paste on mortar shear failure curves

Effect of aggregate content

Figure 6 shows the Mohr-Coulomb failure curves for mortars made with the same cement paste (w/c=0.45) and average aggregate size (#30) but different aggregate volume fractions (s/c=1, 2, and 3). The Mohr-Coulomb failure curves of mortars show that both the cohesion (C_M) and internal friction angle (ϕ_M) of the mortar increase with the increased s/c. As indicated in Equation 6, increased aggregate volume (V_{agg}) in the mortar decreases the interparticle distance (S), which is related to the local force concentrate angle (θ) and probability parameters (P_1 and P_2). Thus, both the cohesion (C_M) and internal friction angle (ϕ_M) of the mortar are influenced as illustrated in Equations 20 and 21.

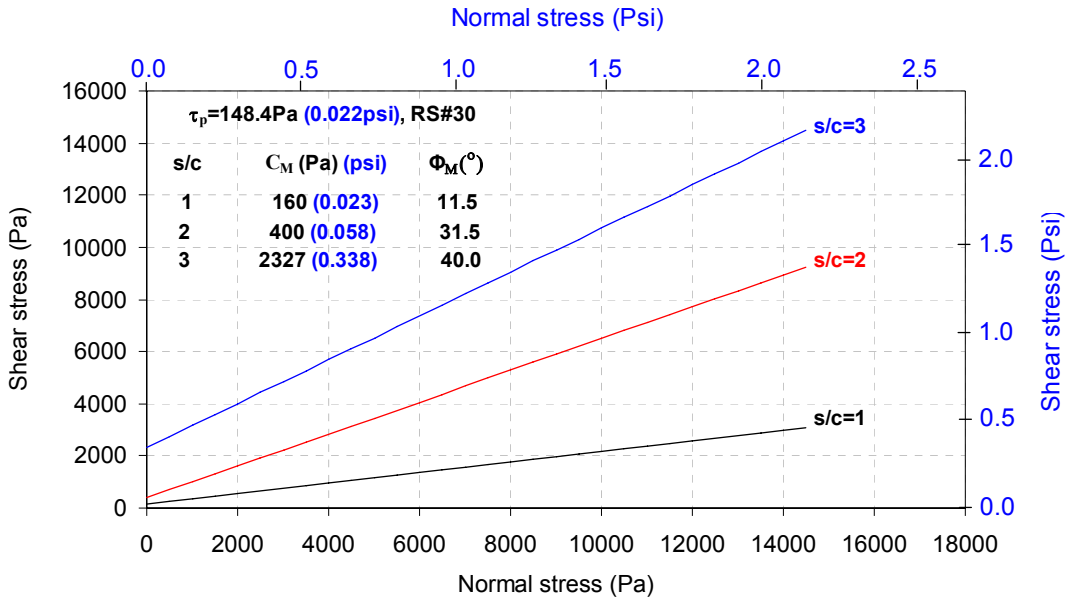

Fig. 6—Effect of aggregate content on mortar shear failure curves

Effect of aggregate size

Figure 7 shows the Mohr-Coulomb failure curves of the mortars made with a given paste (w/c=0.45) and aggregate volume fraction (s/c=2) but different aggregate sizes. The figure illustrates that the mortar made with larger aggregate has lower cohesion (C_M) and internal friction angle (ϕ_M), which suggests that the mortar has higher flowability. As indicated in Equation 6, increased aggregate size (D_0) in the mortar increases the interparticle distance (S), which suggests that a thicker layer of cement paste is coated on the aggregate particles of the mortar, thus, increasing mortar flow ability. This agrees with the common finding that a decrease in maximum size of aggregate generally increases the water demand of the concrete for the same flowability[15].

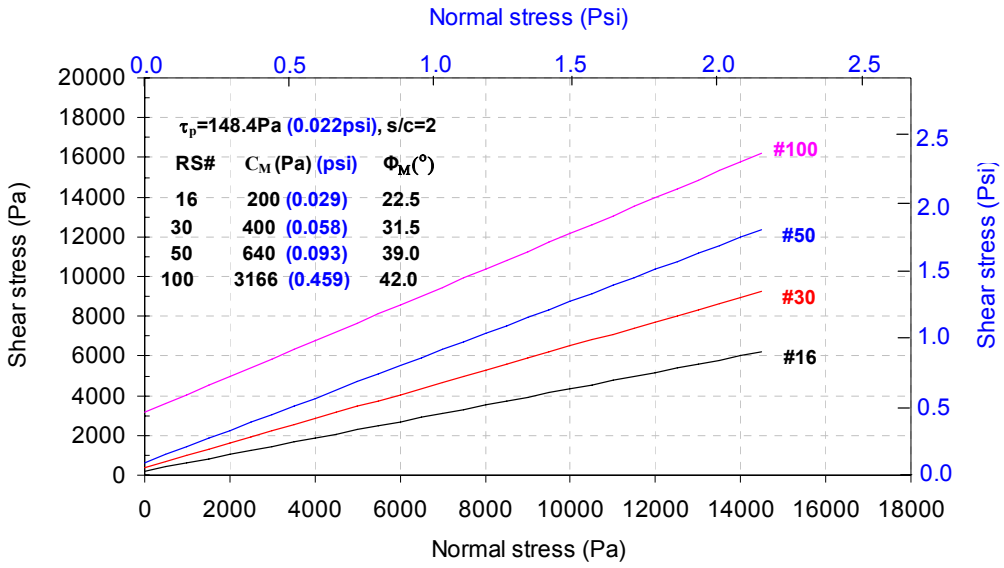

Fig. 7—Effect of aggregate size on mortar shear failure curves

It should be mentioned that Figures 5-7 also indicate that the normal stress has significant effect on failure shear stress of mortar, especially on that of the low flowable mortar. Therefore, in a rheology test, the normal stress, which often results from the self weight

of the tested material above the shear zone and the lateral confine stress from the boundary of container, should not be neglected.

Effect of the mean interparticle distances (S) on relative shear stresses (C_M / τ_P)

As mentioned previously, the distance between aggregate particles has significant effects on the cohesion (C_M) and friction angle (ϕ_M) of the mortar. In the following two sections, these effects are investigated in detail.

Figure 8 shows the relationship between the mean interparticle distances ($\bar{S}>0$) and the relative yield stress of mortar (C_M / τ_P), where $\bar{S}$ is calculated from Equation 6; C_M is the shear stress of a mortar at zero normal stress, also called the cohesion or "true" yield stress of the mortar; and τ_P is yield stress of the cement paste in the mortar. It should be noted that the test data for $\bar{S}<0$ are not included in this figure because it indicates that the volume of the cement paste in the macro unit of mortar is not enough to fill up the voids among the aggregate particles. At this situation, the shear stress resulting from the net cement paste of the mortar (τ_{NP}) as expressed in Equation 17 becomes negative. In an actual mortar, this shear stress (τ_{NP}) should not be negative; therefore, the mortar having a mean interparticle distance $\bar{S}>0$ is assumed and studied in the present study.

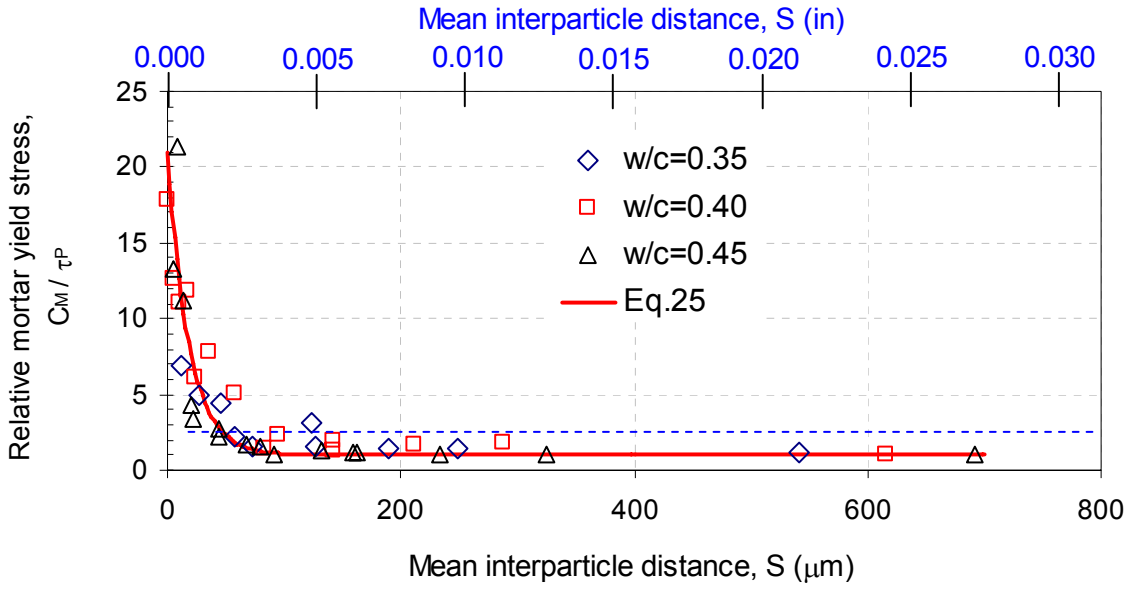

Fig. 8—Effect of the mean interparticle distance on relative yield stress of mortar

The best fitting curve of the test data presented in Figure 8 is given as Equation 25 (R^2 = 0.8074):

$$\frac{C_M}{\tau_P} = 20 * e^{-0.0546*\overline{S}} + 1 \qquad (25)$$

where, $\overline{S}$ is in micrometer (μm)*.

* 1μm= 3.9370e-005in

As illustrated in the Figure 8 and Equation 25, the relative yield stress (C_M / τ_P) decreases with increased mean interparticle distance ($\overline{S}$) of a mortar. When $\overline{S}$ is approximately less than 300 μm, C_M / τ_P increases very rapidly. However, when $\overline{S}$ is larger than 300 μm, C_M / τ_P is converged to 1, which suggests that the yield stress of the mortar is equal to the yield stress of the cement paste in the mortar. This research finding is valuable for concrete practice. It suggests that when a mortar (such as a self-

consolidating grout) has a large mean interparticle distance ($\overline{S}$), the rheological properties of its cement paste would play more important role in controlling the mortar flow ability. For a mortar with given cement paste, aggregate size, gradation, and volume friction can be adjusted in mix design to achieve a workable mortar or concrete.

Effect of the mean interparticle distances (S) on relative friction angles (ϕ_M/ϕ_{agg})

Figure 9 shows the relationship between the mean interparticle distances ($\overline{S}>0$) and relative friction angles of mortar (ϕ_M/ϕ_{agg}), where ϕ_M and ϕ_{agg} are measured from direct shear tests. The best fitting curve of the test data is given as Equation 26 (R^2=0.9505):

$$\frac{\phi_M}{\phi_{agg}} = e^{-0.004\cdot\overline{S}} \tag{26}$$

As illustrated in Figure 9 and Equation 26, the relative friction angle of a mortar (ϕ_M/ϕ_{agg}) decreases steadily (in a hyperbolic logarithm form) with increased interparticle distance ($\overline{S}$) of the mortar. The influence of the interparticle distance ($\overline{S}$) on the relative mortar friction angle (ϕ_M/ϕ_{agg}) is relatively less than that on the relative mortar cohesion (C_M/τ_P).

Probability parameters and final shear failure stress model

Based on the discussions above, the two probability parameters, $P_1 = \frac{\tan\phi_M}{\tan\phi_{agg}}$ (Equation 21) and $P_2 = \frac{C_M}{\tau_P} - 1$ (Equation 22), should also correlate to the mean interparticle distance (S).

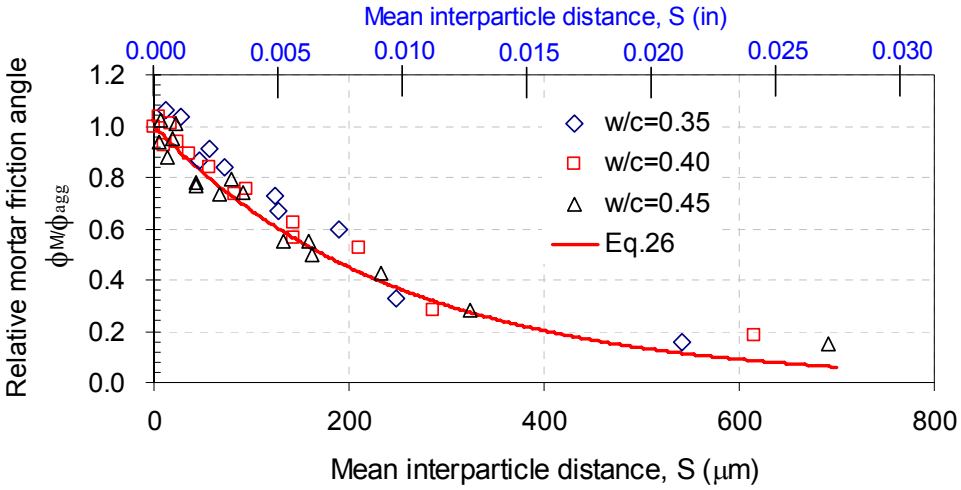

Fig. 9—Effect of the mean interparticle distance on relative friction angle of mortar

Comparing Equations 21 and 22 with Equations 25 and 26, respectively, P_1 and P_2 can be driven as bellows:

$$P_1 = e^{-0.004\cdot\bar{S}} \quad (R^2=0.9505) \tag{27}$$

and

$$P_2 = 20\cdot e^{-0.0546*\bar{S}} \quad (R^2=0.8074) \tag{28}$$

Submitting Equations 27 and 28 into Equations 24, the new shear failure stress model for a fresh mortar can be finalized as:

$$\tau_M = (e^{-0.004\cdot\bar{S}}\cdot\tan\phi_{agg})\cdot\sigma + \left(1+20\cdot e^{-0.0546\cdot\bar{S}}\right)\cdot\tau_P \tag{29}$$

Again, the mean interparticle distance ($\bar{S}$) is related to aggregate size, gradation, and volume fraction and can be determined by Equation 6; and aggregate friction angle (ϕ_{agg}) and yield stress of cement paste (τ_p) are mortar material properties and can be determined from experimental tests or other available models.

CONCLUSIONS

The shear failure behavior of fresh mortar was investigated using a force balance model and a direct shear test. The following conclusions can be made from the present investigation:

1. Both the newly developed shear failure stress model and the experimental results from the direct shear tests illustrated that the shear failure behavior of a mortar followed the Mohr-Coulomb equation. The newly developed model fits the data from the direct shear tests very well.
2. According to the Mohr-Coulomb equation, the internal friction angle (ϕ_M) and cohesion (C_M) of a mortar can be determined. The cohesion (C_M) of a mortar is actually the shear failure stress of the mortar at zero normal stress, or the "true" rheological yield stress of the mortar. Both the internal friction angle (ϕ_M) and cohesion (C_M) of a mortar greatly depended on the mean interparticle distance ($\overline{S}$) of the mortar.
3. Aggregate parameters (size, gradation, and volume fraction) determine the mean interparticle distance ($\overline{S}$) of a mortar, and therefore they significantly influenced the shear failure behavior of the mortar.
4. The relative yield stress of the mortar (C_M / τ_P) decreases in an inverse power form and the relative friction angle of a mortar (ϕ_M/ϕ_{agg}) decreases in a hyperbolic logarithm form with increased interparticle distance ($\overline{S}$) of the mortar. For the mortar having a large mean interparticle distance ($\overline{S}$) (generally for the mortar with a low aggregate volume fraction), the effects of aggregate size and gradation

on the mortar yield stress appeared not significant, while the effect of cement paste property becomes substantial.

5. The normal stress has significant effect on failure shear stress of mortar, especially on that of the low flowable mortar. As a result, in a rheology test, the normal stress, which often results from the self weight of the tested material above the shear zone and the lateral confine stress from the boundary of container, should not be neglected.

LIST OF SYMBOLS

$A_{cross\ agg}$	Cross section area on the slant plane of cement paste bridging two aggregate particles
A_p	Net area of cement paste in a unit volume of mortar
C_M	Cohesion of fresh mortar
D_0	The average diameter of the aggregate particles retained on a given sieve, i
D_i	The average diameter of the i-th group, $D_i = \frac{(D_i)_{max} + (D_i)_{min}}{2}$, where $(D_i)_{max}$ is the maximum diameter of i-th group and $(D_i)_{min}$ is the minimum diameter of i-th group
f_c	Shear force from cement paste, see Figure 4
f_i	Interparticle force, see Figure 4
f_i^n	Component of interparticle force (f_i) on direction normal to the local slant surface, see Figure 4
f_i^t	Component of interparticle force (f_i) on direction of the local slant surface, see Figure 4
i	The order of the sieves used.
V_{agg}	Volume fraction of aggregate in a unit volume of mortar
N_{agg}	Number of aggregate particles in a unit volume of mortar
P	Probability of aggregate contacting to other particles
P_l	Combination parameter of probability for internal friction angle of

	mortar
P_2	Combination parameter of probability for cohesion of mortar
S	Mean interparticle distance
$V_{uncompactedvoids}$	Volume of voids among aggregate particles in a unit volume of mortar at granulate dry state
voids	Un-compacted void content of the aggregate particles
V_{paste}	Volume of cement paste in a unit volume of mortar
$V_{excess\ paste}$	Volume of excess paste in a unit volume of mortar
S	Mean interparticle distance
α	Angle of direction, see Figure 4
β	Angle of direction, see Figure 4
σ_i	Normal force applied on particle, see Figure 4
ϕ_{agg}	Friction angle of aggregate particles in dry granular state
ϕ_M	Friction angle of fresh mortar
θ	Local force concentrate angle, see Figure 4
μ	Friction coefficient of aggregate particles in dry granular state
τ_M	Yield stress of mortar
τ_{NP}	Shear stress from net paste in a unit volume of mortar
τ_{agg}	Shear stress from contact aggregate particle friction in a unit volume of mortar
τ_p	Yield stress of cement paste in mortar

τ_i Shear force generated by particle friction

REFERENCES

1. Peter Domone (2006), Mortar test for self-consolidating concrete, Concrete International, 28: 39-45
2. Okamura H, Ouchi M (2003). Self-Compacting Concrete, Journal of Advanced Concrete Technology; 1(1): 5-15
3. Saak AW, Jennings HM, and Shah SP (2001). New Methodology for Designing Self-Compacting. Concrete, ACI Materials Journal, 98(6): 429-439
4. Mori H (1998). High Fluidity Concrete, Journal of Architecture and Building Society, 113(1420): 41-43
5. Tattersall GH and Banfill PFG (1983). The rheology of fresh concrete, Pitman Publishing Inc.
6. Wallevik OH and Gjorv OE (1990). Modification of the two-point workability apparatus. Magazine of Concrete Research. 42(152): 135-142
7. Hu C and de Larrard F (1996). The rheology of fresh high performance concrete. Cement and Concrete Research. 26(2): 283-294
8. Lu G and Wang K (2007). A DLVO model for yield behavior of fresh cement paste, ACI material Journal, under review
9. Li Z, Ohkubo T, and Tanigawa Y (2004). Yield Model of High Fluidity Concrete in Fresh State, Journal of Material in Civil Engineering, 16(3):195-201
10. Power TC (1968). The properties of fresh concrete, John Wiley and Sons, Inc, New York
11. Kennedy CT (1940). The design of concrete mixes, Proceedings of the American Concrete Institute, 36: 373-400

12. Lu G, Wang K, and Rudolphi TJ (2007). Modeling rheological behavior of a highly flowable mortar using concepts of particle and fluid mechanics, Journal of Cement and Concrete Composites, in press

13. Lu G and Wang K (2007). Mathematics model for granular material direct shear,

14. ASTM C305-99 (American Association State Highway and Transportation Officials Standard AASHTO No. T162), (2003). Standard practice for mechanical mixing of hydraulic cement pastes and mortars of plastic consistency, Annual Book of ASTM Standards, 04. 01

15. Mehta PK, Monteiro PJM (1993). Concrete-structure, properties and materials, 2nd edition. Prentice Hall

16. Powers TC (1968). The Properties of Fresh Concrete, John Wiley & Sons, New York

CHAPTER 6. MODELING RHEOLOGICAL BEHAVIOR OF HIGHLY FLOWABLE MORTAR USING CONCEPTS OF PARTICLE AND FLUID MECHANICS

A paper published in Cement & Concrete Composites

Gang Lu, Kejin Wang , Thomas J. Rudolphi

Abstract

A particle-fluid model was developed for predicting the relationship between the shear stress and shear strain rate of highly flowable mortars. In this model, mortars was considered as a two-phase material, containing a fluid matrix (paste) and a group of well-graded, cohesionless, and rigid particles (fine aggregate) that were uniformly distributed in the matrix. The mortar shear stress was assumed to be the sum of the shear stresses resulting from the cement paste flow, the aggregate particle movement, and the interaction between the cement paste and aggregate. The shear stress resulting from the cement paste flow was assessed using constitutive equations. The shear stress resulting from the aggregate particle movement was evaluated based on the probability of the aggregate particle collision and mechanical collision concept. The shear stress resulting from the interaction between the aggregate and paste was considered as the normal stress that the moving aggregate particles apply onto the cement paste in front of them. The shear rate of the mortar was obtained from the rheological definition of viscosity. Using this model, the effects of mortar mixture properties (such as aggregate size, volume, gradation, and friction as well as paste viscosity and yield stress) on mortar rheology were studied. The results indicated that the present model well explains the mortar flow

behavior, and the predicted results were consistent with those obtained from the rheology tests.

Keywords: *Mortar; Model; Rheology; Shear stress.*

1. Introduction

Modern concrete can be designed and produced to have great flowability that allows the concrete mixture to flow into congested reinforcement areas and fill complicated formwork under its own weight without segregation. Such a self-consolidating concrete (SCC) has generated a tremendous industrial interest because of its economic opportunities (reduced labor and accelerated construction), improved concrete quality, and friendly working environment [1]. A great deal of work has been done developing test methods and evaluating the SCC flow properties since the last decade. However, limited research has been conducted studying the mechanism of the concrete flow and self- consolidation. The SCC mix proportioning is now still based on a trial-and-error process. Clearly, further development and application of SCC requires a better understanding of the fundamental rheological behavior of the concrete materials.

Many models have been developed to study and predict concrete rheological behavior. Among the available models, the Herschel-Bulkley (HB) model is considered as the most suitable for SCC [2, 3]. The HB model is expressed as: $\tau = \tau_0' + a \cdot \dot{\gamma}^b$, where τ_0' is the yield stress, $\dot{\gamma}$ is the shear strain rate, and a and b are concrete material related constants. When the exponent b is equal to 1, the HB model becomes the same as Bingham model, which is commonly used for describing the rheological behavior of conventional concrete

rather than for the behavior of SCC. Clearly, rational and applicable models are currently required for predicting the rheology behavior of SCC other than the empirical data fitting model. It is necessary to develop a new rheology model for SCC along with a profound investigation on the flow mechanism of SCC. And the final format of the required rheology model for SCC should have the similar format as the HB model.

Among all available mortar/concrete rheological models, most are empirical or semi-empirical, which are based on experimental results with little theoretical derivations. Very few models are based on theoretical approaches. Topcu and Kocataskin developed a model that relates concrete composition with flow properties based on a two-phase composite material approach and the law of plastic viscosity [4]. In this model, concrete was considered to consist of two phases: a mortar-matrix phase and a coarse aggregate phase. Using the two-phase material approach, Kurokawa, et. al., studied the effect of coarse aggregate on concrete rheology [5]. In their study, the yield stress of fresh concrete was expressed by the sum of the yield values of matrix mortar and the contribution from the friction of coarse aggregate. The viscosity was expressed by the sum of the viscosity of the matrix mortar and that the volume fraction and friction of the coarse aggregate used.

Kennedy found that rheology of concrete depends on not only the rheology of cement paste but also on the amount of excess paste that coats aggregate particles after filling the voids between the aggregate [6]. He believed that a layer of excess paste would be required for concrete to flow. Su and his colleagues developed a design method for

SCC according to the excess paste theory [7]. Oh and co-workers found that when the thickness of excess paste increased, both the yield stress and viscosity of concrete decreased [8]. The excess paste thickness, defined by the average thickness of the paste coated on the aggregate particle surfaces divided by the average diameter of the aggregate particles, was found to be directly related to the concrete viscosity and yield stress.

Considering fresh concrete as a multiphase material, Pimanmas and Ozawa developed a mathematical model for predicting flow property of fresh concrete based on the energy conservation concept [9]. After carefully studying the shear stress transfer mechanism of fresh concrete, they concluded that the overall shear stress of concrete would be the sum of the shear stresses generated by each phase and the interaction between different phases. They suggested using a probabilistic method to simulate the collision of aggregate particles. However, their model over-simplified the correlation between aggregate volume fraction and friction as a bi-linear relationship.

In the present study, a model for the flow behavior of a fresh highly-flowable mortar is developed primarily based on theoretical derivations. In this model, the shear stress of a flowing mortar is assessed based on a combination of aggregate particle collision mechanics, particle-fluid mechanics, probability concepts, excess paste theory, and consequential stress transfer mechanism. The model development and application will provide researchers and engineers with a fundamental insight into the mechanical and physical behavior of a flowing mortar.

It should also be noted that both fresh concrete and mortar can be treated as a composite material consisting of two different phases − a group of rigid particles and a fluid matrix. Fresh concrete is a composite fluid with large rigid particles (coarse aggregates) dispersed in a mortar. Fresh mortar is a composite fluid with small rigid particles (sands) dispersed in a cement paste. The fundamental difference between concrete and mortar is the properties of the matrix materials and the size of the rigid particles. As a result, the model developed in the present study for mortar can be easily applied to concrete materials.

2. Background and Approach

In this study, a fresh mortar is considered as a granular material (fine aggregate) that is well distributed and suspended in a highly-flowable, viscous fluid (cement paste). Entrapped and entrained air voids in the cement paste are not directly considered. The irregular shaped aggregate particles are simulated as rigid, spherical particles having a gradation similar to the aggregate in the actual mortar.

Since the mortar is highly flowable, excess cement paste is assumed available and that it separates aggregate particles. When the mortar begins to flow, the cement paste deforms first due to its low yield stress. Because cement paste is a viscous material, it generates a viscous stress that resists the mortar to flow. In the flowing mortar, aggregate particles, having different sizes, move at different rates, re-arrange their positions, and change the distances between themselves (Figure 2). As a result, shear stresses are generated in the mortar through the aggregate particle touching, collision, friction, and interlocking.

Additional shear stresses are also generated due to the interaction between cement paste and aggregate particles.

Therefore, the overall shear stress of a flowing mortar (τ_M) can be assumed as the sum of the shear stress resulting from (1) the flow of the cement paste (τ_P), (2) the interaction between the cement paste and aggregate (τ_{FA-P}), and (3) the shear stress resulting from the aggregate movement (τ_{FA}), as expressed by Equation (1):

$$\tau_M = \tau_P + \tau_{FA-P} + \tau_{FA} \quad (1)$$

where

τ_M shear stress of a flowing mortar;

τ_P shear stress resulting from the cement paste flow in the mortar;

τ_{FA-P} shear stress due to the aggregate-cement paste interaction; and

τ_{FA} shear stress generated by the fine aggregate movement.

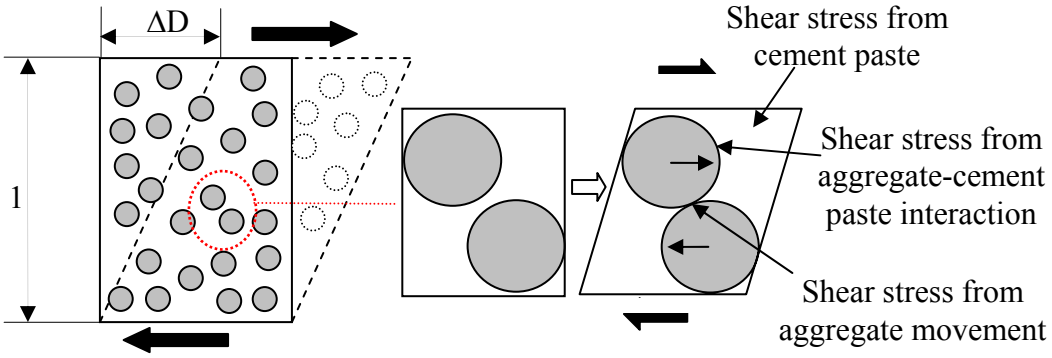

(a) (b)

Figure 1 Material under shear

The yield stress of fresh mortar is given by a yield model for fresh mortar and concrete recently developed by the authors [10], and it is not included in this paper. The shear stress of a flowing cement paste includes two parts, the first part is the yield stress, beyond which the cement paste start flow; the second part is the viscous stress due to the flow of cement paste. Since the flowability of cement paste in high flowable mortar or concrete such as SCC is very high, and the excess paste is always presenting, the yield stress of mortar is controlled by cement paste only [10]. In the present study, the shear stress resulting from the cement paste flow (τ_P) is developed based on fluid mechanics concepts. The shear stress resulting from the interaction between the cement paste and aggregate (τ_{FA-P}) is considered to be caused by the friction generated by the normal stress (F_{AP}) that the moving aggregate particles apply to the cement paste in front of them, which is equivalent to the resistance applied by the cement paste to the aggregate particle movement. The shear stress resulting from the aggregate movement (τ_{FA}) is evaluated using particle collision mechanics, together with the probability concept. Figure 1 illustrates the major procedures for the mortar shear stress analysis. The general concepts used for analyzing the shear stress resulting from the aggregate movement (τ_{FA}) are described by: $\tau_{FA} = N_{collision} \cdot (\Delta P_X)_0$, where $N_{collision}$ is the number of colliding particles, and (ΔP_X) is the momentum change per one collision by two particles.

Based on the continuum mechanics, the energy dissipation (ζ) during a solid particle collision is proportional to the shear stress generated by the collision (τ_{FA}), which is in turn proportional to the momentum change of the colliding particles (ΔP_X). Based on the

first law of thermodynamics, the energy dissipation (ζ) is also a sum of the energy loss directly due to the particle collision ($\Delta E_{collision}$) and the energy loss due to interaction between the aggregate particle and the cement paste ($\Delta E_{interaction}$):

$$\zeta = \tau_{FA}(\partial u / \partial y) = (N_{collision} \cdot \Delta P_X) \cdot (\partial u / \partial y) \quad (2)$$

$$\zeta = \Delta E_{collision} + \Delta E_{interaction} \quad (3)$$

where $\partial u / \partial y$ is the velocity gradient.

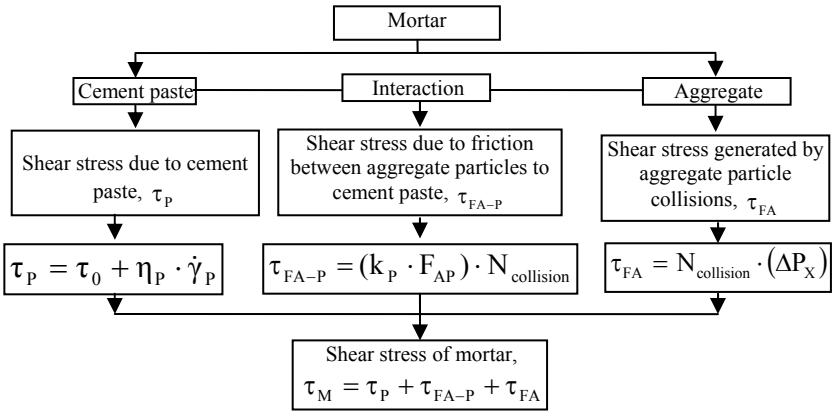

Figure 2 Modeling approach

In the present study, the total momentum change (ΔP_x) is first calculated based on the collision mechanics of a two-particle system. Since aggregate particles in a flowing mortar move without order and unsystematically, the probability concept is applicable. Therefore, the probability of a particle that moves out of its host plane ($P_{collision}$) and the number of aggregate particles in this host plane are computed. Then, the number of the particles that might move out of their original plane and strike on an adjacent horizontal plane can be determined (Figure 3). This number is equal to the number of aggregate particle collisions ($N_{collision}$) that may occur between two adjacent horizontal planes. Thus,

the sub-total momentum change ($(\Delta P_x)_p$) due to the aggregate particle collisions in the two adjacent horizontal planes can be calculated by multiplying the momentum change of the two-particle collision system ($(\Delta P_x)_o$) with the number of collisions ($N_{collision}$) that may occur in the adjacent planes.

Similarly, the energy loss due to the multiple aggregate particle collisions in a mortar unit ($\Delta E_{collision}$) can also be determined from the number of collisions occurring in the mortar unit. The energy loss due to interaction between aggregate particles and cement paste ($\Delta E_{interaction}$) can be calculated according to the basic definition of energy: the average dragging force that cement paste applied on the aggregate multiplied by the average distance between the aggregate particles.

Combining Equations (2) and (3), one can compute the total momentum change (ΔP_x) and finally, calculate the mortar shear stress (τ_{FA}) contributed by the aggregate particle collisions.

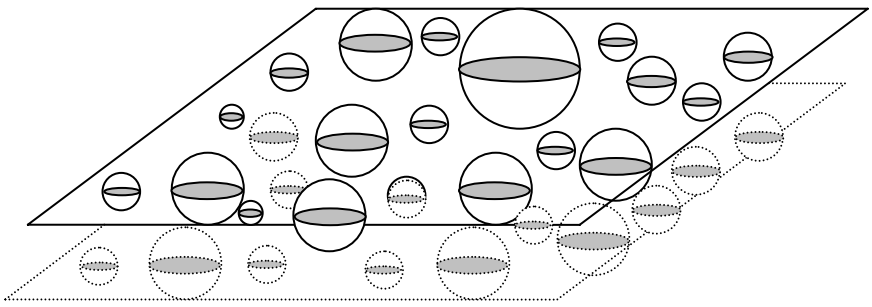

Figure 3 Aggregate particles on two adjacent planes

3. Model Development

In the following sections, each component in the right hand of Equation (1) is evaluated and the related calculations are developed.

3.1 Yield stress of fresh mortar

As previously mentioned, the yield stress of fresh mortar is given by a yield model recently developed by the authors [10]. This is not included in the present paper.

3.2 Shear stress resulting from cement paste flow (τ_P)

In a flowing mortar, cement paste is primarily a viscous fluid, and it provides a viscous stress to resist the flow of the mortar. Therefore, the shear stress of a flowing mortar resulting from its cement paste can be considered as equal to the viscous stress of the cement paste. This viscous stress (τ_P) can be computed from the rheological properties of the cement paste as described in Equation (2). In order to calculate the shear stress generated by cement paste from mortar, the shear rate should be calculated first. Shear strain rate of coarse aggregate phase is regarded the same as global shear strain rate of mortar since aggregates are assumed continuously distributed all over the element of mortar [15]. At a microscopic lever, if two adjacent aggregate particles and cement paste in between of them are considered, as shown in Figure 1, the problem can be simplified as the shear rate in different phases of simple sandwich material unit element shown in Figure 4. Thus,

$$\dot{\gamma}_P = \frac{1+1.65\cdot V_A}{1-1.35\cdot V_A}\cdot\dot{\gamma}_M \tag{4}$$

where $\dot{\gamma}_P$ is the apparent shear rate of paste phase; $\dot{\gamma}_M$ is the apparent shear rate of mortar; and V_A is the volume fraction of aggregate particles. This equation indicates that the shear rate of the cement paste in flowing mortar is higher than the overall shear rate of mortar.

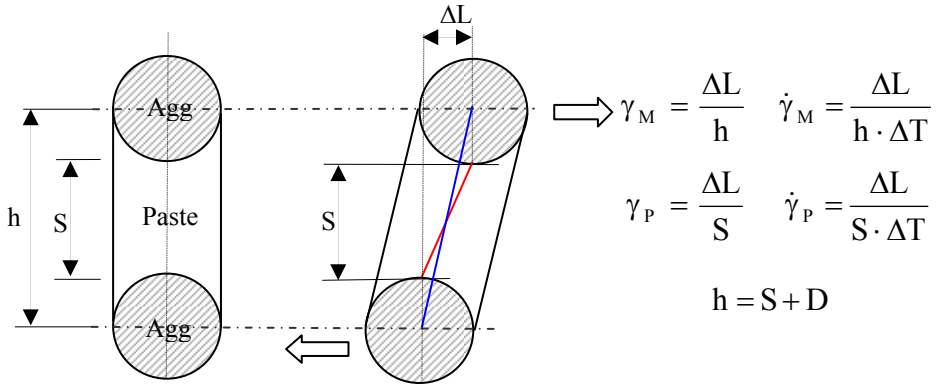

Figure 4 A microscopic mortar unit under shear

Then, following the deformation of the shear stress generated from flowing viscous fluids, the shear stress from cement paste in unit geometry mortar is,

$$\tau_P = \tau_{0P} + \eta_P \cdot \frac{1+1.65V_A}{1-1.35V_A} \cdot (1-V_A) \cdot \dot{\gamma}_M \tag{5}$$

where τ_{0P} and η_P are cohesion and viscosity of cement paste; and V_A is the volume fraction of aggregate phase.

3.3 Number of aggregate particle collisions in a flowing mortar ($N_{collision}$)

3.3.1 Modeling aggregate particle distribution

Figure 5 (a) illustrates a unit volume of an actual mortar, which is composed of well-graded, irregular-shaped aggregate particles in a fluid cement paste. The shaded area in

plane z represents the aggregate particles and the un-shaded area represents the cement paste.

To simplify the collision analysis, these irregular particles are simulated into the sphere particles (Figure 5(b)) [11]. The various diameters of the spherical aggregate particles can be determined based on the actual aggregate gradation as obtained from the sieve analysis [12], according to Equation 6 [13]:

$$D_0 = \log^{-1}\left(\frac{\sum_{i=1}^{k} f_i \cdot \log D_i}{\sum f_i}\right) \tag{6}$$

where

D_0 the average diameter of the aggregate particles retained on a given sieve, i;

f_i volume fraction of the aggregate particles on the given sieve;

D_i the average diameter of the i-th group, $D_i = \frac{(D_i)_{max} + (D_i)_{min}}{2}$, where $(D_i)_{max}$ is the maximum diameter of i-th group and $(D_i)_{min}$ is the minimum diameter of i-th group; and

i the order of the sieves used.

Note that plane y intersects aggregate particles with the areas ranging from 0 to $\pi \cdot \left(\frac{D_0}{2}\right)^2$, where D_0 is the average diameter of aggregate particles given in Equation (6).

The average area that a given horizontal plane intersects aggregate particles in the mortar, as shaded area in Figure 5(b), can be expressed as follows:

$$A_{AVE} = \int_0^{\frac{\pi}{2}} \pi \cdot \left(\frac{D_0}{2}\right)^2 \cdot \cos\alpha \cdot \frac{2}{\pi} \cdot d\alpha = 0.3926 \cdot D_0^2 \quad (7)$$

where A_{AVE} ranges from 0 to $\pi \cdot \left(\frac{D_0}{2}\right)^2$ and D_0 is the average diameter of aggregate particles, which can be obtained from Equation (7).

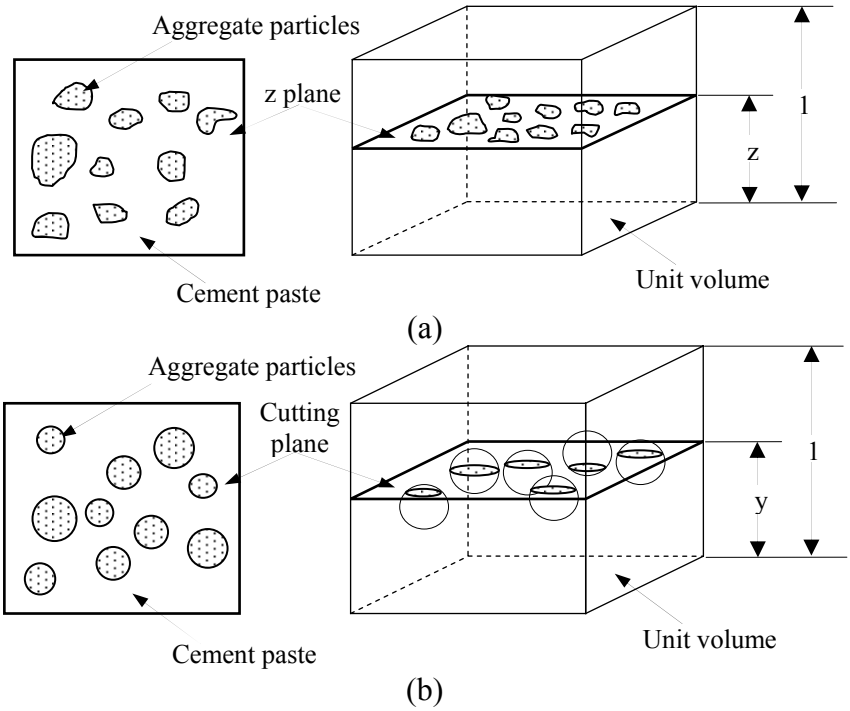

Figure 5 Particles distribution on unit horizontal plane before (a) and after (b) simplification

Assuming that $A_{AVE} = \pi D^2/4$, based on Equation (7), the average diameter of the aggregate particles intersected by a horizontal plane, D, can be calculated as follows:

$$D = 0.7070 \cdot D_0 \tag{8}$$

Note that the aggregate size distribution in any given horizontal plane is considered as the same as that in the entire mortar unit and consistent with the gradation of the aggregate used in the actual mortar. Thus, the total volume of aggregate particles in a unit material element (1x1x1) is equal to the volume fraction of aggregate in mortar, V_A. The total volume of aggregate particles in a unit material element can be also expressed by the number of aggregate particles in the unit, N, multiplies the average volume of the aggregate particles, A_{AVE}. Thus,

$$V_A = N \cdot A_{AVE} \tag{9}$$

where

V_A volume fraction of aggregate phase,

N number of aggregate particles in a unit volume material, and

A_{AVE} average area given by Equation (7).

The number of aggregate particles in a unit material volume was therefore given as

$$N = V_A \Big/ A_{AVE} = 1.2732 \cdot \frac{V_A}{D^2} \tag{10}$$

3.3.2 Probability of number of particle collision in a horizontal plane

Based on the discussions above, the irregular arrangement of the aggregate particles in a given horizontal plane (Figure 6(a)) can be modified into a linear arrangement (Figure 6(b)). Thus, the probability of a particle "*i*" that may move out of its host horizontal plane and be affected by its adjacent particles can be analyzed. From Figure 6, the cone

surface OPQ is tangent to particle *i* and its adjacent particles, such as *j* and *k*. It is assumed that the particle *i* will not collide with any adjacent particles. Thus, the direction of the velocity of the studied particle, V, in Figure 6, should be inside of the cone field *opq* in Figure 7. The cone OPQ and cone *opq* are parallel to each other.

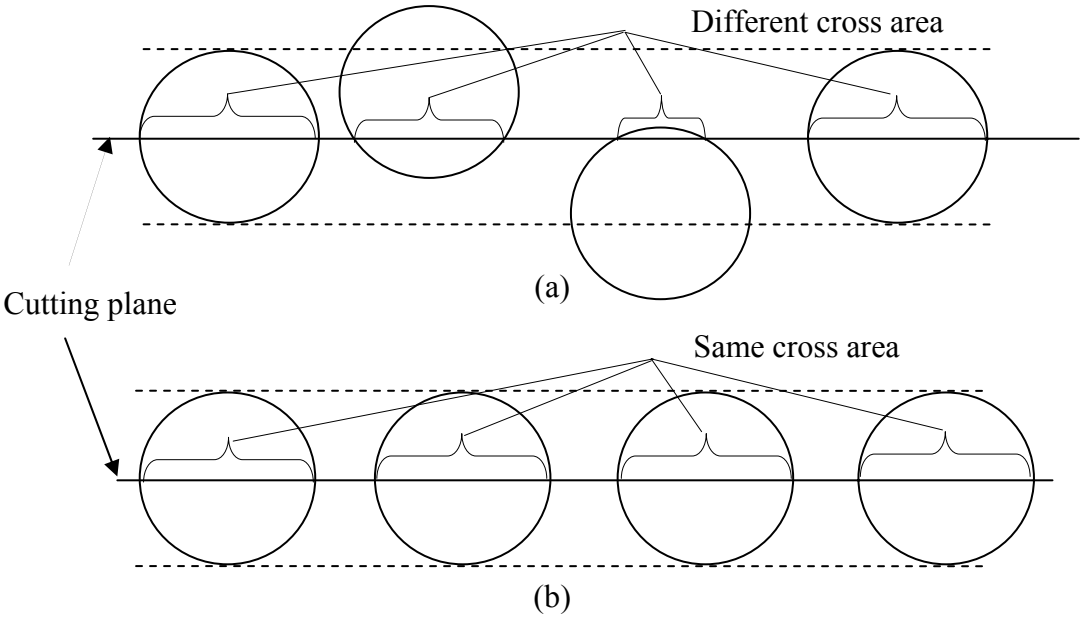

Figure 6 Particles distribution on one horizontal plane

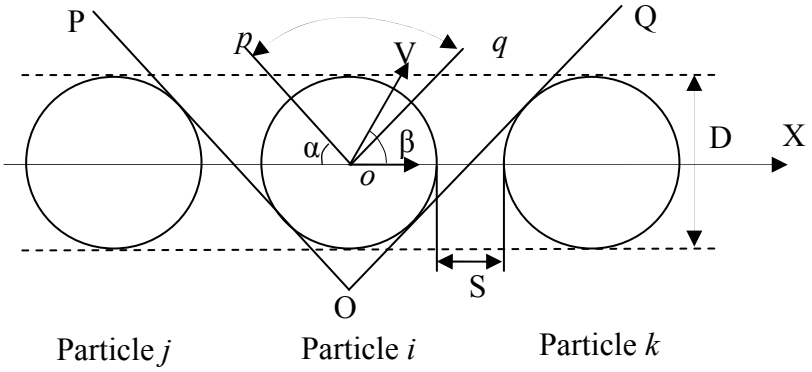

Figure 7 Direction of velocity of a flowing particle (2-D)

In the 3-D consideration, the movement of the individual aggregate particle *i* in Figure 8 was analyzed as the following:

A typical aggregate particle between two adjacent horizontal planes and intersected by only one of the planes is illustrated as Figure 8. The angle α, which describes the area of the intersection (shaded area), is defined as

$$\sin\alpha = \frac{\frac{D}{2}}{\frac{D}{2}+\frac{S}{2}} = \frac{D}{D+S} \tag{11}$$

where

D average diameter of aggregate particles, given by Equation (9) and

S average distance between the aggregate particles in mortar.

The probability $P_{collision}^{particle}$ that an aggregate particle may go out of the horizontal plane (the direction of the particle velocity is within the shaded area in Figure 8) is the ratio of the surface area of the top segment-to-the surface area of the half sphere:

$$P_{collision}^{particle} = \frac{S}{D+S} \tag{12}$$

From Equations (10) and (12), the effective number of collisions, $N_{collision}$ that occurs in this horizontal plane is given by

$$N_{collision}^{plane} = N \cdot P_{collision}^{particle} = 1.2732 \cdot \frac{V_A}{D^2} \cdot \frac{S}{D+S} \tag{13}$$

Equation (13) indicates that the effective number of collisions for a unit plane is correlated with the volume fraction of aggregate particles in mortar (V_A), their average diameter (D), and the distance between the particles (S), which is related to the excess paste thickness [8]. When the distance between the aggregate particles (S) increases, the effective number of collisions ($N_{collision}^{plane}$) in a unit plane decreases.

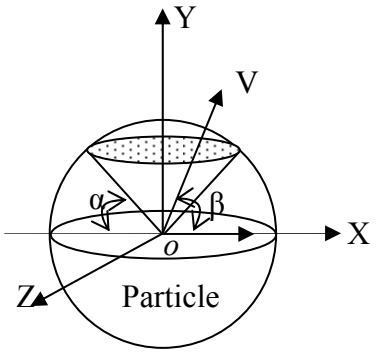

Figure 8 Individual aggregate particle between two adjacent planes (3-D)

3.3.3 Distance between particles in a unit volume of mortar (S)

To calculate the distance between the aggregate particles in a unit volume material (S), Equation (14) first gives the volume of a single particle ($V_{particle}$), and Equation (15) then provides the number of aggregate particles in a unit volume of the mortar ($n_{particle}$):

$$V_{particle} = \frac{4}{3}\pi\left(\frac{D}{2}\right)^3 = \frac{\pi D^3}{6} \tag{14}$$

$$n_{particle} = \mathbf{V_A} / V_{particle} = \frac{6V_A}{\pi D^3} \tag{15}$$

From Equation (15), the total surface area of all aggregate particles in the modeled mortar unit ($A_{particle}$) can be determined from Equation (16):

$$A_{particle} = 4\pi(\frac{D}{2})^2 \cdot n_{particle} = \pi D^2 \frac{6V_A}{\pi D^3} = \frac{6V_A}{D} \quad (16)$$

If the mortar aggregate has 35% air voids, in terms of the aggregate volume, after compaction [11] the total volume of voids in the modeled mortar unit will be

$$V_{voids} = 35\% \times V_A \quad (17)$$

Thus, the average distance between the aggregate particles in the modeled mortar units can be expressed by Equation (18) [8]:

$$S = 2 \cdot \frac{V_P - V_{voids}}{A_{particle}} = \frac{1 - 1.35V_A}{3V_A} \cdot D \quad (18)$$

where V_p is the volume of the cement paste.

Plugging Equations (6), (8), and (18) into Equation (13), one can calculate the number of aggregate particle collision, $N_{collision}$, in a unit horizontal plane.

3.4 Shear stress resulting from the interaction between aggregate and cement paste, τ_{FA-P}

When aggregate particles move along with a flowing mortar, they generate a normal force (F_{AP}) on the paste in front of them (Figure 9). This normal force (F_{AP}) is equal to the drag force (F_{PA}) acting on the aggregate particles by cement paste. Because of this normal stress, a friction force is developed between the aggregate particles and cement paste, which contributes to the mortar shear stress (τ_{FA-P}). Based on Franzini and Finnemore, this normal force applied by the moving aggregate particles to the cement paste can be calculated according to Equation (19) [14]. Thus,

$$F_{AP} = C_D \rho_P \frac{V_F^2}{2} A \tag{19}$$

where

F_{AP} force acting on cement paste by a moving aggregate particle;

C_D coefficient of the cement paste dragging force;

ρ_p cement paste density;

V_F particle fluctuation velocity; and

A projected area of a sphere aggregate particle, defined as $\pi D^2 / 4$, where D is the average diameter of the particle.

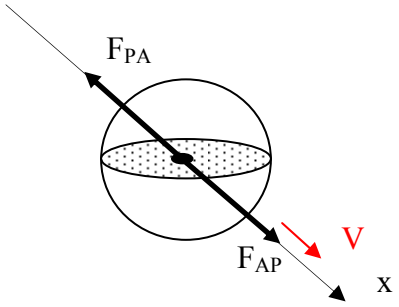

Figure 9 A spherical particle moving in viscous fluid

The total normal stress applied to cement paste due to aggregate movement in a unit mortar, τ_{P-FA}, is equal to the normal force generated by a single particle (F_{AP}) multiplied by the number of particles that move out of their host plane ($N_{collision}$), or the number of collisions in the flowing mortar, as given by Equation (13):

$$\tau_{FA-P} = (k_P \cdot F_{AP}) \cdot N_{collision} \tag{20}$$

where

τ_{FA-P} sub-total normal force acting on paste by aggregate particles in a horizontal plane;

k_p normal stress coefficient;

F_{AP} force acting on cement paste by a single aggregate particle; and

$N_{collision}$ the number of particles that move out of its host plane onto another adjacent plane (see Equation (11)).

Here, the normal stress coefficient, k_p, reflects the fact that the normal force (F_{AP}) increases with the shear resistance of the cement paste. reflects the efficiency that the interface between aggregate particles and cement paste can transfer normal force to the lateral shear force. Also, k_p is not only related to the material properties to the rate of the load applied to the mortar material [15].

3.5 Shear stress resulting from aggregate particle movements/collisions, τ_{FA}

3.5.1 Momentum change $(\Delta P_x)_o$ and energy loss $(\zeta)_o$ due to a two- particle collision

Figure 10 illustrates a velocity diagram of a moving aggregate particle in a modeled mortar unit. Although randomly orientated, the aggregate moving velocity, **V**, can be expressed as

$$\mathbf{V} = \mathbf{v}_i + \mathbf{v}_j + \mathbf{v}_k \tag{21}$$

where $\mathbf{v}_i$, $\mathbf{v}_j$ and $\mathbf{v}_k$ are velocity components along X, Y and Z axis, respectively.

The X component of the particle velocity, $\mathbf{v}_i$, can be further divided into two parts: $\mathbf{v}_{i1}$ and $\mathbf{v}_{i2}$. Assuming that one part of the velocity, $\mathbf{v}_{i1}$, is equal to the overall mean flow velocity of mortar, $\mathbf{v}_M$, $\mathbf{v}_i$ can be expressed as

$$\mathbf{v}_i = \mathbf{v}_{i1} + \mathbf{v}_{i2} = \mathbf{v}_M + \mathbf{v}_{i2} \tag{22}$$

Let $\mathbf{v}_{i2}$ be considered together with $\mathbf{v}_j$ and $\mathbf{v}_k$ and determine

$$\mathbf{v}_F = \mathbf{v}_{i2} + \mathbf{v}_j + \mathbf{v}_k \tag{23}$$

where $\mathbf{v}_F$ is called the fluctuation velocity of flowing particles. Thus, Equation (20) becomes

$$v = v_M + v_F \tag{24}$$

The following section, therefore, determines the v_M and v_F. Physically, the mean flow velocity, v_M, is generated by the drag force that the cement paste applies to a moving aggregate particle, which is in the mean flow direction. The fluctuation velocity, v_F, is generated by the collision of particles, which is randomly oriented. In the present study, all aggregate particles in the modeled mortar unit are assumed to have the same fluctuation velocity.

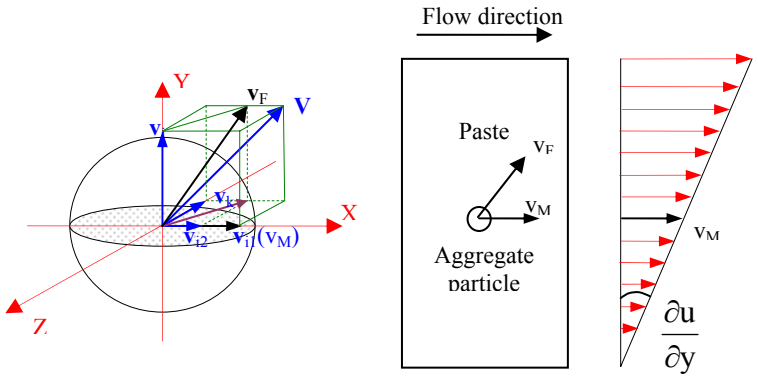

Figure 10 Velocity components of a flowing particle

To analyze the mean flow velocity of colliding particles, a two-particle collision is first considered. As illustrated in Figure 11, the relative positions of two colliding particles A

and B, both having the same mass and diameter but different moving velocities, are determined by angles Φ and Ψ. Based on the collision mechanics, the magnitude of the mean flow velocity between the two colliding particles A and B in the collision direction is [9, 15, 16] is:

$$V_M^n = V_{AB}^M \cdot \sin\Phi \cdot \cos\Psi = D \cdot \frac{\partial u}{\partial y} \cdot \cos\Phi \cdot \sin\Phi \cdot \cos\Psi \tag{25}$$

where

V_{AB}^M relative mean flow velocity between particle A and B (Figure 11);

D average diameter of aggregate particles; and

$\frac{\partial u}{\partial y}$ velocity gradient of mortar.

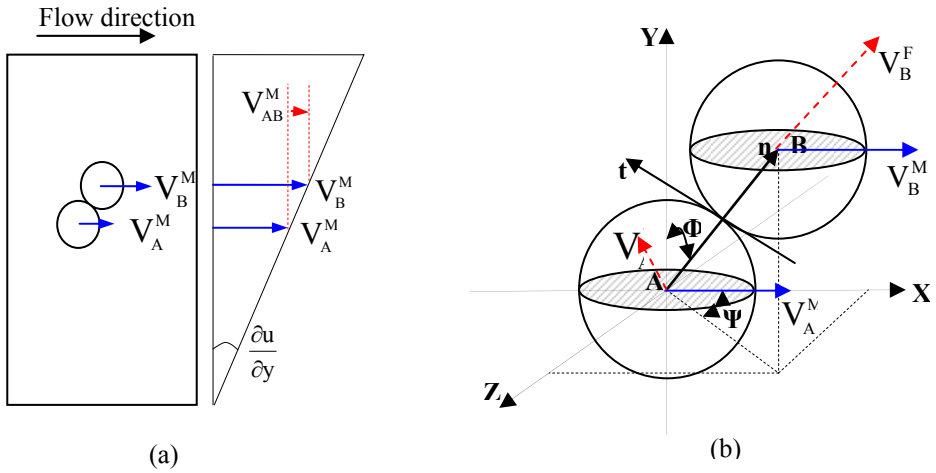

Figure 11 Illustration of collision between two particles

The probability of a collision at a point on the surface of one sphere for this mean flow velocity is [17]

$$P_C^M(\Phi,\Psi) = \frac{\sin\Phi \cdot d\Psi \cdot d\Phi}{\pi} \tag{26}$$

where the range of Φ and Ψ are $\Phi \in \left[-\frac{\pi}{2}\ ,\ \frac{\pi}{2}\right]$ and $\Psi \in \left[0\ ,\ \frac{\pi}{2}\right]$, respectively.

From Equations (24) and (25), the average mean flow velocity between the two colliding particles in the collision direction is

$$(V_M^n)_{AVE} = \iint_{\Phi,\Psi} V_M^n \cdot P_C^M(\Phi,\Psi) = 0.2122 \cdot D \cdot \frac{\partial u}{\partial y} \tag{27}$$

where

D average diameter of aggregate particles; and

$\frac{\partial u}{\partial y}$ velocity gradient of mortar (shear strain rate).

Using a similar procedure (see Equations 21-26), the average fluctuation velocity of particles A and B in the collision direction can be expressed as

$$(V_F^n)_{AVE} = 0.6365 V_F \tag{28}$$

where

V_F magnitude of average fluctuation velocity of aggregate particles.

As shown in Figure 11, the mean flow and fluctuation velocities between two colliding particles along the direction perpendicular to collision, t, are

$$(V_M^t)_{AVE} = 0.4244 \cdot D \cdot \frac{\partial u}{\partial y} \tag{29}$$

and $(V_F^t)_{AVE} = 0$ (30)

where D and $\frac{\partial u}{\partial y}$ are the same as that in Equation (24).

Based on continuum mechanics, the average momentum change, $(\Delta P_X)_0$, along the mean flow direction (X direction in Figure 10 and 11) and the kinetic energy loss, ΔE (=ζ), due to collision of the two spheres are derived as [18]:

$$\left(\Delta P_X\right)_0 = \mu \cdot m \cdot (1+\varepsilon) \cdot \left(0.083 \cdot D \cdot \frac{\partial u}{\partial y} + 0.25 \cdot V_F \right) \tag{31}$$

$$\Delta E = \frac{m}{4} \cdot (1-\varepsilon^2) \cdot \left\{ \left[0.2122 \cdot D \cdot \frac{\partial u}{\partial y} \right]^2 + \left[0.6365 V_F \right]^2 \right\} + \frac{m}{4} \cdot \left\{ \left(0.4244 \cdot D \cdot \frac{\partial u}{\partial y} \right)^2 - \left(0.4244 \cdot D \cdot \frac{\partial u}{\partial y} - \mu \cdot \left[0.2122 \cdot D \cdot \frac{\partial u}{\partial y} \cdot (1+\varepsilon) + 0.6365 V_F \cdot (1+\varepsilon) \right] \right)^2 \right\} \tag{32}$$

where

$\left(\Delta P_n\right)_0$ average momentum change of the two-particle collision in the collision direction,

ΔE energy loss due to the two-particle collision,

D average diameter of aggregate particles,

m average mass of aggregate particles,

$\frac{\partial u}{\partial y}$ velocity gradient of mortar,

V_F average fluctuation velocity of aggregate particles; it is the sum of $(V^n_F)_{AVE}$ and $(V^t_F)_{AVE}$, which are given in Equations (26) and (28),

μ friction coefficient of particles, and

ε coefficient of elastic restitution.

3.5.2 Shear stress resulting from all aggregate particle movements or multiple-particle collisions, τ_{FA}

As mentioned previously, the stress produced from the aggregate particle movements can be determined from the fundamental laws of continuum mechanics, Equation (1) and (2) [18]. The momentum change ΔP_X of two colliding spheres in the mean flow direction (X direction), has been given by Equation (31). The whole momentum change on a horizontal plane can be calculated by multiplying this single two-particle collision momentum, $(\Delta P_X)_0$ with the total number of collision occurring on this plane, $N_{collision}$, are given by Equation (13). Since the horizontal plane considered here is a unit plane, the total force acting on this plane gives the stress instead of the force. Thus, Equation (1) was revised to:

$$\tau_{FA} = N_{collision} \cdot (\Delta P_X)_0 \tag{33}$$

where τ_{FA} is the shear stress generated from the collision of aggregate particles in a horizontal plane.

Similar to momentum change, the total energy loss due to particle collisions of a unit horizontal plane can be determined by multiplying the energy loss of a single two-sphere collision system by the number of collisions:

$$\Delta E_{collision} = N_{collision} \cdot \Delta E \tag{34}$$

Energy loss due to interaction between one aggregate particle and the cement paste as it moves can be calculated according to the basic definition of energy:

$$\Delta E_{\text{interaction}}^{\text{single particle}} = F_{AP} \cdot S \tag{35}$$

where F_{AP} is the force acting on cement paste by aggregate as given in Equation (19), and S is the average distance between the aggregate particles in mortar as given in Equation (18).

Note that Equation (35) provides calculation of the energy loss due to a two-spherical particle collision system. The total energy loss occurring in a unit horizontal plane can be determined as

$$E_{\text{interaction}} = N_{\text{collision}} \cdot E_{\text{interaction}}^{\text{single particle}} = N_{\text{collision}} \cdot C_D \rho_P \frac{V_F^2}{2} A \cdot S \tag{36}$$

where $N_{\text{collision}}$ is the effective number of collisions given by Equation (13) and C_D is the overall coefficient of drag.

Now, inserting Equation (33) into Equation (32) and plugging Equations (35)-(37) into Equation (34), one can establish mortar shear stress by giving the energy dissipation due to aggregate particle collision (ζ) equal to the total energy loss due to the aggregate particle collision and interaction with cement paste (E_{agg}):

$$N_{\text{collision}} \cdot (\Delta P_X)_0 \cdot \frac{\partial u}{\partial y} = N_{\text{collision}} \cdot C_D \rho_P \frac{V_F^2}{2} A \cdot S + N_{\text{collision}} \cdot \Delta E \tag{37}$$

From Equation (37), one can obtain the fluctuation velocity of aggregate particles, V_F. Using Equation (33), the shear stress from aggregate particle movement due to collision and friction, τ_{FA}, is then determined.

Finally, the mortar shear stress expressed in Equation (1) can be re-written as follows:

$$\tau_M = \tau_0 + \eta_P \cdot \frac{1+1.65V_A}{1-1.35V_A} \cdot \dot{\gamma}_m + k_P \cdot N_{collision} \cdot C_D \cdot \rho_P \cdot \frac{V_F^2}{2} \cdot A + \tau_{FA} \quad (38)$$

The viscosity of mortar can be obtained based on its rheological definition:

$$\eta_M = \frac{\tau_M}{\dot{\gamma}} \quad (39)$$

where

η_M mortar viscosity;

τ_M mortar shear stress; and

$\dot{\gamma}_M$ mortar shear rate.

The required inputs for use of the present model (Equations (38)) are

- average diameter of the aggregate particles in the mortar (D),
- material density of aggregate (ρ),
- volume fraction of the aggregate (V_A),
- friction coefficient of the aggregate (μ),
- coefficient of elastic restitution (ε),
- density, yield stress, and viscosity of cement paste (ρ_p, τ_p, η_p, respectively), and
- overall coefficient of drag of cement paste (C_D).

4. Model Application and Verification

4.1 General form of the particle-fluid model

One way to validitate of a newly developed model is to check whether or not the model can be compared with the commonly used models. For the newly-developed model, if all parameters are given or computed based on the equations presented in this paper, Equation (38) will become

$$\tau_M = \tau_0 + A \cdot \dot{\gamma} + B \cdot \dot{\gamma}^2 + C \cdot \dot{\gamma}^3 \quad (40)$$

where A, B, and C are constant factors related to the mortar material properties, and which can be calculated from the equations provided in the previous section of this paper. The yield value τ_0 is a real yield value, and $\dot{\gamma}$ is the shear rate. Equation (40) shows that the new particle-fluid model has a power format, which is similar to both the modified Bingham model and the Herschel-Bulkley model [19]. Feys and colleagues have also verified a similar model to Equation (40) based on experimental data from SCC rheology tests [20]. These instances prove that the present model is rational in physical interpretation.

4.2 Studying the effect of cement paste properties

The basic cement properties used in the present model are yield stress and viscosity. These two basic rheological parameters are predominated by the cement properties, water-to-cement ratio (w/c), and the mixing method of the paste. To study the effect of cement paste properties on the rheological behavior of a mortar, two different cement

pastes (τ_0=8Pa, η=0.12Pa.s and τ_0=16Pa, η=0.24Pa.s), one aggregate size (#16), and one volume content of aggregate (40%) are used in the newly developed particle-fluid model. Figure 12 shows the flow curves computed from the present model of the mortars made with different cement properties. As observed in the figure, both yield stress and viscosity of the mortars increase when the yield stress and viscosity of cement paste increase or w/c of the cement paste decreases. This indicates that a larger force is required to initiate the mortar flow and to maintain a high flow rate, which is consistent with the published results from mortar rheology testing and modeling. [19, 20, 21]

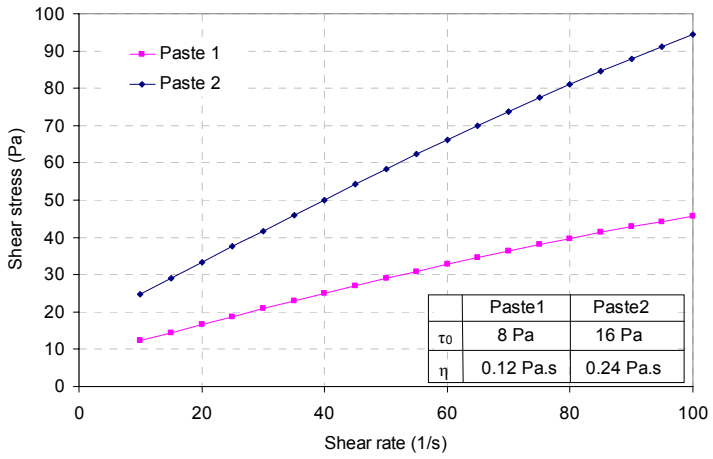

Figure 12 Effect of paste properties on mortar rheological behavior (aggregate size #16 and volume 40%)

4.3 Studying the effect of aggregate type

The effect of aggregate properties on mortar rheology can be appropriately studied under the present model because an important aggregate property parameter, the coefficient of aggregate friction (μ), is required as an input. The coefficient of aggregate friction (μ) is associated with not only aggregate size and gradation but also the aggregate angularity

and surface texture. Based on the results from a direct shear test and a mathematical model, the authors of the paper have obtained the coefficients of friction for various aggregates **[**22**].** Using these friction coefficient values (0.5 for limestone and 0.3 for gravel), the shear stresses of mortars made with a cement paste (τ_0=16Pa, η=0.24Pa.s) and two different types of aggregates (limestone and gravel), with a single size of #16, or 1.18 mm, and volume fraction of 40% are calculated according to the present particle-fluid model.

As observed in Figure 13, for a given mix proportion and a given size of aggregate, limestone, having a higher coefficient of surface friction, provides the mortar with higher shear stress and viscosity than gravel.

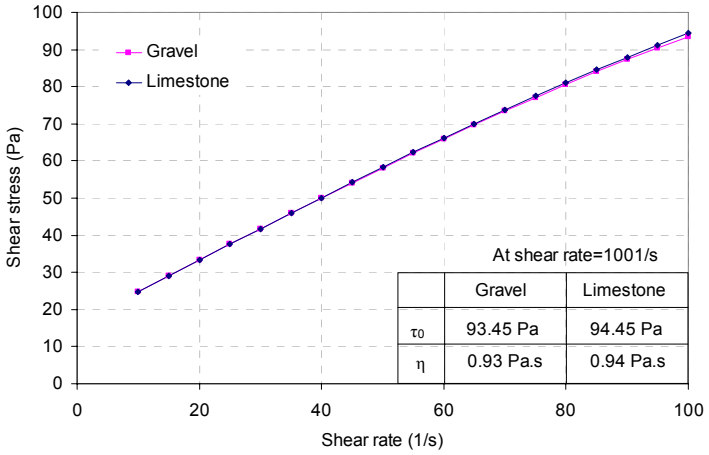

Figure 13 Effect of aggregate type on mortar rheological behavior
(aggregate size #16 and volume 40%; paste: τ_0=16 Pa, η=0.24Pa.s)

4.4 Studying the effect of aggregate content

To investigate the effect of aggregate content on mortar rheology, one cement paste (τ_0=8Pa, η=0.12Pa.s), three aggregate sizes (#16 or 1.18mm, #30 or 0.6mm, and #50 or

0.3mm), and four volume fractions of aggregate (10%, 20%, 30%, and 40%) are considered. As shown in Figure 14, the flow curves of mortars with different aggregate contents are significantly different. When the aggregate content increased, both the yield stress and viscosity of the mortar increase. This may be caused by the higher degree of friction and collision of solid particles, which increases the mortar shear stress and viscosity. Figure 16 also shows that when the aggregate volume fraction increased from 10% to 40%, the mortar flow curves become increasing nonlinear. For a given volume fraction, larger aggregate sizes produced a more nonlinear flow curve compared to a smaller aggregate. This is mainly because that the collision of aggregate particles affects the flow of mortar more for larger aggregate particles than for smaller aggregate particles. The effects of aggregate content on the mortar shear stresses and viscosities at shear rate of 100 s^{-1} are summarized in Figure 15. It is observed in the figure that at a low aggregate volume fraction (10% and 20%), the differences in the mortar rheological parameters (shear stress and viscosity) resulting from different sizes of aggregate are not significant. However, the differences become obvious when the volume fraction increases (30% and 40%).

4.5 Studying the effect of aggregate size

Flow curves of mortars with different aggregate sizes are shown in Figure 16. For a given paste, aggregate material properties and volume fraction of aggregate, the mortar made with larger aggregate has a higher flowability. Again, at a low aggregate volume fraction (10% and 20%), the differences in the mortar rheological parameters (shear stress and

viscosity) resulting from different sizes of aggregate are not significant. However, the differences become obvious when the volume fraction increases (30% and 40%).

The rheological parameters (shear stress and viscosity) of the mortars with different size of limestone aggregate at shear rate of 100 s^{-1} are summarized in Figure 17. The figure clearly shows that smaller aggregate size results in higher yield stress and viscosity. This agrees with the common finding that a decrease in maximum size of aggregate generally increases the water demand of the concrete [23].

In summary, the results obtained from the present particle-fluid model have shown that the cement paste having higher flowability generally provides its mortar with lower viscosity and shear stress. In addition to the properties of the cement paste, aggregate size, gradation, and volume fraction significantly influence mortar rheology, among which the particle size distribution and aggregate gradation are of the most important significance. The present study on the effects of different aggregate types also demonstrates that the surface texture of aggregate has significant effect on the mortar rheology. The flowability of the mortar decreases with its aggregate volume fraction. For the mortar with a low aggregate volume fraction, the effect of aggregate size, gradation and surface texture on the mortar rheology is not significant, but this effect becomes significant as the volume fraction of aggregate increases. All these findings are consistent with the experimental results from mortar rheology tests [20, 21].

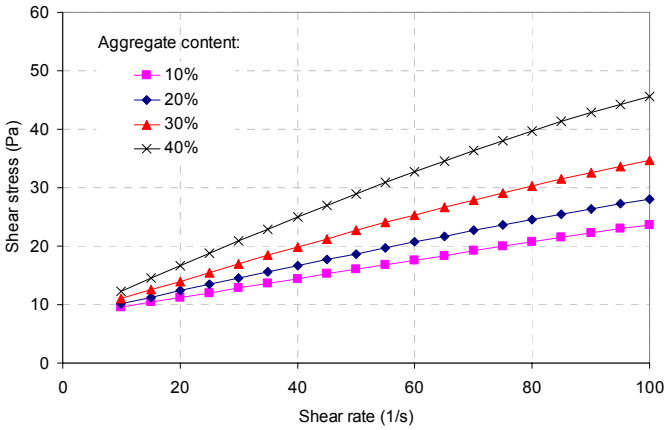

(a) Aggregate size: #16

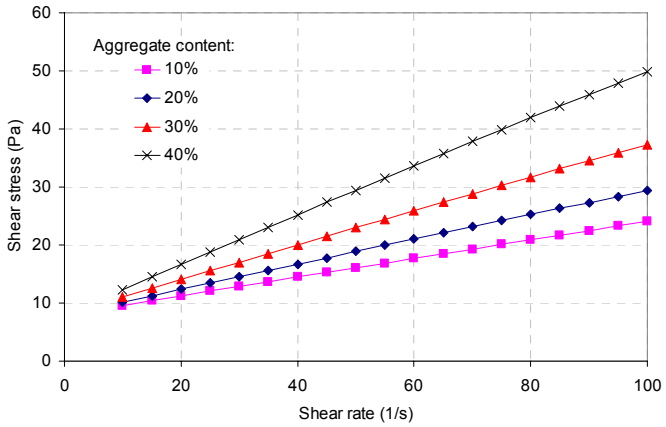

(b) Aggregate size: #30

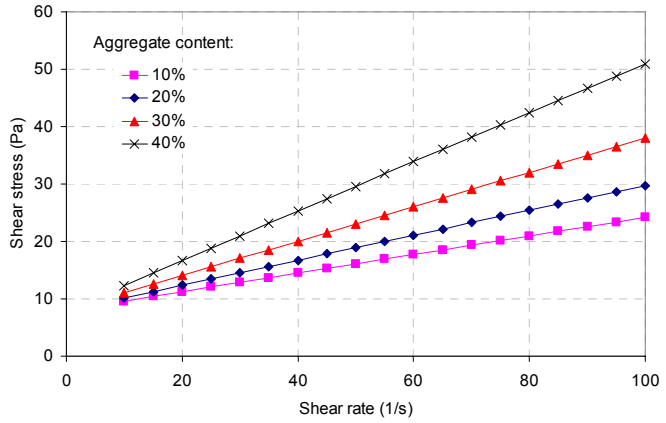

(c) Aggregate size: #50

Figure 14 Effect of aggregate content on mortar rheological behavior (paste: τ_0=8 Pa, η=0.12Pa.s)

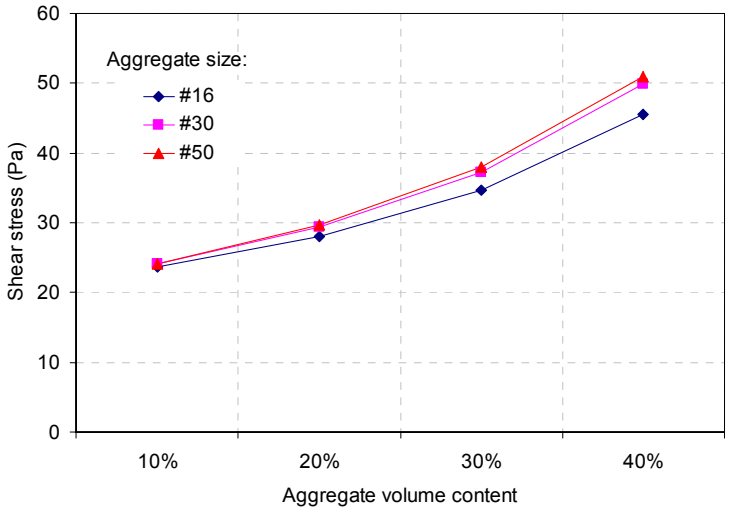

(a) Effect on shear stress

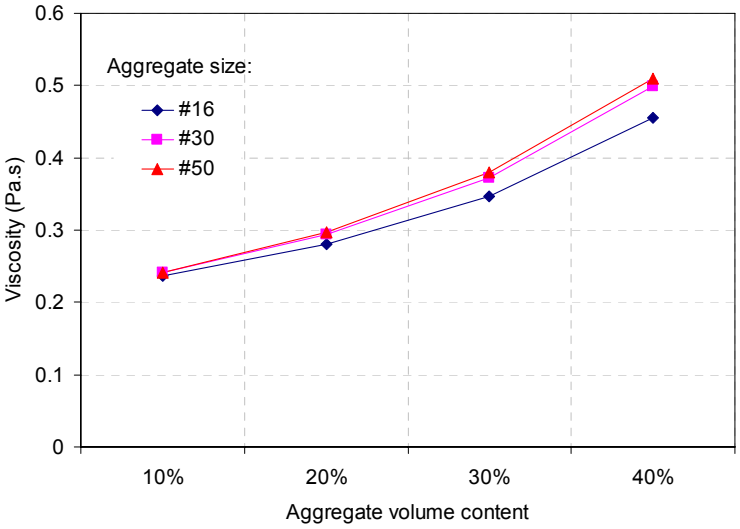

(b) Effect on viscosity

Figure 15 Effect of aggregate content on mortar rheological parameters at shear rate= $100s^{-1}$ (paste: τ_0=8 Pa, η=0.12Pa.s)

5. Summary

A particle-fluid model was developed for studying the flow behavior of highly flowable mortar. In this model, fresh mortar is considered as a two-phase material, with a fluid matrix and a group of rigid particles dispersing in the matrix. The mortar shear stress is considered as the sum of shear stresses resulting from the cement paste flow and the aggregate particle movements as well as the interaction between the cement paste and aggregate. The model predicts a power function between the shear stress and shear of a mortar. Such a prediction is believed to be more suitable for very high-flowable mortar than any available models. Using the present model, the effects of cement paste properties and aggregate properties (surface texture, size, volume fraction) were investigated. The results obtained from the particle-fluid model are consistent with those obtained from the experimental tests. The model rationally explains and predicts the flow behavior of a highly flowable mortar made with various materials and mix proportions.

If concrete is considered as a two-phase material, a group of coarse aggregate particles dispersed in a flowable mortar matrix, this particle-fluid model can also be easily adapted for studying the rheological behavior of highly flowable concrete, such as self-consolidating concrete.

References

[1] Okamura H, Ouchi M. Self-Compacting Concrete, Journal of Advanced Concrete Technology 2003; 1(1): 5-15.

[2] Larrard D, Ferraris CF, Sedan T. Fresh concrete: A Herschel-Bulkley material. Material and Structures 1998; 31(211): 494-498.

[3] Bird RB, Dai GC, Yarusso BJ. The rheology and flow of viscoplastic materials. Rev Chem Eng 1983; 1: 1-70.

[4] Topcu IB, Kocataskin F. A two-phase composite materials approach to the workability of concrete. Cement and Concrete Composites 1995; 17(4): 319-325.

[5] Kurokawa Y, Tanigawa Y, Mori H, Nishinosono K. Analytical study on effect of volume fraction of coarse aggregate on Bingham's constants of fresh concrete. Transactions of the Japan Concrete Institute 1996; 18: 37-44.

[6] Kennedy CT. The design of concrete mixes. Proceedings of the American Concrete Institute 1940; 36: 373-400.

[7] Su N, Hsu K, Chai H. A simple mix design method for self-compacting concrete. Cement and concrete research 2001; 31(12): 1799-1807.

[8] Oh SG, Noguchi T, Tomosawa F. Toward mix design for rheology of self-compacting concrete. RILEM International Symposium on Self-Compacting Concrete. University of Tokyo, 1999.

[9] Pimanmas A, Ozawa K. Mathematical modeling of shear constitutive relationship for flowing fresh concrete. In: Proceedings of ICUEACC, Bangkok, Thailand, 1996. p. D.128-D.133.

[10] Lu G, Wang K. A yield model of highly flowable concrete, to be submitted

[11] Harr ME. Mechanics of Particulate Media---A Probabilistic Approach. New York:McGRAW HILL, 1977.

[12] ASTM C33-03, Standard specification for concrete aggregates, Annual Book of ASTM Standards, Vol. 04. 02, 2003

[13] Cadle RD. Particle size; theory and industrial applications. New York: Reinhold Publishing Corporation, 1965.

[14] Franzini JB, Finnemore EJ. Fluid Mechanics with Engineering Application. New York: McGRAW HILL, 1997.

[15] Duran J. Sands, Powders, and Grains—An Introduction to the Physics of Granular Materials. New York: Springer-Verlag, 1999.

[16] Goldsmith W. Impact, the theory and physical behaviour of colliding solids, Edward Arnold, London, 1960.

[17] Mehrabadi MM, Nemat-Nasser S, Oda M. On statistical description of stress and fabric in granular Mechanics. International Journal for Numerical and Analytical Methods in Geomechanics, 1982, 6(1): 95-108

[18] Fung YC. Continuum Mechanics. New Jersey: The Prentice-Hall, 1977.

[19] Ferraris CF. Measurement of the rheological properties of high performance concrete: State of the art report, Journal of research of the National Institute of Standards and Technology, 1999, Vol. 104, 5: 461-477

[20] Feys D, Verhoeven R, DeSchutter G. Fundamental study of the rheology of Self Compacting Concrete, composed with Belgian materials. In: The 7th National Congress on theoretical and applied Mechanics NCTAM 2006.

[21] Hu J. A study of effects of aggregate on concrete rheology. PhD thesis. Ames, Iowa State University, 2005

[22] Lu G, Wang K. A mathematics model for granular material direct shear, to be submitted

[23] Mehta PK, Monteiro PJM. Concrete-structure, properties and materials, 2nd edition. Prentice Hall, 1993

List of symbols

a, b, and c	constant factors related to the mortar material properties
A	projected area of a sphere aggregate particle
A_{AVE}	average cross area of aggregate particles on a horizontal plane in mortar
$A_{particle}$	total surface area of all aggregate particles in the unit volume of mortar
C_D	coefficient of the cement paste dragging force
D	average diameter of aggregate particles
D_0	average diameter of the aggregate particles retained on a given sieve, i
D_i	average diameter of the i-th group, $D_i = \frac{(D_i)_{max} + (D_i)_{min}}{2}$
$(D_i)_{max}$	maximum diameter of i-th group
$(D_i)_{min}$	minimum diameter of i-th group
ΔE	energy loss due to the two-particle collision
$\Delta E_{collision}$	total energy loss due to particle collision
$\Delta E_{interaction}^{single\ particle}$	Energy loss due to interaction between the aggregate particle and cement paste
$\Delta E_{interaction}$	Energy loss due to interaction between the aggregate particle and cement paste
F_{AP}	force acting on cement paste by a single aggregate particle
f_i	volume fraction of the average particles on the i-th sieve
k_p	normal stress coefficient

m	average mass of aggregate particles
N	number of aggregate particles in a unit plane material
$N_{\text{collision}}^{\text{plane}}$	number of particles that move from one plane to its adjacent plane
n_{particle}	number of aggregate particles in a unit volume of mortar
$P_{\text{collision}}^{\text{particle}}$	the probability that an aggregate particle may go out of the horizontal plane
$P_C^M(\Phi,\Psi)$	probability of a collision occurring at certain location
$(\Delta P_X)_0$	average momentum change of the two-particle collision in the mean flow direction
$(\Delta P_n)_0$	average momentum change along collision direction
S	average distance between the aggregate particles in mortar
V_A	volume fraction of aggregate
V_F	magnitude of particle fluctuation velocity
V_P	total volume of voids in unit volume of mortar
V_M^n	relative mean flow velocity between two colliding particles
$(V_M^n)_{AVE}$	average relative mean flow velocity between two colliding particles along **n** direction
$(V_F^n)_{AVE}$	average relative fluctuation velocity between two colliding particles along **n** direction
$(V_M^t)_{AVE}$	average relative mean flow velocity between two colliding particles along **t** direction

$\left(V_F^t\right)_{AVE}$	average relative fluctuation velocity between two colliding particles along **t** direction
$V_{particle}$	volume of single particle
V_{voids}	total volume of voids in unit volume of mortar
$\mathbf{v}$	aggregate particle velocity
v_F	aggregate particle fluctuation velocity
$\mathbf{v}_i$	velocity components along X axis
v_j	velocity components along Y axis
v_k	velocity components along Z axis
α	angle of direction, see Figure 7
β	angle of direction, see Figure 7 and 8
Φ	angle of direction, see Figure 11
Ψ	angle of direction, see Figure 11
ε	coefficient of elastic restitution
ρ_p	cement paste density
ζ	energy dissipation, which is always positive definite
η_P	viscosity of the cement paste in mortar
η_M	mortar viscosity
$\dot{\gamma}_M$	apparent shear rate of the mortar
$\dot{\gamma}_P$	apparent shear rate of cement paste
τ_M	shear stress of mortar

τ_0	yield stress of the mortar
τ_P	shear stress resulting from the cement paste flow in mortar
τ_{FA-P}	shear stress due to the aggregate-cement paste interaction
τ_{FA}	shear stress generated by the fine aggregate movement
μ	friction coefficient of particles
$\frac{\partial u}{\partial y}$	velocity gradient of mortar

CHAPTER 7. GENERAL CONCLUSIONS

Summary

In this study, the mechanism of the origin of the shear stress of granular material, the yield stress of cement paste and mortar, and shear stress of mortar flowing have been investigated theoretically. Meantime, the corresponding rheology tests have been performed to verify the validity of the theoretical investigations by using direct shear boxes and vane rheometer.

In studying of the granular material direct shear, the mathematical approach was performed. The 3-D probabilistic and mechanical two-particle contact models were developed to calculate both the shear stress generated on shear plane when granular material is under direct shear and volume change due to shear. Totally 142 direct shear tests on different granular materials were performed and verified the present models successfully.

A yield stress model of cement paste was developed based on the DLVO theory. In this model, cement particles are considered as rigid spheres suspended in water. The interparticle force between two adjacent cement particles is assumed to be generated by the electrostatic and dispersion forces of the cement particles. The mean interparticle force of the cement paste system along the shear direction is determined based on a probability approach. The shear stress of the cement paste is then obtained by multiplying the mean interparticle force with the number of particles in a unit volume of the cement paste. Totally 6 direct shear tests and 7 rheometer tests were performed on cement pastes

with different water to cement ratio to validate the model as well as the former rheometer results on cement pastes with different water to cement ratio.

The shear failure behavior of fresh mortars was investigated using a force balance approach from a microscale to macroscale level. In this approach, fresh mortar was considered as a two-phase material containing a matrix of cement paste and a group of rigid, spherical, non-cohensive aggregate particles. The shear force of a micro mortar unit, consisting of two contacted aggregate particles surrounded by a layer of cement paste, was first assessed from all forces balanced on the micro slant surface of failure. The shear force was assumed resulting from the friction between these two contacted particles and the shear force carried by the cement paste of the micro unit. The shear force of a macro-unit volume of the mortar was then calculated based the number of the contacted aggregate particles in the mortar and the shear force carried by the rest of cement paste. The number of the contacted aggregate particles in the micro-unit volume of mortar was estimated based on the probability concept. In order to verify the validity of the newly developed model, 47 fresh mortar mixtures made with different water-to-cement ratios (w/c), sand-to-cement ratios (s/c), and different aggregate size and gradations were tested using a direct shear apparatus. The experimental results were compared with those obtained from the model. The study indicated that the newly developed shear failure stress model fits the data from the direct shear tests very well. Both the model and experimental results revealed that the shear failure behavior of mortar follows the Mohr-Coulomb equation. The internal friction angle (ϕ_M) and cohesion (C_M) obtained from the Mohr-Coulomb curves of mortar decrease with the

interparticle distance (S), which is in turn associated with the aggregate size, gradation, voids, and volume fraction. The research results provide researchers and engineers an insight onto proportioning of workable mortar and concrete mixtures.

The shear stress and shear strain rate of highly flowable mortars were lastly modeled based on the consideration of the particle-fluid interaction. In this model, mortar was considered as a two-phase material, containing a fluid matrix (cement paste) and a group of well-graded, non-cohesive, and rigid particles (fine aggregate) that were uniformly distributed in the matrix. The mortar shear stress was assumed to be the sum of the shear stresses resulting from the paste flow, the aggregate particle movement, and the interaction between the cement paste and aggregate. The shear stress resulting from the paste flow was assessed using constitutive equations. The shear stress resulting from the aggregate particle movement was evaluated based on the probability and mechanical concepts of aggregate particle collision. The shear stress resulting from the interaction between the paste and aggregate was considered as the normal stress that the moving aggregate particles apply onto the cement paste. The shear rate of the mortar was obtained from the rheological definition of viscosity. Using this model, the effects of mortar mixture properties (such as aggregate size, volume, gradation, and friction as well as paste viscosity and yield stress) on mortar rheology were studied.

Findings

The major findings of this study are included as the following:

1. Granular material direct shear

The work briefly presented here is a part of a microscopic rheology model of fresh concrete which main objective is to better understand mechanisms governing the shear behavior in granular materials. The present models are the simplest model which still describes the 3D behavior of granular flow with direct shear. Overall shear resistance of granular materials is described as a function of friction coefficient of granular materials, which is one of the most important properties of material. Based on current considerations, the shear resistance of granular materials is directly correlated to inter-particle friction, or friction coefficient of granular materials, and it is independent of the size and size distribution of granular materials. These findings explained the observation that same granular materials with different size and size distributions have nearly constant friction angle.

2. cement paste yield behavior

In the present study, a yield stress model of cement paste is developed based on the DLVO theory. In this model, cement paste is considered as a suspension system and cement particles are rigid spheres in the suspension medium. The shear stress of cement paste is determined by the interparticle electrostatic and dispersion forces alone with probability approach. To verify the validity of the newly developed model, two types of tests (direct shear and rheometer tests) are performed for a group of cement pastes with different w/c, and the model has been applied to three sets of published experimental data. The results indicate that:

The newly-developed model can not only predict the yield stress of a cement paste but also correlate the yield stresses from different experimental methods using an experimental scaling parameter (D).

Effect of normal stress on the yield behavior of the cement pastes with w/c ≤0.4 is more significant than that of cement pastes with a higher w/c. Therefore, the normal stress, possibly resulting from the material self weight and external loads, should be considered in future rheological tests.

The "true" yield stresses measured from the direct shear test and rheometer tests are very close, especially at a low w/c (≤0.4), both of which are much higher than the Bingham yield stress measured from the rheometer test.

3. mortar yield behavior

The shear failure behavior of fresh mortar was investigated using a force balance model and a direct shear test. The following conclusions can be made from the present investigation:

Both the newly developed shear failure stress model and the experimental results from the direct shear tests illustrated that the shear failure behavior of a mortar followed the Mohr-Coulomb equation. The newly developed model fits the data from the direct shear tests very well.

According to the Mohr-Coulomb equation, the internal friction angle (ϕ_M) and cohesion (C_M) of a mortar can be determined. The cohesion (C_M) of a mortar is actually the shear failure stress of the mortar at zero normal stress, or the "true" rheological yield stress of the mortar. Both the internal friction angle (ϕ_M) and cohesion (C_M) of a mortar greatly depended on the mean interparticle distance ($\overline{S}$) of the mortar.

Aggregate parameters (size, gradation, and volume fraction) determine the mean interparticle distance ($\overline{S}$) of a mortar, and therefore they significantly influenced the shear failure behavior of the mortar.

The relative yield stress of the mortar (C_M / τ_P) decreases in an inverse power form and the relative friction angle of a mortar (ϕ_M/ϕ_{agg}) decreases in a hyperbolic logarithm form with increased interparticle distance ($\overline{S}$) of the mortar. For the mortar having a large mean interparticle distance ($\overline{S}$) (generally for the mortar with a low aggregate volume fraction), the effects of aggregate size and gradation on the mortar yield stress appeared not significant, while the effect of cement paste property becomes substantial.

The normal stress has significant effect on failure shear stress of mortar, especially on that of the low flowable mortar. As a result, in a rheology test, the normal stress, which often results from the self weight of the tested material above the shear zone and the lateral confine stress from the boundary of container, should not be neglected.

4. mortar flow

A particle-fluid model was developed for studying the flow behavior of highly flowable mortar. In this model, fresh mortar is considered as a two-phase material, with a fluid matrix and a group of rigid particles dispersing in the matrix. The mortar shear stress is considered as the sum of shear stresses resulting from the cement paste flow and the aggregate particle movements as well as the interaction between the cement paste and aggregate. The new model shows a power function between the shear stress and shear of a mortar, which agrees with the widely-accepted "modified Bingham" model and Herschel-Bulkley (HB) model. Different from these commonly-accepted models, the new particle-fluid model itself illustrates the factors that affect mortar behavior (such as cement paste density and rheological properties as well as aggregate characteristics and volume fraction). Using this new model, the effects of these factors were investigated, and the results obtained from the new model are consistent with those from the published experimental tests.

Limitations and Recommendations

In the present study, some assumptions were made in the theoretical development of the rheology model for granular material and cementitious material. These assumptions shall be re-evaluated and/or modified to improve the models in future study.

In the modeling of the granular material direct shear, aggregate particles were simplified to be spheres, and effect of aggregate shape was not directly considered in the models. Also, the initial condition of the granular material was assumed as fully compacted, voids

ratio was not able to study independently because of the complexity. Thus, in the future the initial situation of the granular material should be studied.

Furthermore, in study the yield behavior of cement paste and mortar, both the cement particles and fine aggregate particles were simplified as the rigid spheres. The effect of cement and fine aggregate particles shape were not directly considered in the models. The deformation of these particles was not considered due to the complexity. In cement paste yield model, the interparticle action between two adjacent cement particles was only considered as the electrostatic and dispersion forces of the cement particles, since the interparticle distance was assumed larger than zero. This omits the actual situation that the interparticle friction exists. The mixtures of cement paste and mortar were assumed to perform uniformly under deformation in the calculation of yield stress, which might not be practical since material at different locations might deform differently.

Finally in modeling the flow behavior of fresh mortar, the mortar was ideally considered as a two-phase material with a rigid spherical fine aggregate particles dispersing in the viscose fluid. The air voids in mortar was not considered, as well as the different shape effect of aggregate particles. This should be considered in the future.

In the present research, the effects of chemical admixtures and SCMs on the rheological performance of cementitious materials were not considered. It is necessary to consider the effect on the rheological properties of cement paste on a wider range in the rheology model, since different admixtures are more often used in current concrete.

Due to the limitation of time and source of materials, the accuracy, reliability, and reproducibility of model was restricted because of the relative small amount of data. A larger series of measurements and materials with a broader range of properties have to be tested in order to improve the validity of model. Additional data including the field data, assuming that the aggregate property parameters and mix designs are available, can improve the accuracy and wider applicable range of the model by setting up a bigger data base.

ACKNOLEDGEMENTS

Firstly, I would like to express my sincere appreciations to my adviser, Professor Kejin Wang, for her intellectual supports, encouragements and enthusiasm throughout my stay at The Iowa State University. I am in debt to her not only for her invaluable guidance and discussions that made this dissertation possible, but also in various other aspects, such as stimulation of my creativity and support to my career development.

I would also like to express my deepest gratitude to my miner advisor Dr Thomas Rudolphi, for his kindness and direction during this study. I am also very grateful for Dr. Bruce Thompson, Dr. Halil Ceylan and Dr. Max Porter's time and efforts on serving my Ph.D. committee and providing valuable comments on my dissertation.

Special thanks are given to Dr. Chiara F. Ferraris at the National Institute of Standards and Technology for her valuable inputs and discussions on part of this research and proofreading manuscript I submitted for publication.

My appreciation also goes to the personnel of the CP Tech Center (Ames, IA) for their helps, and to all friends who make the academic life more bearable.

I am always in debt to my family for their endless understanding and support.

Finally, special appreciations to my wife, Yang, who has the courage to walk with me.